Pipe Jacking
Research Results and Recommendations
by
George Milligan & Paul Norris

Published by the Pipe Jacking Association

on behalf of

The Pipe Jacking Research Group

Copies are available from the:

Pipe Jacking Association
56 Britton Street
London EC1M 5NA
Telephone: 0171-353 8805
Fax: 0171-291 1939

Price £18
Strictly payment with order

FOREWORD

PIPE JACKING RESEARCH AT OXFORD UNIVERSITY

Research into pipe jacking has been in progress at Oxford University since 1986. It was prompted by a survey carried out by Craig for the Construction Industry Research and Information Association (CIRIA Technical Note 112, 1983) and promoted initially and supported financially by the Pipe Jacking Association (PJA) and the Concrete Pipe Association (CPA).

Craig included in his report a list of research requirements, which became the overall objectives of the research programme. These may be summarised as: - friction loads in different ground conditions

- characteristics of pipe joints and joint packing materials
- effects of cyclic loading on pipes
- effects of lubricants in reducing friction
- development of a site investigation test to predict friction forces

As a result of increasing interest in the prediction and control of ground movements due to tunnelling, the measurement of ground movements and pressures has now been included within the list of objectives.

The first stage of the research programme involved laboratory testing of model concrete pipes and a number of common joint packing materials. The second stage involved monitoring of field behaviour of pipes at full scale during pipe jacking on five active construction sites, in a variety of different ground conditions. Specially designed instrumentation was incorporated into one of the pipes in the pipe string, to measure pipe-soil interaction, pipe joint characteristics, pipe compression, and pipe joint pressures. Effects of lubrication were investigated on two of the sites. Total jacking forces and rate of movement of the pipe string were measured in the jacking pit. All results were correlated with a detailed site log, observed ground conditions and full tunnel alignment surveys.

For both stages, support for a research assistant was obtained from the Science and Engineering Research Council (SERC). For the second stage, five of the major water companies - Northumbrian, North West, Severn-Trent, Thames and Yorkshire - gave financial support as well as providing sites for the work and covering additional site costs arising from the research. The project therefore represented an outstanding example of research co-operation between clients and designers, contractors and pipe suppliers, research council and academia.

The project has so far been very successful and obtained much data of immediate practical importance to the industry. To help disseminate this information as quickly and widely as possible, the PJA held a one-day workshop in March 1993 for all members of its constituent companies. The report that follows was initially produced as a working document for that event. The management group for the research, with representatives from all of the funding organisations, has decided that it is in the best interests of the industry that the report is made available in this publication to all those interested in pipe jacking and microtunnelling. Proceeds from its sale will help to support further research, which at present is progressing into stages 3 and 4 with continuing funding from SERC, the PJA and the five water companies.

CONTENTS PAGE No.

1. Introduction 1

2. Pipeline alignment 3
   2.1 Significance of pipeline alignment 3
   2.2 Alignments achieved in practice 3
   2.3 Measurement and control of pipeline alignment 3

3. Tunnel stability and ground closure 5
   3.1 Tunnel stability 5
   3.2 Bentonite slurry support and lubrication 5
   3.3 Ground closure 6

4. Pipe/soil interface behaviour 7
   4.1 Local interface stresses 7
   4.2 Pipe-soil friction 7
   4.3 Effects of misalignment 8
   4.4 Time factors 8
   4.5 Lubrication 8

5. Total jacking forces 9
   5.1 Forces due to face loads 9
   5.2 Average friction forces 9
   5.3 Forces due to self weight of pipes 10
   5.4 Forces due to ground pressures 10
   5.5 Fully lubricated drives 11

6. Pipe barrel stresses 12
   6.1 Load paths through pipes 12
   6.2 Pipe barrel stresses 12
   6.3 Elastic analysis and design 12

7. Pipe joint stresses 13
   7.1 Joint stress distributions 13
   7.2 Joint design 13

8. Ground movements 15
   8.1 Short-term settlement and heave 15
   8.2 Long-term settlements 15

9. Further research 16

10. Main conclusions 17

11. References 18

12. Figures 18

PIPE JACKING - RESEARCH RESULTS AND RECOMMENDATIONS

George Milligan[1] and Paul Norris[2]

1. Introduction

This report presents the most important technical findings of the Oxford University pipe jacking research project, in particular those arising from the site monitoring of actual construction activities. This involved the incorporation into five pipe jacks of an instrumented pipe and other instrumentation as shown in Figure 1.1. Reference should be made elsewhere (see section 10) for: details of the planning, sponsorship, funding and management of the project; instrumentation design, calibration and performance; and site selection and monitoring procedures.

The report starts by addressing the importance of pipeline alignment, the inadequacy of current specifications, and the results achievable in practice. The method of calculating three-dimensional angular misalignments between pipes from standard line and level measurements is given, and a simple site procedure for ensuring that steering corrections are made rationally is proposed.

Total pipe jacking forces depend greatly on whether the ground collapses or squeezes onto the pipe during jacking, or whether the initial overbreak around the pipe is maintained. These questions are approached via a simple understanding of the geotechnical conditions, for both cohesive and cohesionless soils, and the effectiveness of bentonite slurry support systems discussed.

Information is then provided on the measured local interface stress behaviour between the pipe and the ground and its relation to the soil parameters, in a wide variety of different ground conditions. Increases in frictional resistance during delays in jacking, and reductions due to the use of lubrication, are illustrated.

Resulting total jacking resistance is then considered, in terms of contributions due to face resistance, pipe weight and soil pressures. The way in which the total force is transmitted through the pipe barrel and the joint between pipes is analysed in detail, leading to rational approaches for pipe design under the installation loads.

Finally, the ground movements likely to occur during and after construction of a pipeline or tunnel by pipe jacking are reviewed. The areas of uncertainty still outstanding are then summarised and the further research programmes to investigate them detailed.

This report is written with the intention of benefitting all those involved in pipe jacking, whether client, consultant or contractor. Specification, design, estimating, site operation and control, resolution of claims, or preferably avoidance of the situations that lead to claims, and even the costs of insuring works, should all benefit from a better fundamental understanding of the processes involved. In the long term this should lead to more economical and safer construction and improved performance.

Most of the information in this report has been obtained from the research work on the five schemes detailed in Table 1.1. While the research work has of necessity concentrated on pipe jacked tunnels of man-entry size, the basic principles should apply equally to microtunnelling provided the consequences of the reduced diameter are taken properly into account, for example in assessing the stability of the excavated bore and hence the likely contact stresses between pipe and ground.

1. Department of Engineering Science, Oxford University and Geotechnical Consulting Group
2. Mott MacDonald, formerly Department of Engineering Science, Oxford University

	1	2	3	4	5
Date	August 1990	January 1991	March 1991	July 1991	December 1991
Location	Bolton, Lancs	Gateshead, Tyneside	Honor Oak, SE London	Chorley, Lancs	Cheltenham, Glos
Client	NW Water Bolton M.B.C	Northumbrian Water	Thames Water	NW Water Chorley D.C.	Severn Trent Water Cheltenham BC
Consultant	---	---	Binnie/Taylor Woodrow	Halcrow	---
Contractor	Laserbore	DCT	Barhale	Barhale	Lilley
Pipe Supplier	Buchan	ARC	Buchan	Spun Concrete	Spun Concrete
Pipe I.D (mm)	1200	1350	1800	1500	1200
Ground Type	Stiff Glacial Clay	Weathered Mudstone	London Clay	Dense Silty Sand	Loose Sand & Gravel
Cover (m)	1.3 - 1.5	7 - 11	11 - 21	7 - 10	4 - 7
Drive Length (m)	60	110 *	78	158	384
Position of Test Pipe	Pipe No.3	Pipe No.10	Pipe No.15	Pipe No.16	85m from front end.
Lubrication	No	No	No	No/Yes	Yes
Packer +	MDF	MDF	MDF	MDF	MDF
Excavation	Hand	Hand	Hand	Hand	Slurry T.B.M.

Notes: * Monitoring only for part of drive
+ MDF = Medium Density Fibreboard

Table 1.1 Details of schemes monitored (Norris 1992b)

2. Pipeline alignment

2.1 *Significance of pipeline alignment*

In the sections that follow, it will be seen that the degree of misalignment between pipes within the pipe string is of considerable significance for a number of reasons, for instance in generating additional interface friction between pipes and soil and most notably in controlling the total jacking load that can be transmitted safely through the pipe joints. By misalignment is meant the angular deviation between the central axes of successive pipes. In an ideal pipe jack, no such deviations would exist, but in practice irregularities in ground conditions, excavation methods, etc., will inevitably cause the shield at the front to stray from the ideal course; corrections are continually made with the steering jacks to maintain the line and level as close as possible to that required.

The normal practice at present is to specify limits to the allowable errors in line and level at any point along the tunnel, typically 50 or 75mm. While these may be necessary to maintain adequate clearance from obstructions or other services, or to provide correct hydraulic flow conditions, they are quite insufficient as a means of controlling the angular deviations between successive pipes within acceptable limits for transmission of large axial forces. Likewise, the allowable angular deviations specified in BS5911 relate only to the satisfactory performance of the joint sealing arrangements, not the transmission of longitudinal load.

2.2 *Alignments achieved in practice*

Figures 2.1 to 2.4 show the measured pipe joint angles ß (in three dimensions) along the pipes as constructed on four of the five instrumented sites, for various different ground conditions, cover depths, and locations within the pipe string (see Table 1.1). These joint angles were all accurately measured by the special instrumentation, but could also be determined less precisely from conventional line and level measurements, using the analysis shown in Figure 2.5. The joint angles calculated in this way are also shown. Four out of the five drives were within specified line and level throughout and typical joint angles ranged between zero and 0.3° in these reasonably well-controlled drives, with maximum values up to about 0.5°.

Successive tunnel surveys throughout the schemes showed that the alignment of the pipeline (in its unloaded state) did not change significantly as the pipeline was extended; thus local curvatures once established remain throughout the drive. This is particularly important if control during the early stages of a drive is poor, and gives rise to serious joint angles, as this is the location at which highest pipe loads will be generated later in the drive. The special instrumentation also allowed any straightening of pipe joints under load to be detected; generally any such tendency was found to be small, as shown typically in Figures 2.6 and 2.7. Only in the fully lubricated scheme 5 (Cheltenham), was any significant straightening observed, with changes in ß of about 0.08°.

2.3 *Measurement and control of pipe misalignment*

The observations reported in Section 2.2 mean that conventional line and level measurements at the shield are sufficient for practical purposes to determine joint angles, assuming that no significant change in alignment occurs due to the application of jacking loads or the passage of successive pipes. Where it is required for any reason to determine joint angles more precisely, for instance to check maximum angles where damage to pipes has occurred, this could be done using a Demec gauge to measure the distances between

points on adjacent pipes at three locations around a joint. The joint angle ß is then calculated from changes in these distances using the analysis presented in Figure 2.8.

Normal measurements of line and level may also be used in a simple method of making sensible decisions on steering adjustments to keep angular deviations within acceptable limits. Consider the lead pipe in the tunnel, for which the current line and level errors are measured to be X_1, Y_1, plotted as point A on the "control diagram", Figure 2.9. The tunnel is now advanced by one pipe length, usually 2.5m, after which the line and level errors are X_2, Y_2, point B on the diagram. If the tunnel is then to be advanced a further pipe length, pipe N°2 will end up in the position previously occupied by pipe N°1, with the offsets of its two ends given by points A and B. If pipe N°1 were to continue along exactly the same alignment, with no angular deviation at the joint with pipe N° 2, the new line and level errors at its front end would be given by point C with co-ordinates X_3, Y_3 such that $(X_3-X_2) = (X_2-X_1)$ and $(Y_3-Y_2) = (Y_2-Y_1)$, as shown on the figure. However if there is an angular deviation of the joint of ß = 0.1°, the end point of pipe N° 1 could lie anywhere on the circle with radius R_1; for ß = 0.2° the corresponding circle would have radius R_2, and for ß = 0.5° radius R_3. In each case the radius of the circle would be given by $R = L$ß where ß is in radians and L is the pipe length. Converting ß to degrees and putting L as 2500mm, gives R = 43.6ß (mm).

The controlling engineer, lead miner or computer may then make a rational decision as to how line and level should be corrected over this next pipe length. The aim would be to head towards zero error (X = 0, Y =0) but without exceeding an acceptable angular deviation of, say, 0.1°. The line and level at the end of this stage, point D, should then be within an area as shown hatched in the figure. This would require the front end of the pipe to go from B to D, the necessary adjustments to the steering jacks being indicated by the change in direction from line BC to line BD. In the example shown this would indicate an adjustment to the vertical alignment but very little to the horizontal alignment. For the next pipe length, the process is repeated starting from what are now the last two data points, B and D. On site it would probably be most practical to have the control diagram on a plastic sheet so that points could be marked with a felt tip pen and easily removed once no longer needed, with the circles drawn to the correct scale on a transparent overlay sheet.

The method easily allows flexibility of decision-making; for instance corrections can be deliberately biased towards controlling level at the expense of line should the former be of greater consequence. It would also be possible to plan "moves" ahead if it is necessary to get an off-line drive back accurately on line by a particular chainage, for instance at an existing shaft, while ensuring that angular misalignments are acceptable. However the greatest benefit on site might be psychological, in emphasising to all concerned the importance of keeping angular deviations small, and providing a simple graphical method of observing the actual deviations occurring as the tunnel progresses.

Note that in all the above discussion of joint angles, these may easily be converted into differential joint gaps, or vice versa. A joint angle ß is related to a maximum differential joint gap δ at the internal surface of the pipe by the relation

$$\delta = \pi ß D/180$$

where ß is expressed in degrees and D is the internal diameter of the pipe.

3. Tunnel stability and ground closure

3.1 *Tunnel stability*

The stability of the excavated bore is of considerable importance in pipe jacking, for a number of reasons: sudden collapses may endanger miners or damage tunnelling machinery; large ground movements above the pipeline may be caused, damaging foundations, road pavements or other service runs; and ground collapsed onto the pipeline will greatly increase the resistance to jacking and probably lead to excessive total jacking forces. The first two of these generally relate to the excavated face at the front of the shield. Ground conditions should be carefully assessed to anticipate possible face instabilities, particularly in mixed ground, soft clays and silts, or cohesionless soils below the water table. Where any possibility of collapse exists, consideration should be given to the use of earth-pressure balance or slurry support tunnelling machines. Face stability in cohesive soils may be assessed from the analysis given in Figure 3.1. Note that if the shield is kept tight against or embedded into the face the ratio P/D is zero. When the undrained strength is reasonably high, no face pressure is needed. When face pressure is needed, it must be kept within limits to ensure that neither excessive settlement nor heave occurs. A factor of safety of 2.0 on collapse will usually ensure this, but in soft clays at shallow depth the safe range of pressures is very limited as shown in the example in the figure.

Along the pipeline behind the shield, the ideal situation is that the overbreak, due to the shield being of slightly larger external diameter than the pipes, should remain open so that the pipes are sliding along the base of an open bore. The total jacking forces will then be minimised. Stability in cohesive soils is assessed as shown in Figure 3.2, and is controlled in the short term by the undrained strength of the soil. Stability in cohesionless soils is assessed as shown in Figure 3.3, and depends on the angle of friction of the soil. Note that in the latter case some internal pressure in the bore is necessary to maintain stability. For fine sands above the water table this may be supplied by capillary suctions, as was the case in scheme 4 of the research. Alternatively it may be provided by fluid pressure from a bentonite slurry filling the overbreak at a sufficient pressure to maintain stability. This was the approach successfully adopted in scheme 5.

3.2 *Bentonite slurry support and lubrication*

Lubrication of any kind can only work effectively if a discrete layer of the lubricant is maintained between the two sliding surfaces, in this case the exterior of the pipe and the adjacent excavated soil surface. Once the gound has collapsed onto the pipe, the effect of lubrication will be greatly reduced. The first and most important function of bentonite slurry or other lubricant is therefore to provide sufficient internal pressure to stabilise the tunnel bore as discussed above. The slurry must be designed to form a filter cake in the surrounding soil without excessive bleeding of material and be pressurised to the necessary level to overcome ground water pressures and stabilise the tunnel. Clearly it must fill the complete overbreak space before this can be achieved. In this situation, large diameter concrete pipes are theoretically buoyant. Successful lubrication of scheme 5 was achieved with slurry pressures of around 50 kPa, against a theoretical support pressure of about 10 kPa. Buoyancy of the pipes was also observed as changes in the surveyed pipe level following injection of lubricant (see Figure 2.4); that the pipe was able to lift by some 20mm indicates that the full overbreak of 20mm on diameter had been maintained. Confirmation of this was obtained from the contact stress cells, which registered total stresses equal to the slurry pressure, very low or

zero effective contact stresses with the soil at the bottom of the pipe, slightly higher effective contact stresses at the top of the pipe, and very low shear stresses.

In contrast, lubrication was also used for part of scheme 4 through mixed fine sand, silt and clay soils above the water table. In general, capillary suctions were sufficient to keep the bore stable along most of the drive, but the lubricant did not always fill the overbreak void and its effectiveness varied greatly. In some places the measured interface friction was greatly reduced, but elsewhere did not differ from the values obtained over the unlubricated length (Figures 3.4 and 3.5).

In clays of low permeability, plain water should theoretically be able to stabilise the tunnel bore and provide buoyancy to the pipe to minimise contact stresses and reduce jacking forces. However there is a danger that water, or even aquaeous slurries, may soften the clay and reduce the local ground stability and induce swelling in the soil so that the overbreak closes and contact stresses between pipe and ground are increased. Some evidence of this was obtained in scheme 1, where the ground was affected by water from a burst water main and heavy rain, and significant increases in jacking resistance were subsequently measured. However the precise reason for this increase is not known; it may be connected with a chnage in mode of sliding from frictional to cohesive, as discussed in Section 4.2. Polymer lubricants which do not give up water to the soil may still be very effective in these situations.

3.3 *Ground closure*

Even when the excavated tunnel is stable, the ground may close onto the pipe due to the "elastic" unloading of the ground around the tunnel. The reductions in vertical and horizontal diameter of the opening may be estimated from an elastic analysis as given in Figure 3.6. If these reductions exceed the initial overbreak, contact between soil and pipe will occur, radial stresses will develop, and resistance to jacking start to increase. Of the five schemes monitored, the calculated reduction in diameter was less than the initial overbreak in all except scheme 3. Here the calculated reduction in horizontal diameter is about 30mm, sufficient to close the overbreak; large contact stresses were developed in this case, in fact sufficient to damage the instrumentation.

In very stiff, heavily overconsolidated clay a further mechanism of ground closure may have to be considered. Localised stresses around the tunnel opening may be large enough to cause local plastic yielding of the soil: the resulting ground strains cannot be predicted without complex analyses (e.g. by finite elements) but as the minimum stresses to cause local yielding are exceeded the deformations will increase rapidly above those predicted from the purely elastic analysis.

4. Pipe/soil interface behaviour

4.1 *Local interface stresses*

The contact stress cells incorporated into the instrumentation allowed direct measurement of both radial (normal) and shear stresses at the interface between pipe and ground. Pore pressures were also measured at the interface close to the contact stress cells. Subtraction of the pore pressure from the total radial stress should give the effective radial stress, but in practice the results were often difficult to interpret for various reasons.

Figure 4.1 clearly indicates the pipes sliding along the base of a stable bore, with contact only at the bottom; stresses varied widely about mean values, probably mainly due to irregularities in the excavated surface. Similar effects were observed in scheme 2, but in scheme 3 in heavily overconsolidated London clay very large radial stresses and pore pressures were measured, particularly on the sides of the pipe. Local stresses of more than 500 kPa were sufficient to damage the instrumentation.

Results for scheme 4 are shown in Figure 4.2; again contact is mainly along the base of the tunnel, while intermittent and lower stresses on the sides and top indicate occasional contact occurring at these locations. As already mentioned in Section 3.2, in scheme 5 the instruments generally recorded the fluid pressures from the lubricating fluid and very low shear stresses. Some contact occurred between pipes and soil at the locations in the drive of maximum curvature.

4.2 *Pipe-soil friction*

Results relating local shear and radial stresses from all pushes during jacking have been plotted for each drive of schemes 1 to 3 (before instrument failure) in Figures 4.3 to 4.5. The results for scheme 4 have already been given in Figures 3.4 and 3.5. The relation between shear and total normal stresses appears to be frictional in all the ground materials, in that shear stresses increase more or less linearly with normal stresses. However in the cohesive soils, at higher stresses the shear stresses seem to tend toward a limiting value, which is probably controlled by the undrained strength of the soil multiplied by an adhesion factor such as is applied in the design of piles.

Scheme No.	Soil type	Friction angle (°)
1	Glacial clay	19
2	Mudstone	17
3	London clay	12.7
4	Silty sand	38
4	Sandy silt	30

Table 4.1 Measured local interface friction angles

For the frictional behaviour, the apparent interface friction angles are as given in Table 4.1. Values are given in terms of total stress. Values in terms of effective stress were similar but with greater scatter of data; lack of full saturation at the interface and the difference in location of the contact stress and pore pressure measurements introduced some uncertainty into the determination of effective stress and the total stress values are considered at present

to be more reliable. The values obtained are reasonable in comparison with the known typical values for these soil types.

4.3 *Effects of misalignment*

Misalignments in the pipeline must inevitably induce contact stresses between pipe and ground, for instance as shown in Figure 4.6. Site data showed that scenario (b) of this figure was a good model in many cases, with typical radii of pipeline curvature as given in the figure. The coincidence of sharp curvature and high local interface stresses is clearly shown by the results for schemes 4 and 5 in Figure 4.7. the pipeline appears in scheme 4 to act as a prestressed beam spanning between the high points, while in scheme 5 the deviations are mainly horizontal and the only large stresses are at the sides.

4.4 *Time factors*

In cohesive soils it is well known that the force needed to restart a jack after a stoppage is usually higher than that needed to maintain subsequent motion. A typical set of data from scheme 3 is shown in Figure 4.8; similar results but with much smaller increases were observed in the low plasticity clay of scheme 1. The mechanism is probably that pore pressures generated during pushing dissipate during a stoppage, so that the effective stress increases even though the total stress decreases; similar effects have been observed in high-speed interface ring-shear laboratory tests on London clay. Relations between increase in jacking load and the natural logarithm of stoppage time are shown in Figure 4.9; in scheme 3 significant increases occurred for stoppages of only a few minutes, and of around 25% in the first hour.

4.5 *Lubrication*

As already noted above, effective lubrication in which a complete annulus of lubricant was maintained between pipe and stable ground reduced the interface shear stresses in scheme 5 to very low values of around 2kPa. This is higher than the shear stress of the pure bentonite slurry (about 0.05 kPa), but is consistent with the shear strength of a slurry contaminated with sand. In scheme 4 the annulus was not completely filled, although a layer of soil-lubricant mixture typically 10mm thick was seen to have formed adjacent to the pipe over its bottom half, and the effectiveness of the lubrication was rather variable.

5. Total jacking forces

5.1 *Forces due to face loads*

The records of the total jacking forces, measured by load cells on the main jacks, are shown for each of the five monitored schemes in Figures 5.1 to 5.5. The intercept of the line of average increase in jacking force on the zero axis gives an indication of the face resistance. This was relatively small in the cohesive soils of schemes 1 and 3, but large in the mudstone of scheme 2. In scheme 4 the face resistance was very closely related to the excavation and trimming process at the shield. Generally the miner excavated to a diameter slightly larger than the outside diameter of the shield, and face resistance was very small. However occasionally the shield was used to trim the final 10 to 20 mm of excavation, and the face resistance then increased markedly by almost 1000 kN (100 T). In the machine-driven scheme 5 the large face resistance of about 1200 kN included the slurry face pressure and the resistance of the shield trimming the excavation. The measured face loads are summarised in Table 5.1.

		Measured face load	Average friction force	Average friction stress	Craig (1983)
Scheme		kN	(kN/m)	(kPa)	(kPa)
1	Dry Wet	120	7.2 29.8	1.5 6.2	5 - 18
2	First 40m	950	8.0	1.5	2 - 3
3		300	54.4	7.6	5 - 20
4	Unlub. Lub.	100 - 800	23.1 9.4	4.2 1.7	5 - 20
5	Unlub. Lub.	1200	100 10	22 2.2	10 - 15

Table 5.1 Average face resistance and pipeline friction

5.2 *Average friction forces*

Average friction forces for the five schemes are also included in Table 5.1. In the final two columns the resistance is expressed as an average interface shear stress and compared with the values from past experience quoted by Craig (1983). The measured values are generally at or below the Craig values, either because of the stable ground conditions or the good directional control of the jacks or a combination of the two. It is of course somewhat misleading in most cases to express the resistance as a mean shear stress, since only the bottom of the pipeline is really in contact with the soil. Points to note from the figures are: the marked increase in resistance in scheme 1 after heavy rainfall; the very low resistance for sliding on the mudstone in scheme 2 in comparison with the length over boulder clay; the very "peaky" trace in scheme 3 due to the time effects discussed above; and the marked change from unlubricated to fully lubricated behaviour in scheme 5. The rapidly increasing

resistance in scheme 5 after about 110m is probably associated with the problems of misalignment at 110 and 130m.

5.3 *Forces due to self weight of pipes*

When the pipeline is sliding along the base of a stable bore it is reasonable to assume that the average resistance should be related simply to the weight of the pipe. Using the measured local interface friction coefficients, results for the three schemes for which this model is appropriate are given in Table 5.2. Agreement between theory and measurement is quite good, though the measured values are somewhat higher, probably as a result of increased contact stresses due to misalignments. However it would seem that this approach could be useful in suitably favourable conditions; increasing the calculated resistance by about 25% to cover increases due to misalignment should give a reasonable estimate of jacking resistance.

Scheme	Field skin friction δ (°)	W tan δ (kN/m)	Av. friction (kN/m)
1	19	6.1	7.2 (dry) 29.8 (wet)
2	17	7.0	8.0
4	38 (unlub.) 15 (lub.)	18.7 6.5	23.1 9.4

Table 5.2 Pipe self weight friction

In softer clays a more appropriate model may be that of Haslem (1986), shown in Figure 5.6, in which the undrained adhesion between pipe and soil is multiplied by a contact width determined from elasticity theory. The only monitored site on which this situation occurred was in the later stages of scheme 1, after heavy rain had softened the soil. The calculation in Figure 5.6 compares very closely with the measured resistance; however more data from softer clay is needed to validate this model.

5.4 *Forces due to ground pressures*

When the ground closes onto the pipeline, the resistances will increase considerably above those considered in Section 5.3. On the monitored sites this occurred in scheme 3 and at the start of scheme 5. The evidence obtained from scheme 3 was insufficient, due to the early failure of the instruments under the very high ground pressures, to allow theoretical calculations of these pressures in heavily overconsolidated clays to be advanced.

For scheme 5, it is possible to compare the frictional resistance over the unlubricated early part of the drive with that calculated from the ground stresses shown in Figure 5.7 and following an analysis originally derived by Terzaghi (1943). The ground movements assumed in this analysis are well supported by measurements as discussed in Section 8.2. The calculation gives a total jacking resistance of 110 kN/m, compared with a measured value over the first 20m of about 100 kN/m. This shows very satisfactory agreement for drives through loose to medium-dense cohesionless materials.

5.5 *Fully lubricated drives*

As discussed above, a fully lubricated drive is one in which an annulus of lubricant is maintained between the pipe and the soil surface of a stable tunnel bore. Such conditions were achieved for much of the length of scheme 5, and the resulting jacking resistance was only about 1000 kN over a length of 100m, an average of 10 kN/m, which is equivalent to a mean interface shear stress of only 2.2 kPa, not much in excess of the shear strength of the bentonite slurry lubricant. Clearly, effective lubrication should allow long pipeline lengths to be jacked, provided good directional control is also maintained.

6. **Pipe barrel stresses**

6.1 *Load paths through pipes*

As the pipe string "wriggles" through the ground, the location of the point of maximum compression in any pipe joint will change. Such points are defined here by an angle α from the top of the pipe. Plots showing typical variations in α along a drive for the instrumented pipe joints are shown in Figures 6.1 and 6.2. The difference in α between the two ends of the pipe indicate the load path through the pipe; zero difference means that loading is essentially along one edge of the pipe, a difference of 180° that loading is diagonally across it. Either of these conditions is possible, resulting from misalignments of the types shown in Figure 4.6; as is any intermediate value, due to three-dimensionsal misalignments from simultaneous variations in line and level.

The site measurements also show that load paths may be anything from edge loading to diagonal. However, careful study of the data has shown that the diagonal case only occurs when the load is relatively small, such as close behind the shield where quite rapid changes in α occur as a result of steering operations, or at very small joint misalignment angles as the pipeline passes through a point of contraflexure in the tunnel. Neither of these situations is normally very critical for the design of the pipes; an exception would be the case immediately behind the shield in a drive with a very high face resistance. The most critical situations usually result from edge loading with high jacking forces and relatively large joint misalignment angles (ß), due to over-rapid corrections of tunnel alignment.

6.2 *Pipe barrel stresses*

Direct measurements were made of mean pipe barrel strains in the longitudinal direction using extensometers bolted to the inner surface of the instrumented pipe. A typical set of plots is shown in Figure 6.3. These may immediately be seen to correlate with the load path information in Figure 6.1; loading is initially mainly along the bottom of the pipe for the first 10m of the drive, transferring rapidly to the top at about 15m, then to the right hand side for the remainder of the drive. These observations may in turn be related to the tunnel alignment plot in Figure 2.2.

6.3 *Elastic analysis and design*

Longitudinal stresses were then determined from these strains, and compared with stresses calculated from the measured forces on the pipe, on the basis of simple stocky-column elastic theory. Agreement was generally very good. Maximum stresses in compression were within the normally recognised elastic range for the concrete, while tensile stresses on the unloaded side of the pipe were less than the tensile strength and hence would not lead to tensile cracking. This was true even for the most extremely loaded pipes, under conditions which were inducing local pipe failures at joints. It therefore appears that pipe barrels may be safely designed using simple compression theory, and that joint failure is likely to occur before the pipe barrel shows any sign of distress, at least within the range of conditions covered by the research. Only nominal longitudinal reinforcement is required, if any. Hoop reinforcement will generally be needed in larger diameter pipes to resist bending due to ground pressures, and possibly complex three-dimensional stress conditions near the pipe ends due to the jacking loads, but no information on this has been obtained from the research.

7. Pipe joint stresses

7.1 *Joint stress distributions*

The thin pressure cells incorporated into the joints at either end of the instrumented pipe allowed measurements to be made of the distribution of stress around the joints and its correlation with the joint misalignment angle. Typical results from four sites are shown in Figures 7.1 to 7.3. The pressures measured in individual cells are clearly related to the magnitude and orientation of the joint misalignment, and also depend on the total force transmitted. However, even at quite small misalignment angles the stresses in the joint are highly localised, perhaps acting over less than a quarter of the pipe circumference and reaching high local values at the point of maximum compression of the joint.

Precise back analysis of the results is complicated by the stress-strain behaviour of the packing material, in this case medium density fibreboard, which had been found in the laboratory testing to be the best of the common wood-based materials (see Figure 7.4). The material is initially quite compressible, but on unloading acquires a permanent compression and is then much stiffer on subsequent reloading. As the material is compressed and recompressed under different stresses at different points around the joint as it progresses through the tunnel, its behaviour at any time will reflect its stress history up to that time. However eventually it will tend everywhere towards the "previously compressed" material behaviour.

The measured joint stresses may be compared with those calculated by linear-stress theories such as that of the Australian Concrete Pipe Association (see Figure 7.5). Four such comparisons are presented in Figures 7.6 and 7.7, using appropriate linear approximations to the packer stiffness as shown in the inset figures. Agreement is generally good, with the theoretical calculation giving somewhat higher edge stresses than measured in some cases. This approach would therefore appear to provide a reasonably conservative design method.

7.2 *Joint design*

Joint design based on the above approach requires information only on a maximum allowable concrete stress, the stiffness of the packing material, and its location within the joint, to provide the maximum allowable jacking force for any specified maximum joint misalignment angle. Note that any specified joint angle should include any lack of squareness of pipes; BS5911 allows maximum angles due to lack of squareness of around 0.15°, and two pipes with opposing errors could give an angle of 0.3° in a perfectly straight pipeline. However a check on pipes manufactured in the UK showed that actual lack of squareness was typically around 0.05°, and there was no indication from the research that this was a significant factor in joint design when using pipes of this quality (see Table 7.1).

When the jacking force is well distributed over the pipe end area, it would be appropriate to use a concrete strength as in normal structural design of 0.4 times f_{cu}, the characteristic cube strength of the concrete. However, for the highly localised stresses at the joints in the extreme design conditions, a joint face stress of $0.8f_{cu}$ appears more appropriate. If a joint face strength test is performed, and the minimum stress of $70N/mm^2$ achieved, then it should be satisfactory to use this higher value.

The packer stiffness should for safety be taken as the unload-reload stiffness of the material measured over the appropriate stress range; its thickness should likewise be that of the material after precompression to the maximum expected joint stress. It should be as wide as possible, while keeping it some 20mm back from the edge of the concrete to reduce the

risk of local spalling.

Figures 7.8 to 7.10 show design charts produced on this basis, for various combinations of pipe diameter, packer width and stiffness, and allowable concrete strength. The very rapid reduction in allowable joint load with misalignment angle is apparent; typical maximum joint angles of say 0.5° will limit the jacking force for even the best combination of the above to about 400T. Figure 7.11 indicates the improved jacking forces that might be obtained with a packing material of lower stiffness and greater recovery. However it is important that any such material should also have the low Poisson's ratio of the wood-based materials, otherwise large bursting stresses will be set up in the joint.

Supplier	Spigot (β_{es})° A	Spigot (β_{es})° B	Socket (β_{em})° A	Socket (β_{em})° B	Maximum angle from BS5911 Part 120:1989	Pipe diameter (mm)
ARC	0.02	0.00	0.07	0.00	0.15	1200
	0.03	0.08	0.03	0.03	"	1200
(Spun process)	0.03	0.08	0.08	0.08	"	1200
	0.05	0.03	0.05	0.03	"	1200
Method of	0.02	0.02	0.02	0.02	"	1200
measurement CEN	0.08	0.03	0.03	0.03	"	1200
	0.05	0.09	0.00	0.09	0.14	1350
	0.02	0.05	0.02	0.05	"	1350
	0.00	0.02	0.00	0.02	"	1350
	0.03	0.02	0.07	0.02	"	1350
	0.04	0.05	0.04	0.05	"	1350
	0.00	0.02	0.00	0.02	"	1350
Spun Concrete	0.02	0.02	0.02	0.05	0.15	1200
	0.07	0.05	0.04	-	"	1200
(Spun process)	0.03	0.03	0.03	0.03	"	1200
Method of	0.07	0.07	0.07	0.06	0.13	1470
measurement CEN	0.08	0.04	0.03	0.00	"	1470
	0.07	0.04	0.07	0.04	"	1470
	0.05	0.01	0.05	0.05	0.15	1800
	0.04	0.02	-	0.02	"	1800
	0.01	0.01	0.05	0.01	"	1800
CV Buchan	0.08		-		0.15	1800
	0.09		-		"	1800
(Vertically cast)	0.09		-		"	1800
	0.06		-		"	1800
Method of measurement plumb line on roller line	0.09		-		0.14	1820
	0.08		-		0.14	1820

Notes 1. A & B refer to two planes at 90° to each other
2. - No reading taken

Table 7.1 Pipe end squareness audit (Norris 1992b)

8. **Ground movements**

8.1 *Short-term settlement and heave*

During pipe jacking, ground movements may occur due to instability of the face or the tunnel bore, or from the elastic unloading of the ground caused by the excavation. These have been discussed above in Section 3. In the research programme, detailed measurements of ground movements were only made in scheme 5. Here an array of inclinometers and magnetic settlement plates were installed at one cross section of the tunnel and vertical and horizontal movements measured. In the short term, as the tunnelling machine approached the array, movements were observed upward and ahead of the machine as shown in Figure 8.1. Surprisingly, no longitudinal movements were picked up by the inclinometer A on the centreline of the tunnel, while those recorded by inclinometer B are hard to understand. The upward movements were barely measurable at the surface, indicating that some compression occurred in the loose soils above the tunnel. These movements were probably the result of the high face load applied by the shield and face slurry pressure. The total face resistance of about 1200kN (see Figure 5.5) is equivalent to a pressure of 730 kPa over the face area, which is considerably greater than the theoretical passive earth pressure at that depth.

8.2 *Long-term settlements*

Long-term settlements will occur due to the closing of the overbreak, unless it is completely grouted as soon as construction of the pipeline is complete. Ground movements may then be assessed using the methods developed from other forms of tunnelling, with the advantage that the maximum "ground loss" is limited to the volume of the overbreak. The best estimates at present are made from empirical observations of settlements, as shown in Figure 8.2. The shape of the settlement trough has been found to approximate to an error function, and field observations allow an estimate to be made of the parameter (i), which controls the width of the trough, for cohesive and cohesionless soils. Equating the volume of the trough to the volume of the overbreak assumes of course that no volume change occurs in the soil. Dense cohesionless soils will tend to expand, reducing the settlements, while loose soils may compact and give increased settlements.

In scheme 5, the measured long-term settlements showed the expected form, except that the whole array appeared to experience an additional settlement of about 4mm, the full lateral extent of which could not be determined (see Figure 8.3). This was attributed speculatively to general compaction of the fairly loose gravelly sand due to vibrations from the tunnelling machine. Subtracting this, the surface settlements at three tunnel cross-sections were only 3 to 9mm, as shown in Figure 8.4. However it should be noted that settlements were not complete at the time of the last measurement, the trends with time for the centre-line settlements being as shown in Figure 8.5. In addition, the surface settlements were clearly influenced by the stiff road pavement. The movements measured immediately below the pavement were rather greater (Figures 8.3 and 8.5) and the centreline settlement (after subtraction of 4mm) was about 11mm at the end of the measurement period and approaching the calculated value of 12.8mm in the long term.

9. Further Research

While much has been learnt from the work to date, a number of aspects require further investigation. Briefly, these may be listed as:-

- radial pressure distributions on pipes, and the relation of these to soil conditions, overbreak size etc.;
- shear to normal (radial) stress relations for a wider variety of soils, in particular soft clay, and tunnel depths (stress levels);
- ground movements for various combinations of soil type and tunnel depth, overbreak volume etc.;
- stress concentrations on pipe ends at the thrust ring and adjacent to interjack stations, at which loading conditions may be severe, although the additional system flexibility associated with the interjack or main jacking set-up may allow some self-righting of eccentric loading;
- improvements to pipe joint details and packer material properties so as to allow larger jacking loads to be transmitted through misaligned joints.

The first four of these require a continuation of the site-based work, with some parallel laboratory testing to investigate interface friction behaviour. This will constitute stage 3 of the research, lasting three years from November 1992. Stage 4 will take place almost in parallel for three years from early 1993, and will concentrate mainly on the final aspect listed above; it will involve computer modelling of existing and possible alternative joint details, followed by physical modelling in the laboratory and perhaps on site of those showing most promise. The research assistant on stage 4 will also assist with site work on stage 3 as necessary. Some contributions to the work, such as to the laboratory testing for stage 3, will be made by 4th-year undergaduate projects, and there is a good possibility of acquiring a fully-supported research student (SERC or overseas) to work on some aspect of the problem, for instance the determination of short and long-term ground movements.

Stage 3 will be supported financially by SERC, the Pipe Jacking Association and a consortium of major water service companies. Stage 4 will be fully supported by SERC. Progress of the work will be monitored by a management group with representatives from the funding bodies, as was found to be very successful in stage 2; involvement of the PJA was very important in obtaining the co-operation of contractors and pipe suppliers, while the water companies provided the necessary sites on which to work and carried the additional site costs on each contract.

10. Main conclusions

The main conclusions from the work may be summarised as follows:-

(i) The contact stresses between pipe and ground depend on the stability of the tunnel bore, the initial stresses in the ground and the stiffness of the soil. In cohesionless materials they are well predicted by the Terzaghi model.

(ii) Pipe-soil interface sliding behaviour is frictional in nature even in cohesive soils, except that the undrained strength provides an upper bound in cohesive soils. The field behaviour is consistent with that measured in laboratory interface tests (modified shearbox).

(iii) In stable tunnel bores, the resistance to sliding of the pipes is related simply to the self weight of the pipes.

(iv) Effective lubrication requires complete filling of the overbreak, and in cohesionless soils sufficient pressure to maintain the stability of the tunnel bore. Bentonite slurries are suitable in silty, sandy and gravelly soils, but in stiff clays aquaeous slurries may accelerate swelling of the clay leading to increased contact stresses between pipe and ground.

(v) Face loads are likely to be relatively high with slurry or earth-pressure-balance tunnelling machines, but care is needed to ensure that the face is not overloaded, leading to excessive ground movements. High face loads will occur in hand drives in strong soils when the shield is used to trim the excavation.

(vi) Design of pipe barrels for jacking loads may be safely based on simple stocky-column elastic theory.

(vii) Local pipe joint stresses may be very high, but may be calculated in relation to maximum joint angles with adequate accuracy using the Australian CPA linear-stress approach. Local stresses up to 0.8 times the characteristic concrete cube strength may be allowed; alternatively the allowable stress may be based on the joint face strength test.

(viii) Within reason, joint packing materials should be as thick as possible, and as wide as possible without encroaching within 20mm of the face of the concrete. Of the common wood-based materials, medium density fibreboard or chipboard are the best. Packers should be considered as part of the pipe and fitted at the pipe works.

(ix) It is possible for pipe manufacturers to provide curves showing allowable jacking loads related to joint angles for the particular concrete strength and packing material. It would be reasonable for specifying Engineers to require contractors to remain within these allowable loads by a suitable combination of interjacks and good site control of alignment. Conventional line and level specifications should then only be related to hydraulic or other requirements. Pipe end squareness should be included when defining allowable joint angles. This approach would benefit manufacturers of high-quality pipes and contractors able to exercise good control on site.

(x) Site supervision by both clients' and contractors' staff should emphasise the control of joint angles, which may be calculated from conventional line and level measurements. A simple graphical method has been proposed which allows rational decisions about steering corrections to be made to minimise subsequent joint angles.

11. **References**

References from stage 2 of the research work

Norris, P. and Milligan, G.W.E. (1991) *Field instrumentation for monitoring the performance of jacked concrete pipes.* FMGM 91, Proc. 3rd. Int. Symp. on Field Measurements in Geomechanics, Oslo.

Milligan, G.W.E. and Norris, P. (1991) *Concrete jacking pipes, the Oxford research project.* Proc. 1st. Int. Conf. on Pipe Jacking and Microtunnelling, Pipe Jacking Association, London.

Norris, P. (1992a) *Instrument design, manufacture and calibration for use in monitoring the field performance of jacked concrete pipes.* Report No. OUEL 1919/92, Department of Engineering Science, Oxford University.

Norris, P. and Milligan, G.W.E. (1992a) *Pipe end load transfer mechanisms during pipe jacking.* Proc. Int. Conf. on Trenchless Construction, No Dig 92, Washington.

Norris, P. and Milligan, G.W.E. (1992b) *Frictional resistance of jacked concrete pipes at full scale.* Proc. Int. Conf. on Trenchless Construction, No Dig 92, Paris.

Norris, P. (1992b) *The behaviour of jacked concrete pipes during site installation.* D.Phil. thesis, University of Oxford.

Other references

Atkinson, J.H. and Mair, R.J. (1981) *Soil mechanics aspects of soft ground tunnelling.* Ground Engineering, Vol.14, No.5.

Craig, R.N. (1983) *Pipe Jacking: a State-of-the-art Review. Technical Note No. 112.* CIRIA, London.

O'Reilly, M.P. and New, B.M. (1982) *Settlements above tunnels in the United Kingdom - their magnitude and prediction.* Proceedings Tunnelling '82 Symposium, Institution of Mining and Metallurgy, London, pp. 173-181.

Poulos, H.G. and Davis, E.H. (1974) Elastic solutions for soil and rock mechanics. Wiley, New York.

Terzaghi, K. (1943) Theoretical soil mechanics. Wiley, New York.

12. **Figures**

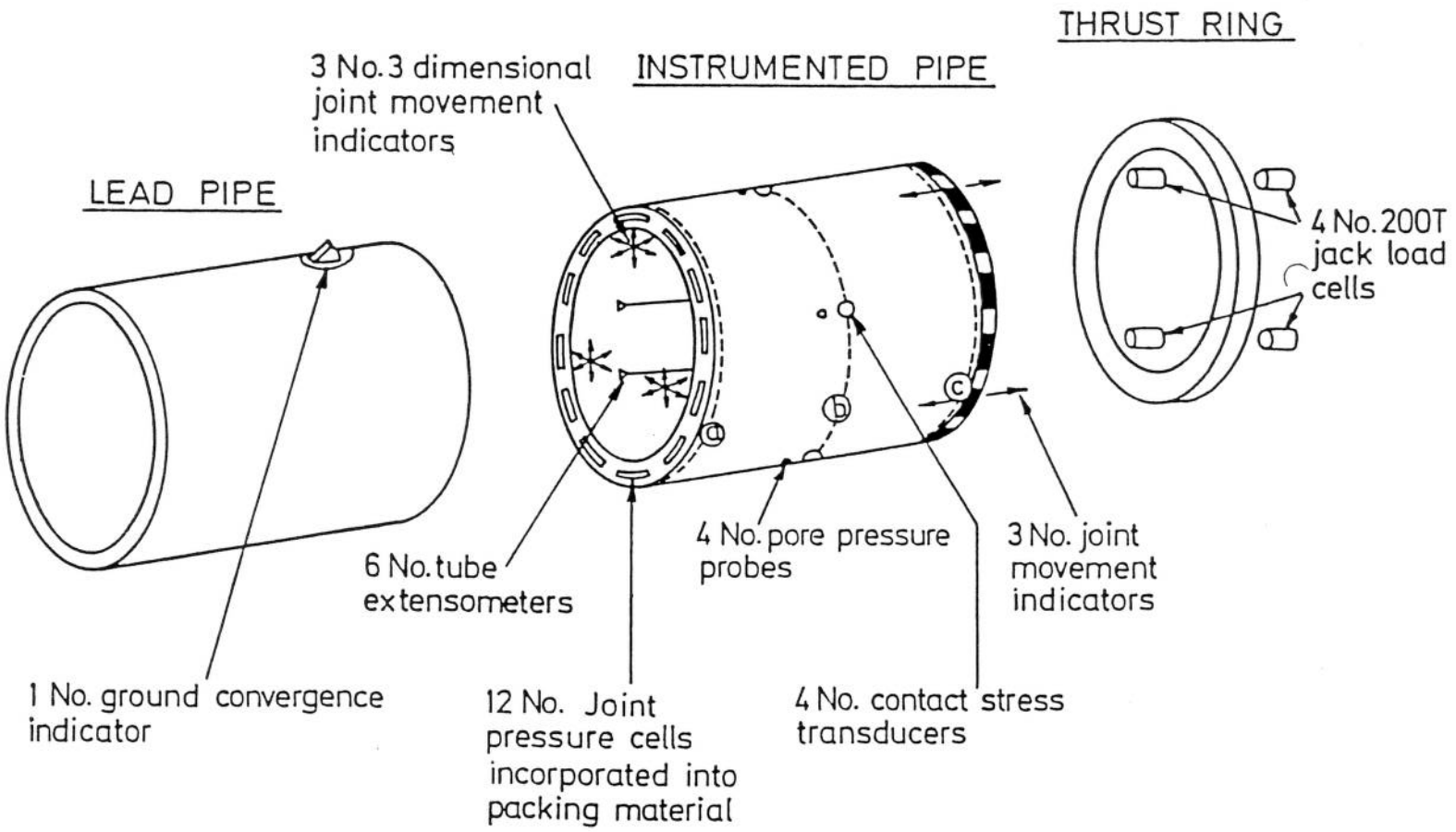

Figure 1.1 Schematic of instrument arrangement (Norris 1992b)

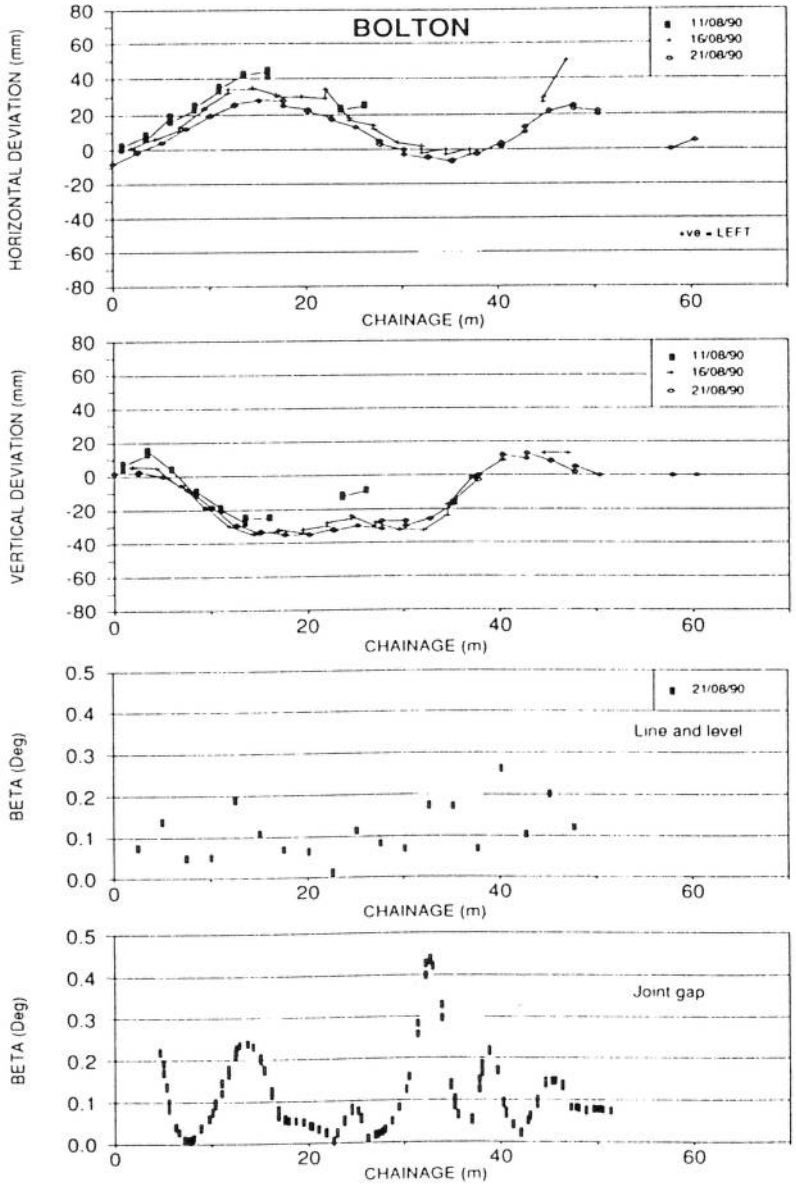

Figure 2.1 Tunnel alignment surveys for scheme 1 (Norris 1992b)

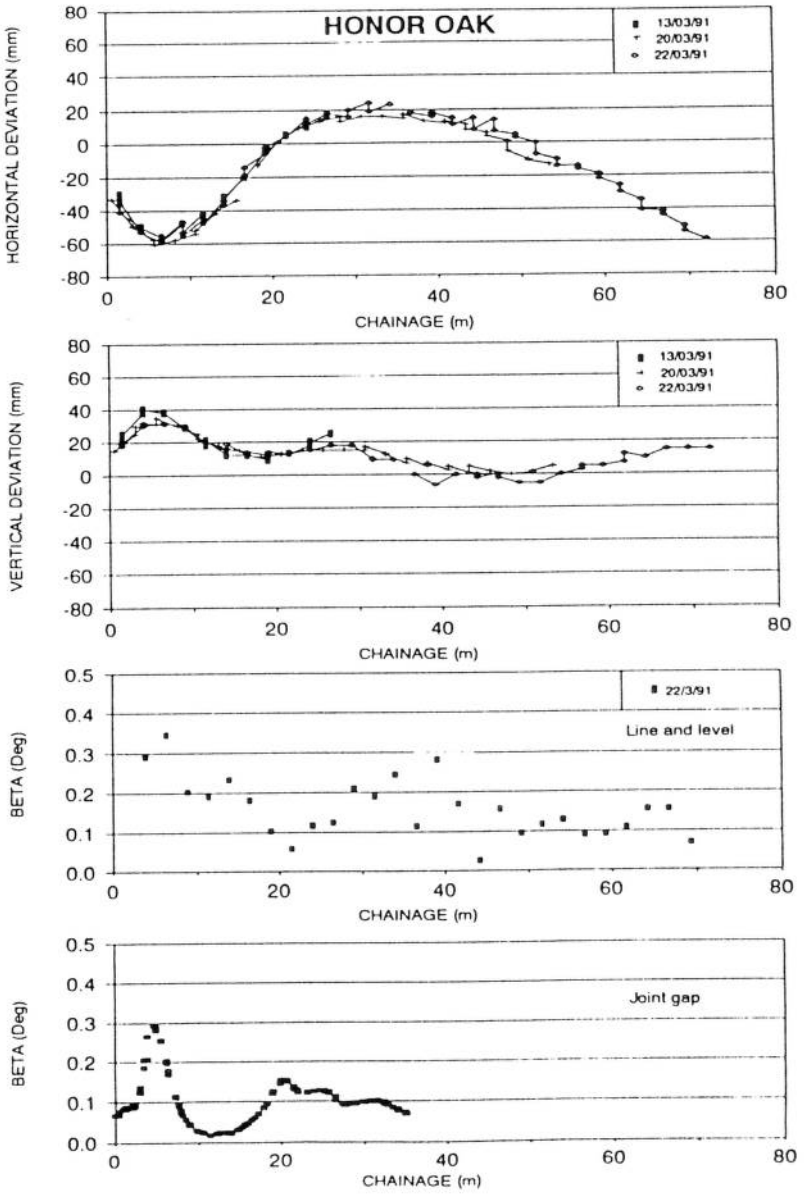

Figure 2.2 Tunnel alignment surveys for scheme 3 (Norris 1992b)

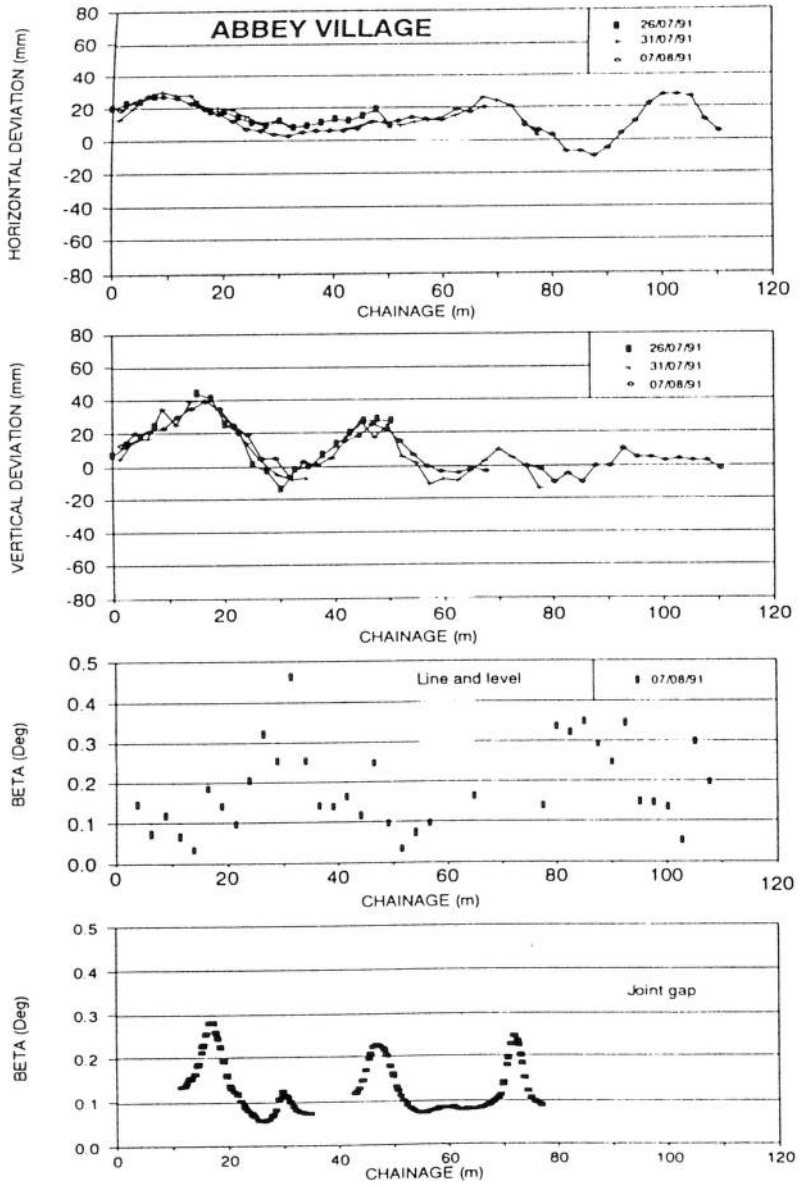

Figure 2.3 Tunnel alignment surveys for scheme 4 (Norris 1992b)

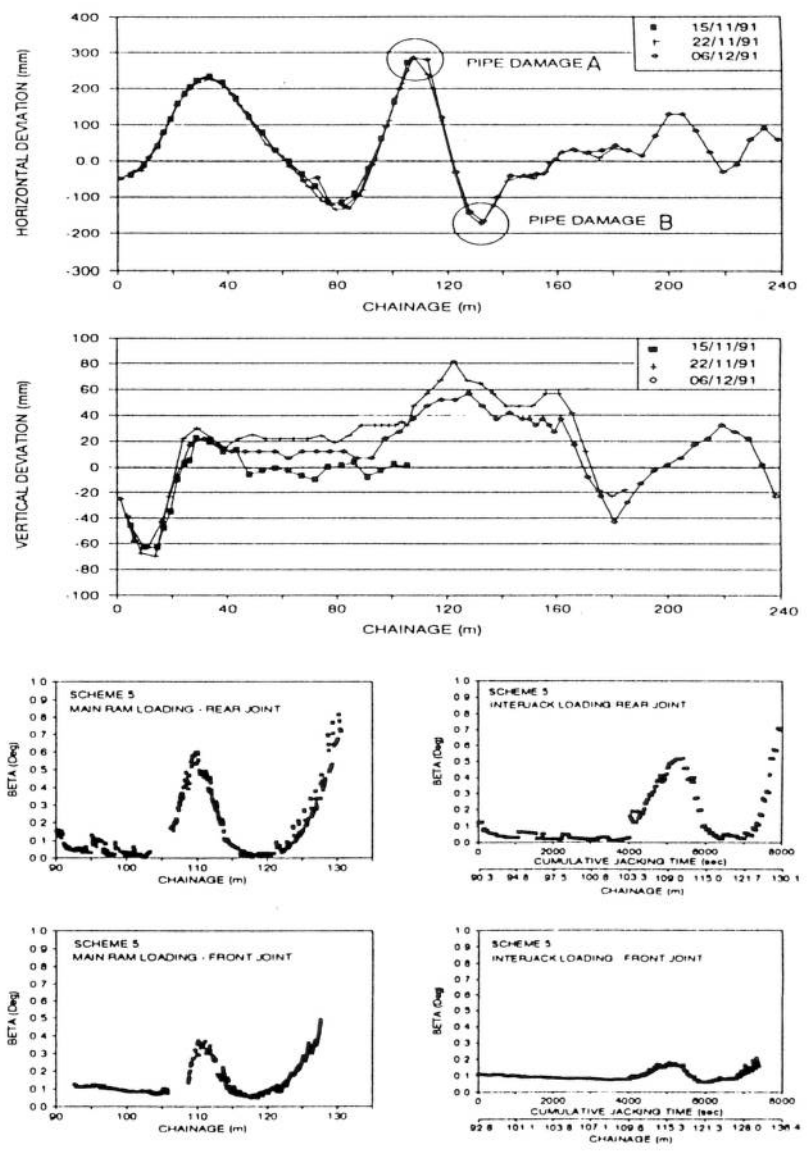

Figure 2.4 Tunnel alignment surveys for scheme 5 (Norris 1992b)

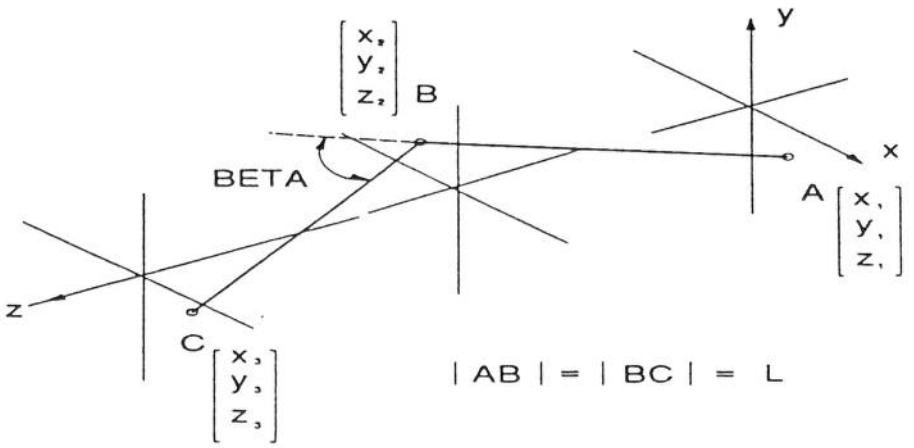

AB and BC represent the centrelines of two successive pipes, with the *x,y,z* co-ordinates being the line error, level error and chainage respectively at the pipe ends.

The direction cosines of AB are

$$l=\frac{x_2-x_1}{L},\quad m=\frac{y_2-y_1}{L},\quad n=\frac{z_2-z_1}{L}$$

likewise the direction cosines of BC are

$$l'=\frac{x_3-x_2}{L},\quad m'=\frac{y_3-y_2}{L},\quad n'=\frac{z_3-z_2}{L}$$

then the misalignment angle ß is given by

$$\cos\beta = l.l' + m.m' + n.n'$$

In practice the values of *z* cannot be obtained sufficiently accurately, but *n* may be determined from the relation

$$l^2+m^2+n^2=1$$

and similarly for *n'*.

Alternatively, for the small deflection angles occurring in practice, the value of ß may be calculated more simply from

$$\sin\beta=\beta(radians)=\frac{\sqrt{(2x_2-x_1-x_3)^2+(2y_2-y_1-y_3)^2}}{L}$$

Figure 2.5 Determination of joint angle ß from line and level surveys

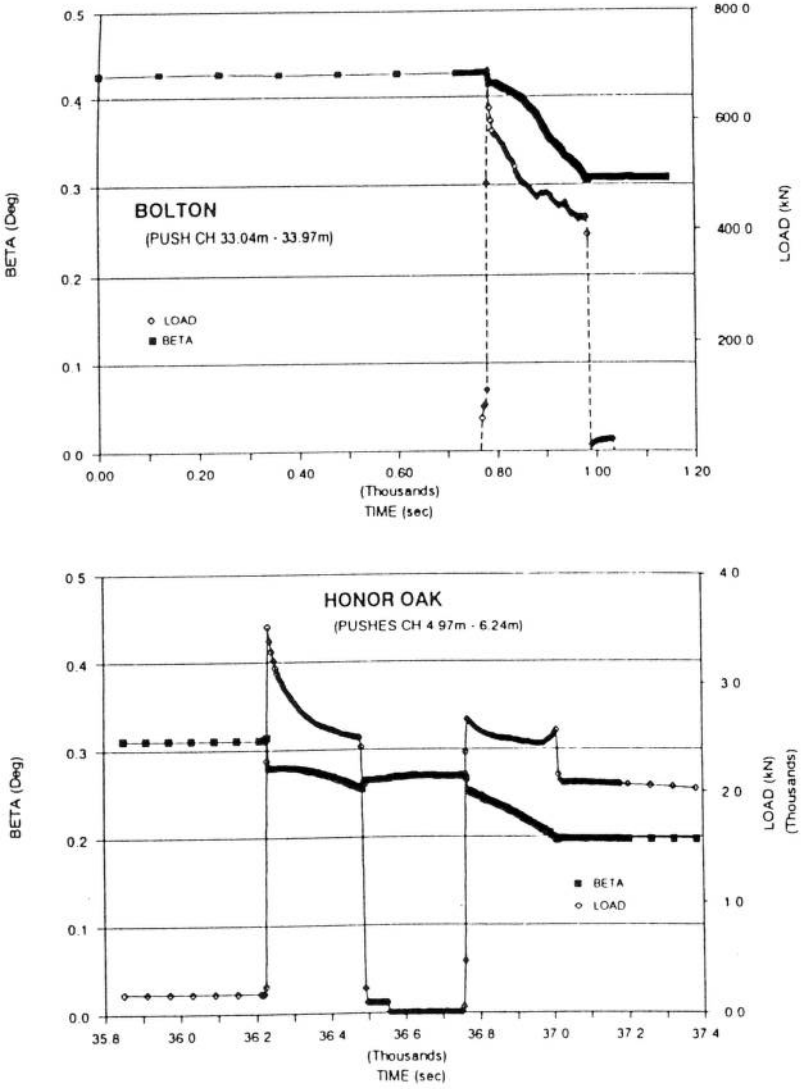

Figure 2.6 Change in ß on application of jacking load, schemes 1 and 3 (Norris 1992b)

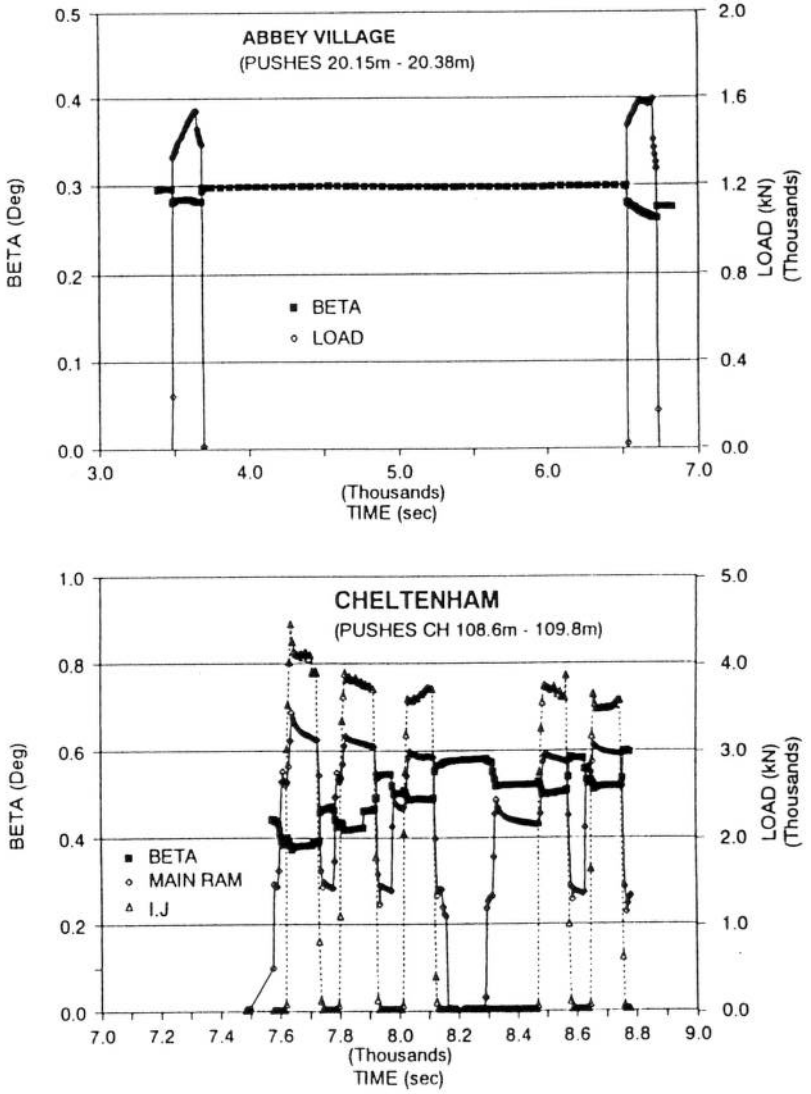

Figure 2.7 Change in ß on application of jacking load, schemes 4 and 5 (Norris 1992b)

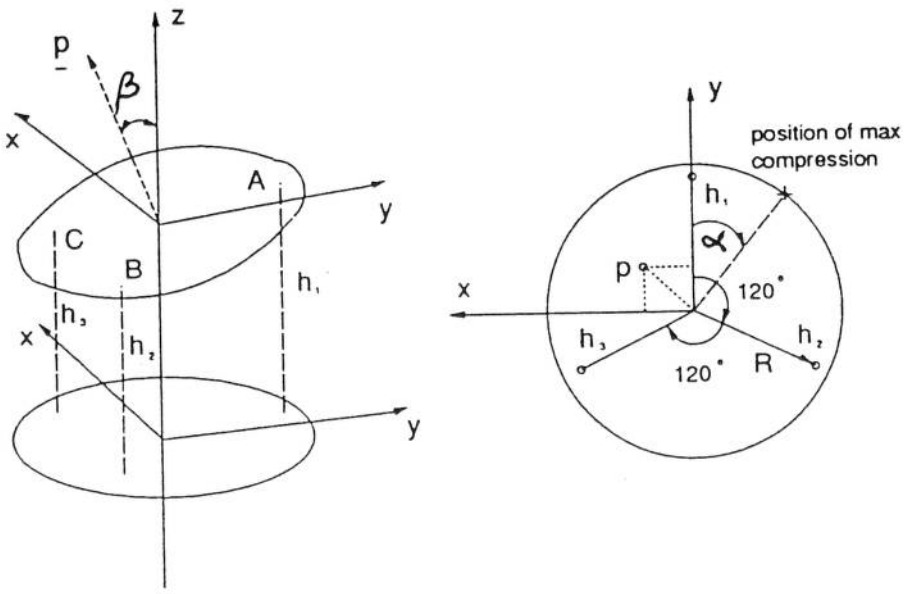

If a joint gap has widths h_1, h_2 and h_3 at three points at a radial distance R and equally spaced around the pipe, it can be shown that

$$\beta = \cos^{-1}\left[\frac{1}{\sqrt{\frac{(h_2-h_3)^2}{3R^2}+\frac{(h_2+h_3-2h_1)^2}{9R^2}+1}}\right]$$

and that

$$\alpha = \tan^{-1}\left\{\frac{\sqrt{3}(h_3-h_2)}{(h_2+h_3-2h_1)}\right\}$$

where ß is the angular rotation at the joint and α is the angular position of the point of maximum compression as shown above.

Note that the second equation always gives two possible solutions for α; the correct one may be identified using the table below.

RANGES FOR α	$h_3 > h_2$	$h_3 < h_2$
$h_2 + h_3 > 2h_1$	0° - 90°	270° - 360°
$h_2 + h_3 < 2h_1$	90° - 180°	180° - 270°

Figure 2.8 Deflections of an instrumented joint (Norris 1992b)

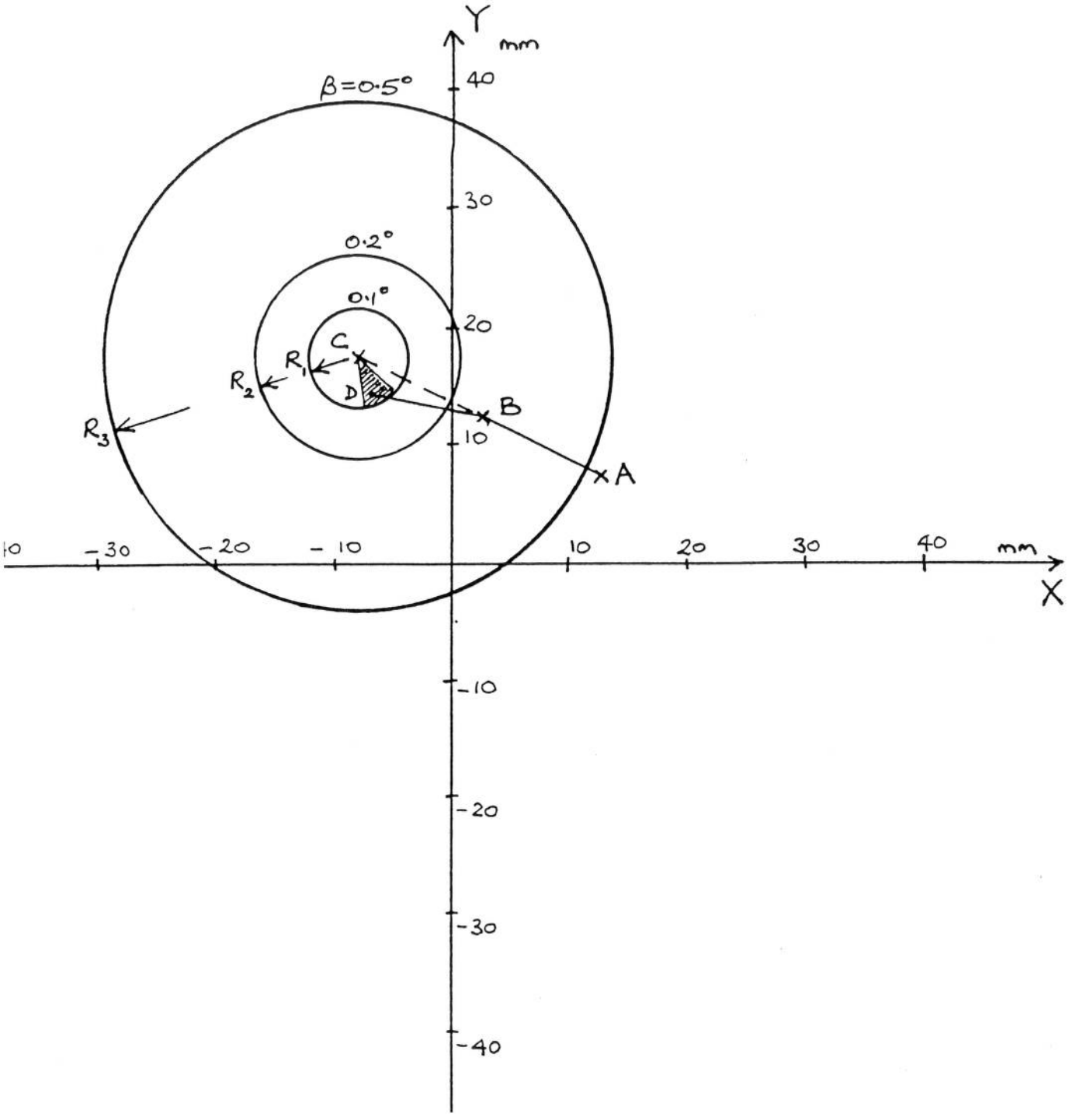

Figure 2.9 Control diagram for pipe jack alignment

In cohesive soils, the pressure σ_T required to maintain stability of the tunnel face is given by

$$\sigma_T > \gamma(C+D/2) - T_c s_u$$

where γ = unit weight of soil, s_u= undrained strength of soil
and T_c= stability ratio - see plot below (Atkinson and Mair 1981).
In pipe jacked tunnels the unsupported length P is usually small or zero, and P/D=0.
e.g. for γ = 20 kN/m^3, C = 4m, D = 2m, the plot gives T_c = 8
hence σ_T = 100 - 8.s_u kPa
and for s_u > 12.5 kPa, no support is needed.

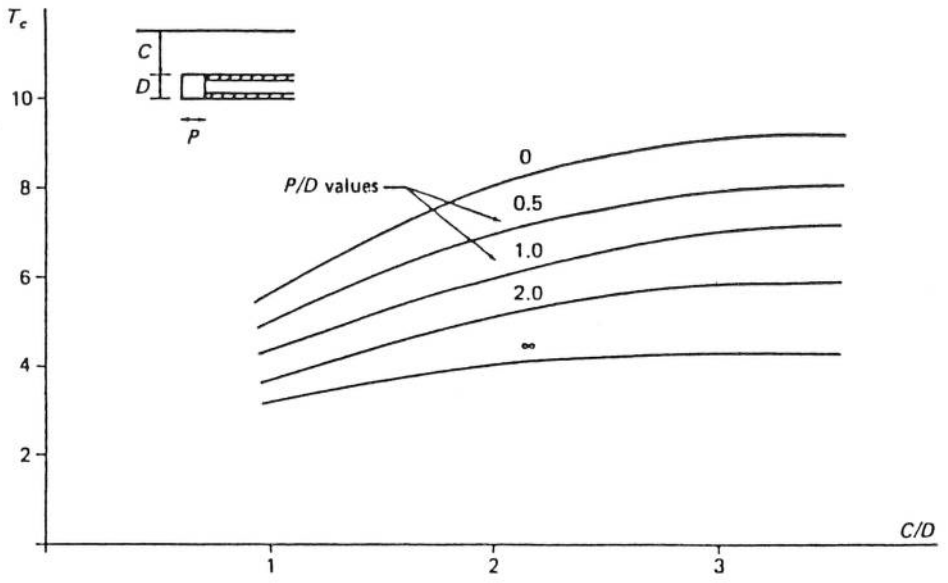

To prevent blow-out due to excessive face pressure,

$$\sigma_T < \gamma(C+D/2) + T_c s_u$$

In both cases, a factor of safety of 1.5 to 2.0 on s_u is needed to limit heave and settlement in soft clays, for example see below (Mair 1987).
In this case, say γ = 20 kN/m^3, D = 2.0m, s_u = 10 kPa, then $\gamma D/s_u$ = 4.
For C/D = 2.0, σ_T must lie between 6 and 14 times s_u, i.e. between 60 and 140 kPa.

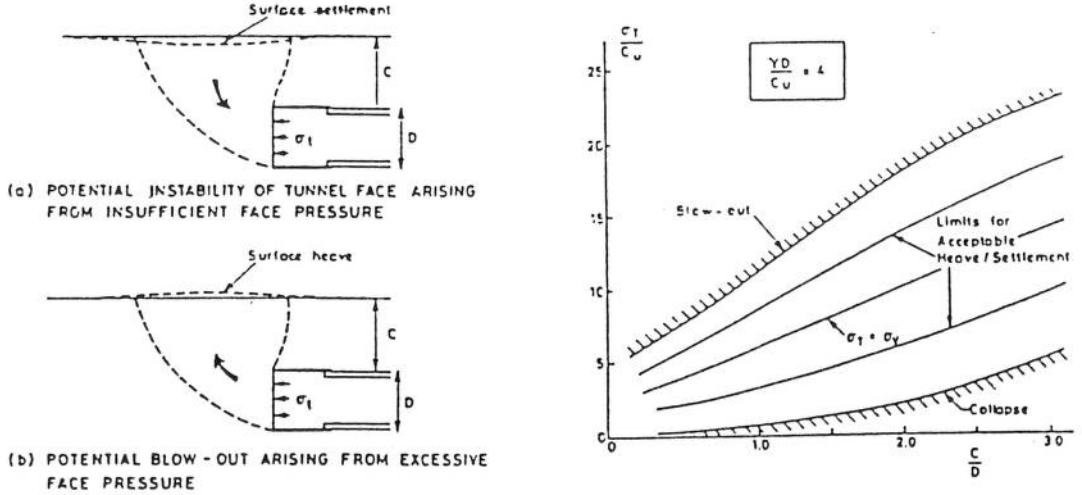

Figure 3.1 Face stability in cohesive soils

For the tunnel behind the shield, the conditions correspond to the case in Figure 3.1 of P/D → ∞. The equation for calculating the support pressure required to prevent collapse is as before

$$\sigma_T = \gamma(C + D/2) - T_c . s_u$$

which may be re-arranged to give

$$\frac{\sigma_T}{s_u} = \frac{\gamma . D}{s_u}(C/D + 1/2) - T_c$$

This gives rise to plots shown below. Again, values of σ_T less than zero indicate that the tunnel is stable without any support pressure. Note that for microtunnels $\gamma D/s_u << 1.0$ in most cases, and the tunnel bore will normally be stable.

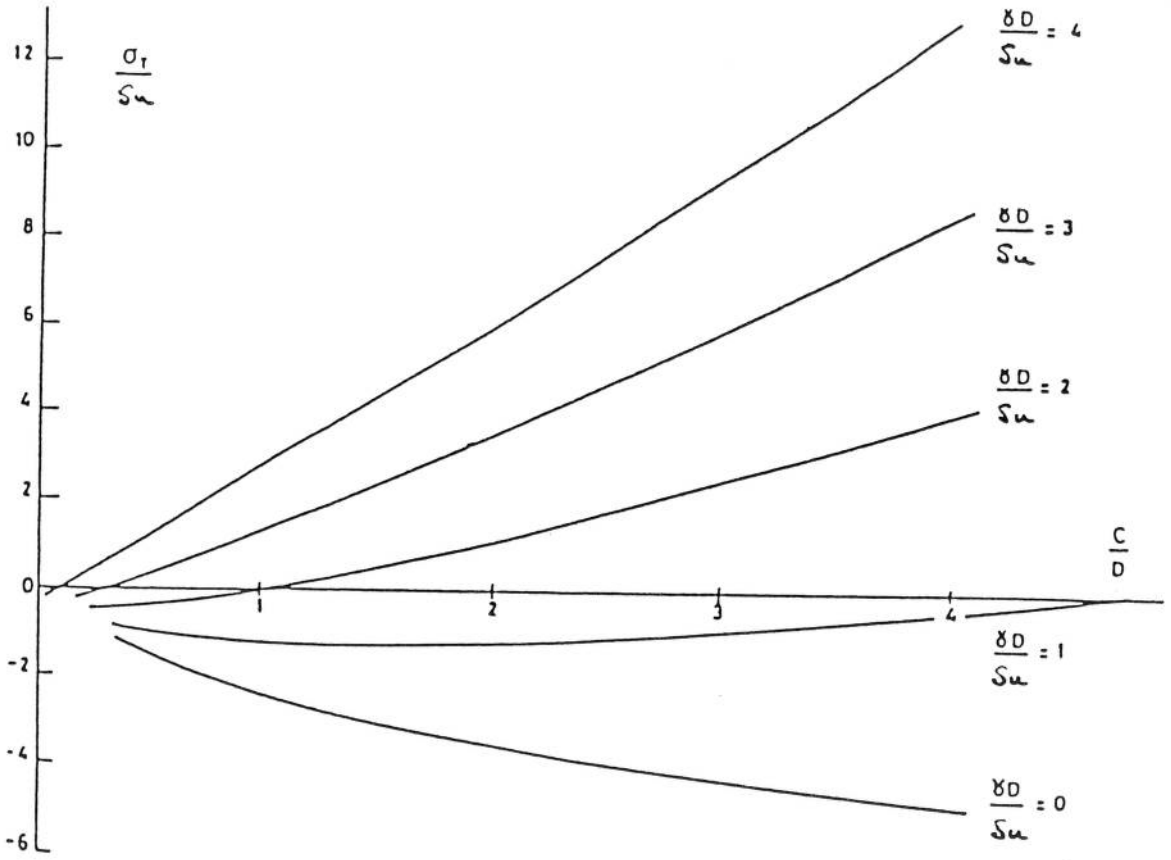

For example, for C/D = 2, and $\gamma D/s_u$ = 4, from Figure 3.1 T_c = 4
then σ_T/s_u = 4 x 2.5 - 4 = 6, or directly from plot above.
i.e. for s_u = 10 kPa, σ_T = 60 kPa.

Figure 3.2 Tunnel stability in cohesive soils

For tunnels in cohesionless soil without a surcharge on the surface, the required support pressure σ_T is independent of the cover depth and is given by

$$\sigma_T = \gamma . D . T_\gamma$$

where T_γ is the stability number given by the plot below; it is a function only of ϕ, the friction angle for the soil.

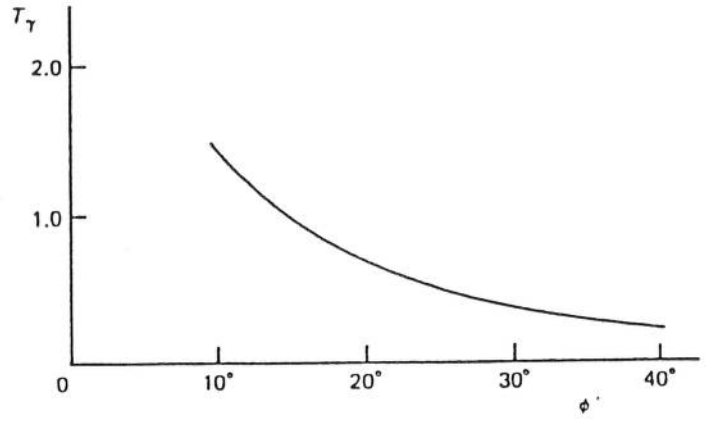

For example, if γ = 18 kN/m^3, D = 1.6m, and ϕ = 35°,
then from the plot T_γ = 0.3 and σ_T = 18 x 1.6 x 0.3 = 8.6 kPa

Alternatively, if the tunnel is at shallow depth and a large surcharge σ_s acts on the surface, the weight of soil may be neglected and then

$$\sigma_T = \sigma_s . T_s$$

with the stability number T_s as given in the plot below.

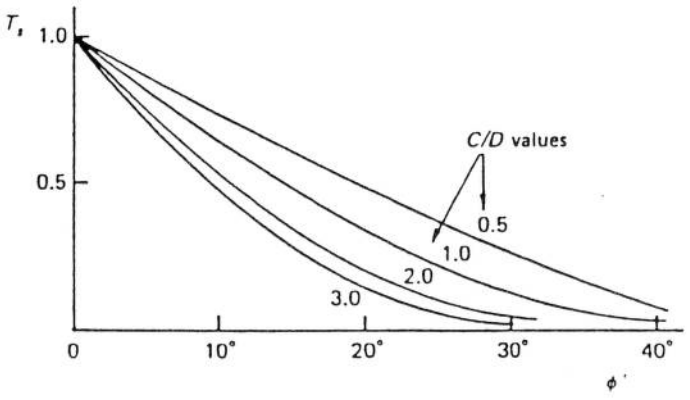

Note that both solutions apply to dry soil. Water pressure, if present, must be added to σ_T and the buoyant weight of soil used in the first equation.

Figure 3.3 Tunnel stability in cohesionless soils

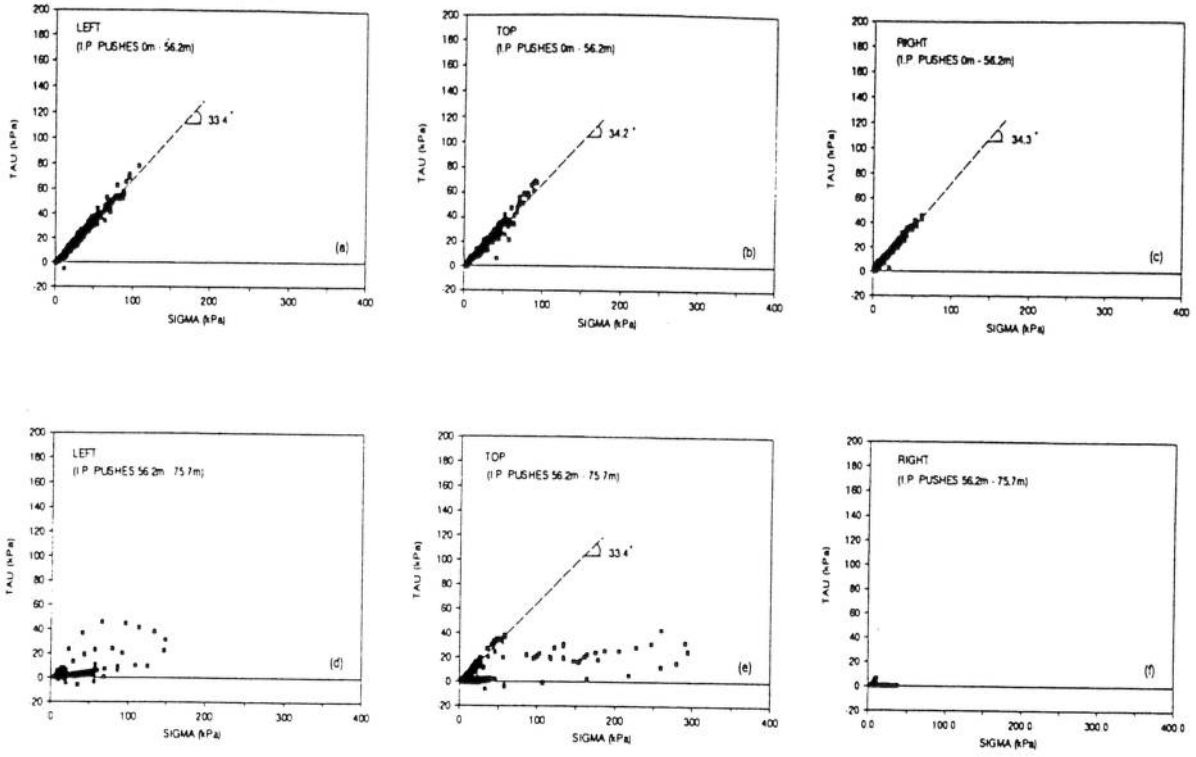

Figure 3.4 Shear stress/total radial stress relations from scheme 4; prior to lubrication (a-c) and during lubrication (d-f) (Norris 1992b)

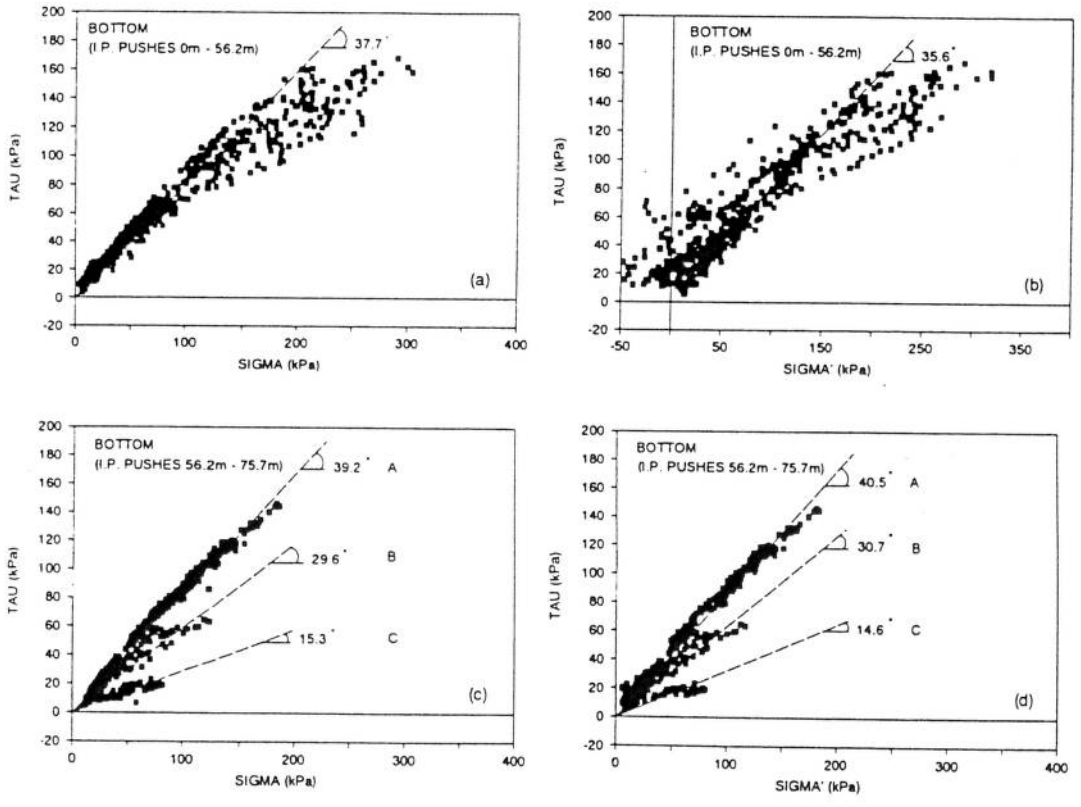

Figure 3.5 Shear stress/radial stress relations from scheme 4; total and effective stress responses on the bottom of the pipe prior to lubrication (a & b) and during lubrication (c & d) (Norris 1992b)

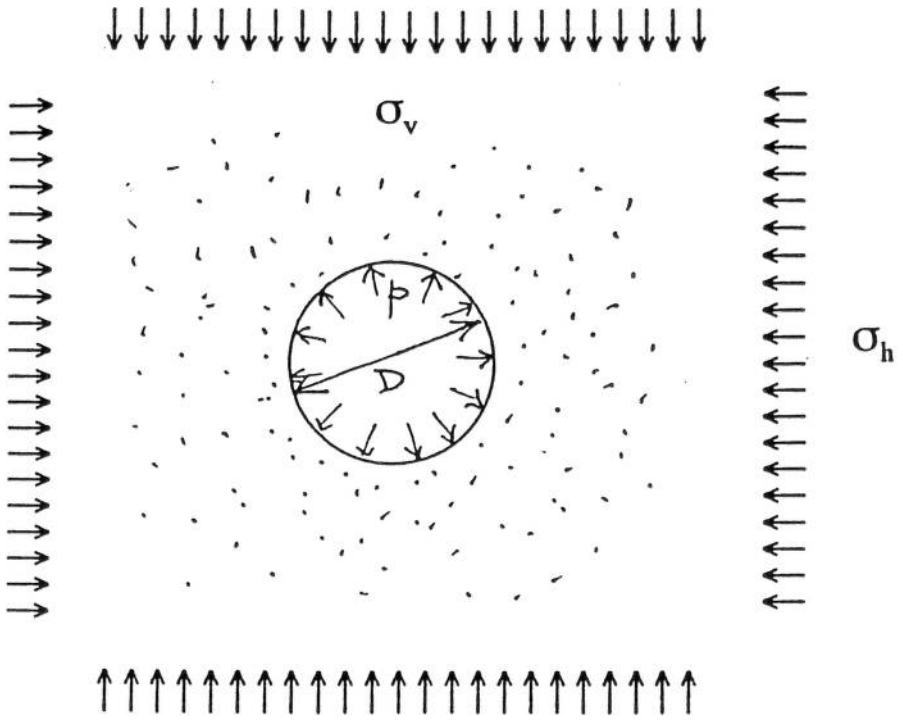

For initial vertical and horizontal stresses in the ground σ_v and σ_h, the reduction in vertical diameter of the tunnel bore due to elastic stress relief is given by

$$\delta_v = \frac{(1-\nu^2)}{E} D(3\sigma_v - \sigma_h)$$

and similarly the reduction in the horizontal diameter is given by

$$\delta_h = \frac{(1-\nu^2)}{E} D(3\sigma_h - \sigma_v)$$

where E and ν are the Young's modulus and Poisson's ratio for the soil.

If an internal support pressure p is applied, the symmetrical increase in radius is given by

$$\delta_p = \frac{(1+\nu)}{2E} pD$$

For example, in scheme 5, D = 1.45m, σ_v = 5.4 x 19 = 103 kPa
take $K_0 = 1 - \sin\phi = 0.47$, hence σ_h = 0.47 x 103 = 48 kPa
taking E = 100 MPa, ν =0.2, gives δ_v = 3.63mm
and for p = 50 kPa, δ_p = 0.44mm
thus total maximum inward movement = 3.63 - (2 x 0.44) = 2.8mm, and initial overbreak of 20mm on diameter would not be closed.

Figure 3.6 Calculation of ground closure

For a tunnel with initial vertical and horizontal stresses in the ground

$$p_z = \sigma_v = \gamma.z$$

$$p_x = \sigma_h = N.p_z$$

the radial stress σ_r at the tunnel surface is zero and the maximum value σ_{max} of the circumferential stress σ_c may be obtained from the figure below for the appropriate value of N. Note that the largest values occur for $N > 1$, i.e. in beds of heavily overconsolidated clay.

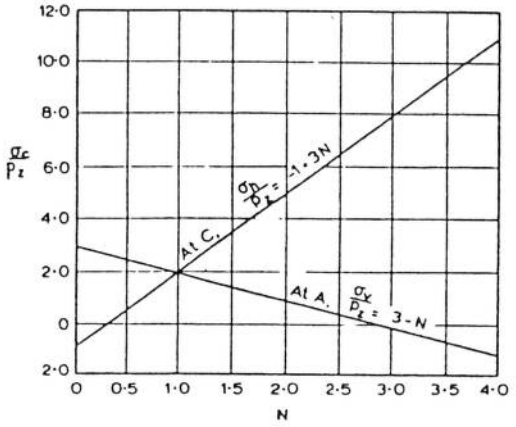

Circumferential principal stress at surface of circular tunnel as function of N (Terzaghi and Richart, 1952).

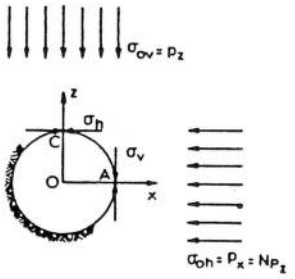

If there is an internal pressure in the tunnel (e.g. due to bentonite lubricant) of $\sigma_T = p$, then this causes stresses at the tunnel surface of

$$\sigma_\theta = -p, \qquad \sigma_r = +p$$

For local yielding to occur,

$$\sigma_\theta - \sigma_r = 2s_u$$

$$\therefore (\sigma_c - p) - p = \sigma_c - 2p = 2s_u$$

Figure 3.7 Conditions for local yielding at the tunnel surface

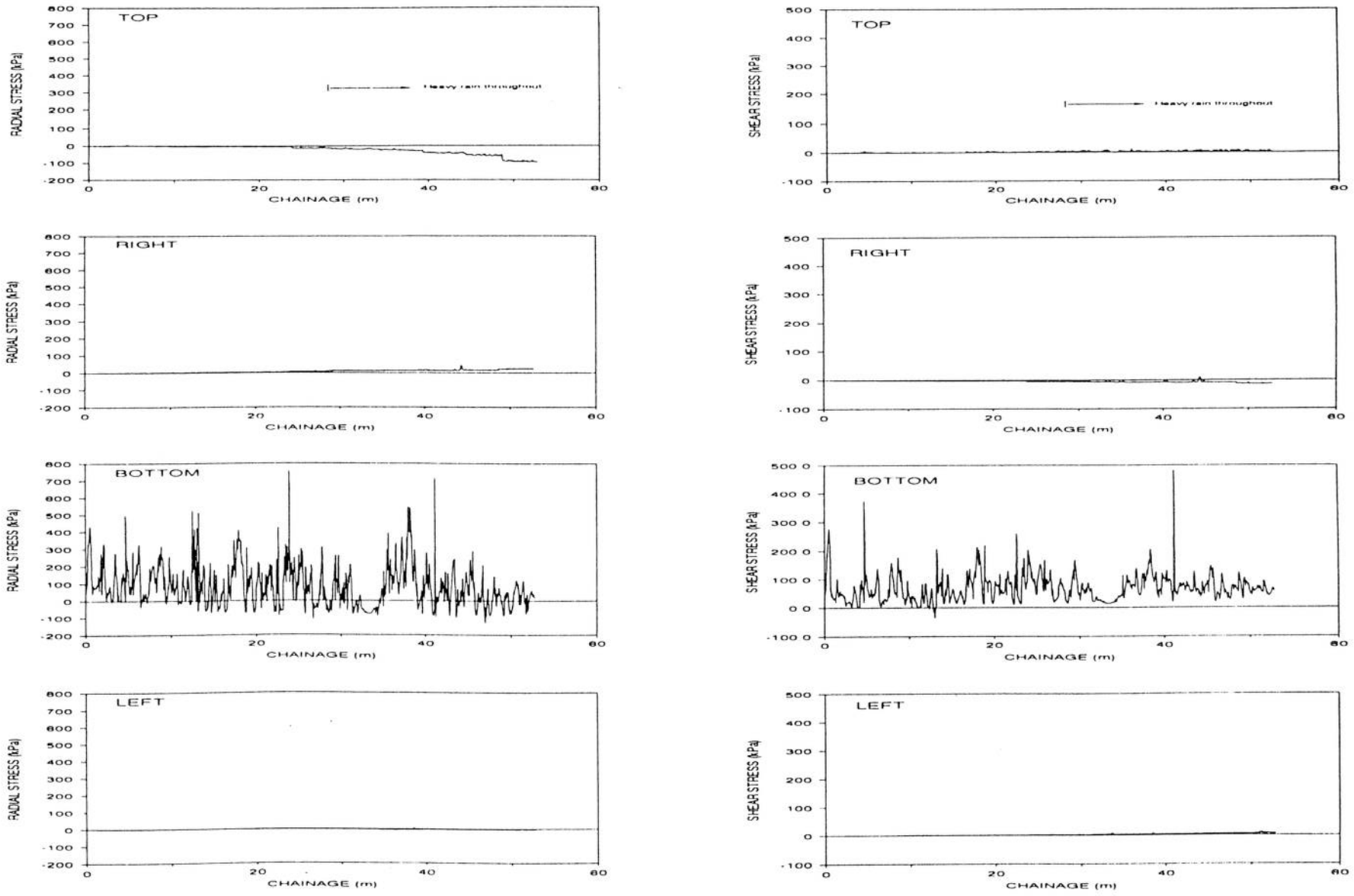

Figure 4.1 Variations in total radial and interface shear stresses in scheme 1 (Norris 1992b)

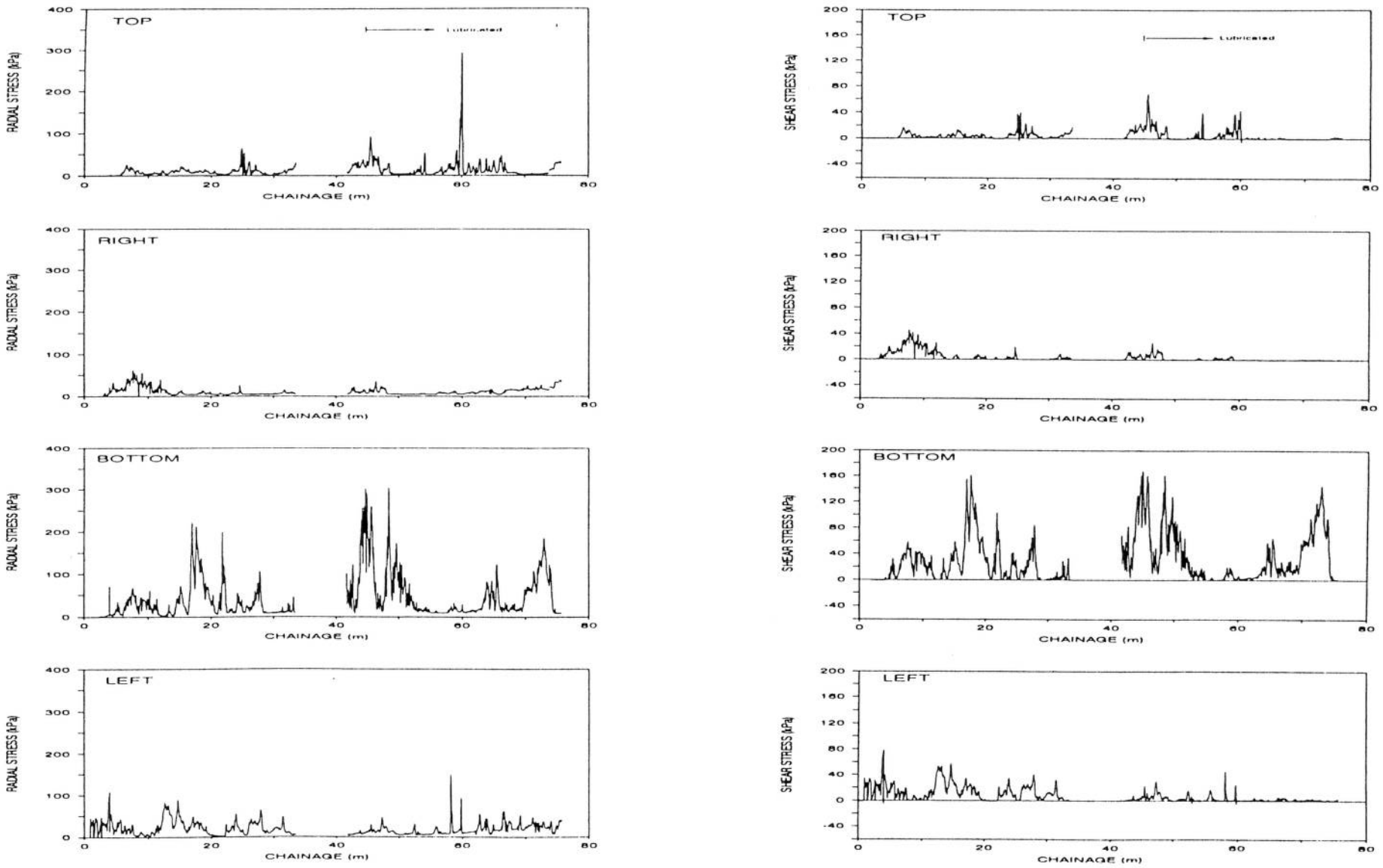

Figure 4.2 Variations in total radial and interface shear stresses in scheme 4 (Norris 1992b)

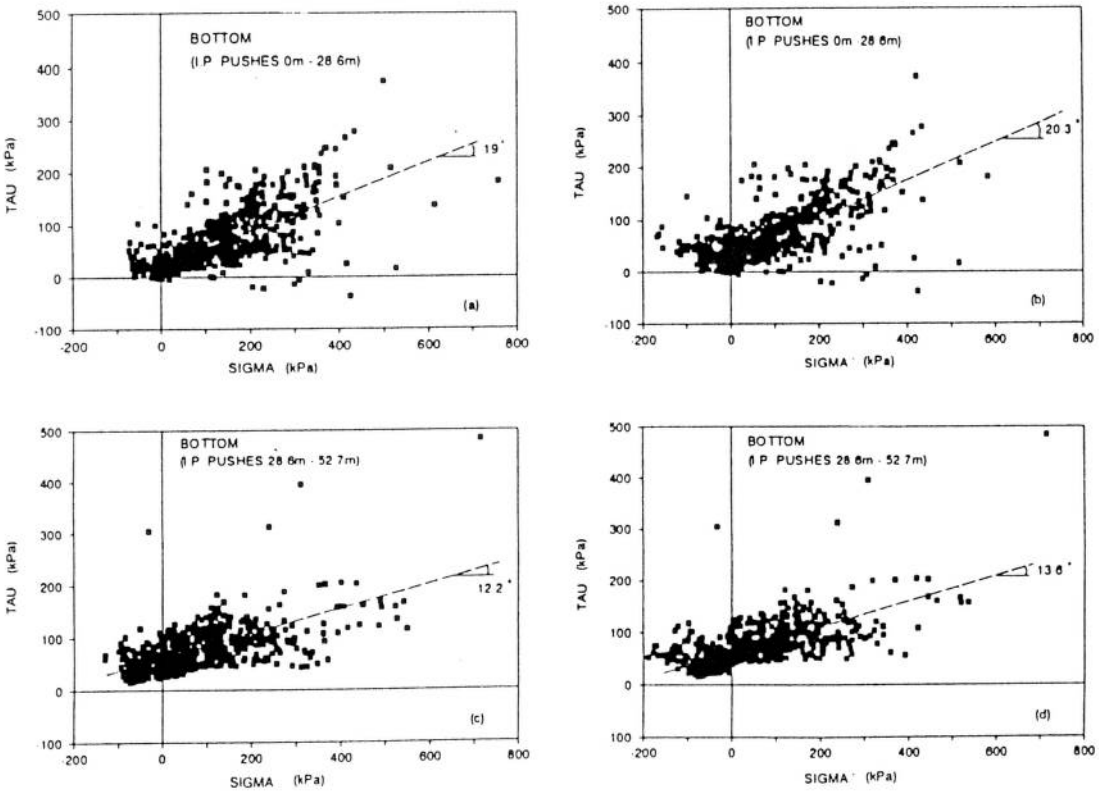

Figure 4.3 Shear stress/radial stress relations from scheme 1; total and effective stress responses prior to heavy rain (a & b), and after wetting (c & d) (Norris 1992b)

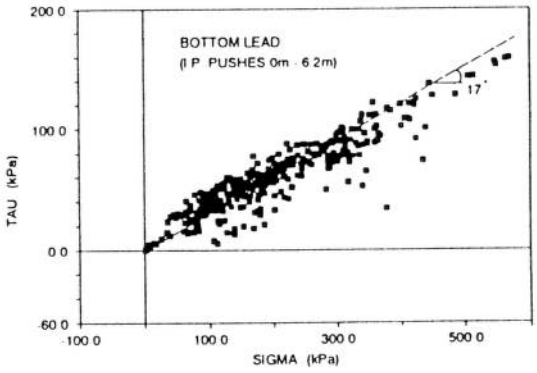

Figure 4.4 Shear stress/total radial stress relation from scheme 2 (Norris 1992b)

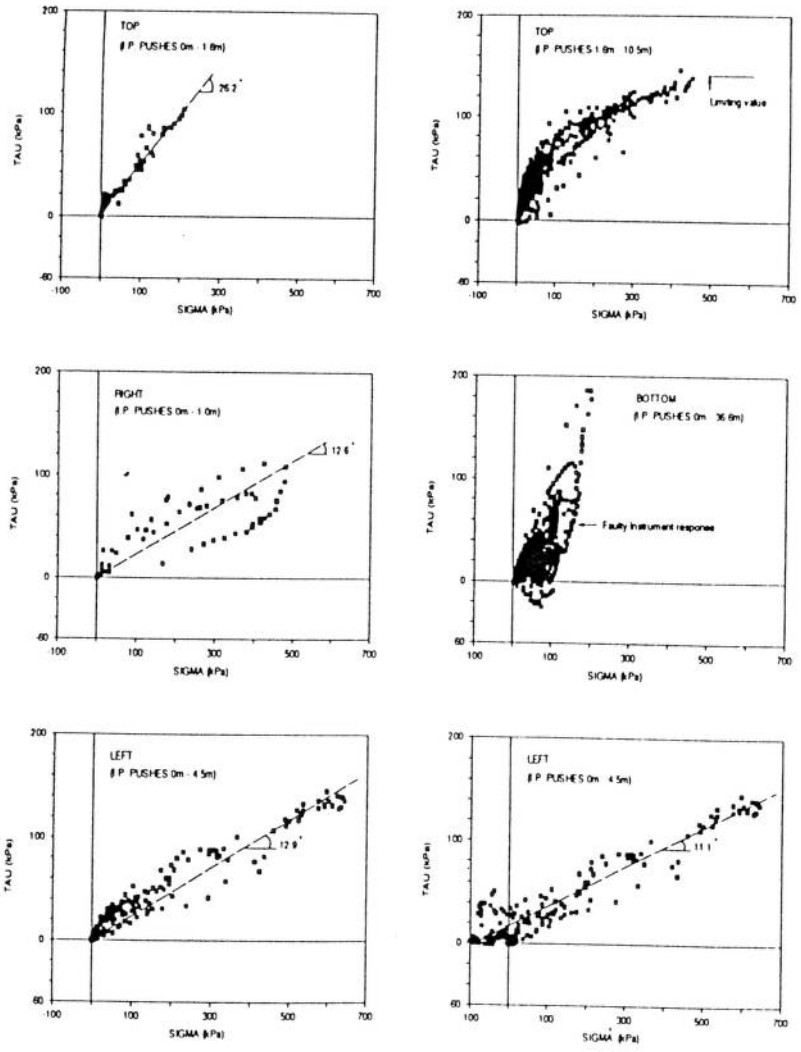

Figure 4.5 Shear stress/radial stress relations from scheme 3 (Norris 1992b)

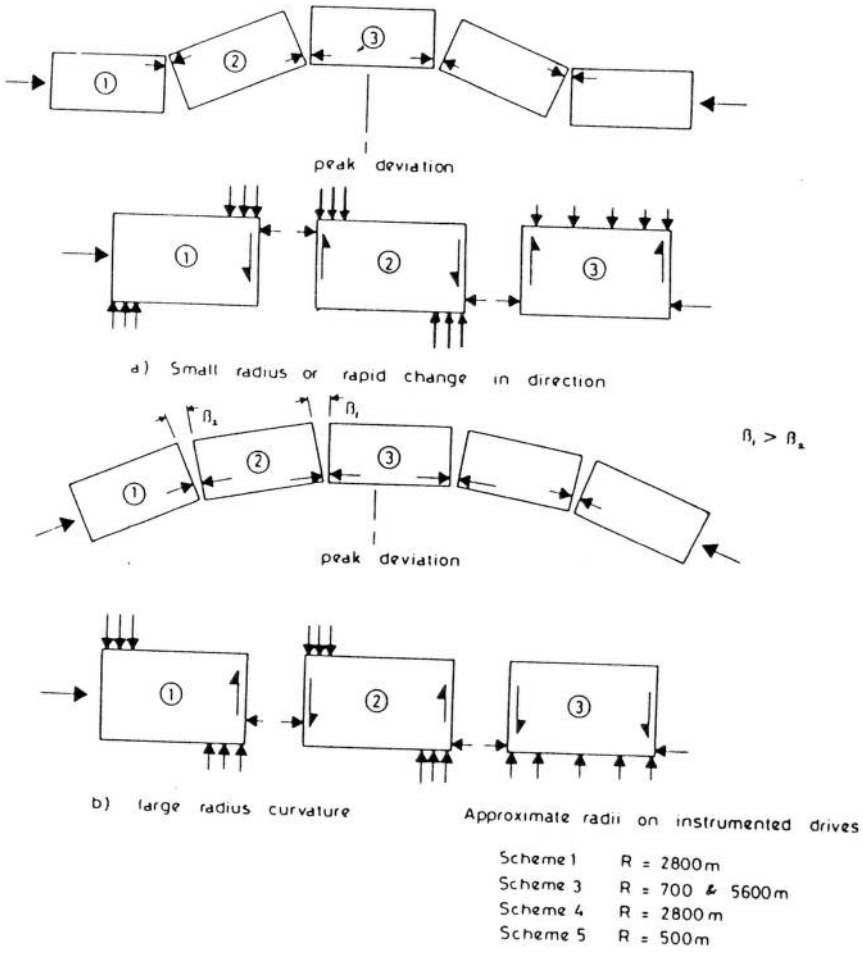

Figure 4.6 Theoretical misalignment forces (Norris 1992b)

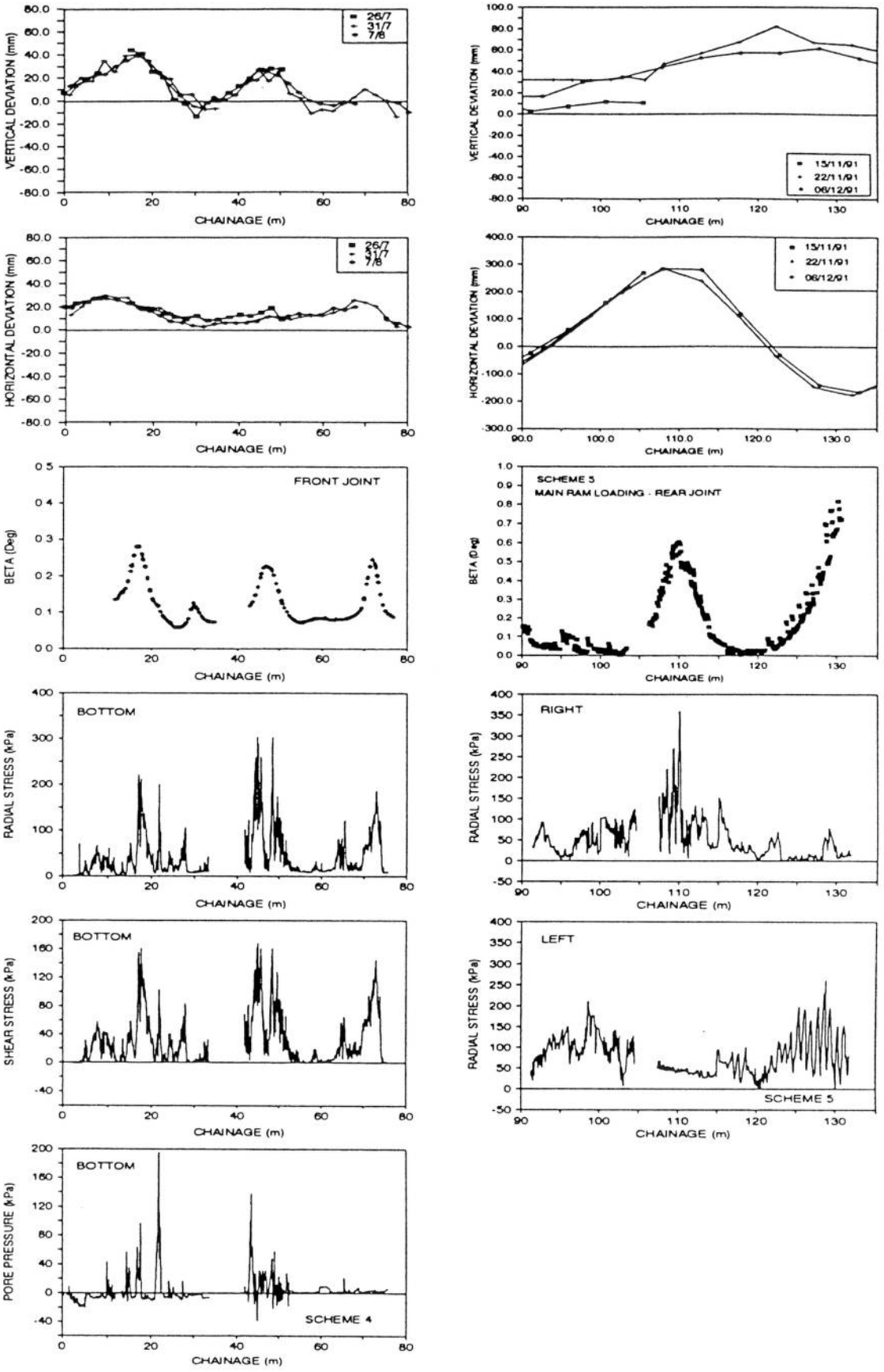

Figure 4.7 Comparison of tunnel alignment data and local interface stresses (Norris 1992b)

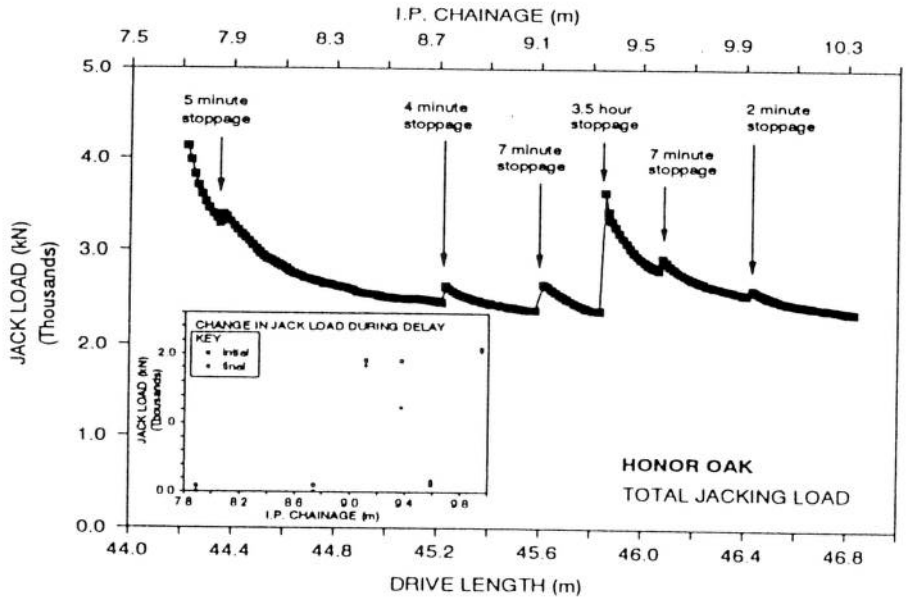

Figure 4.8 Changes in jacking load during stoppages on scheme 3 (Norris 1992b)

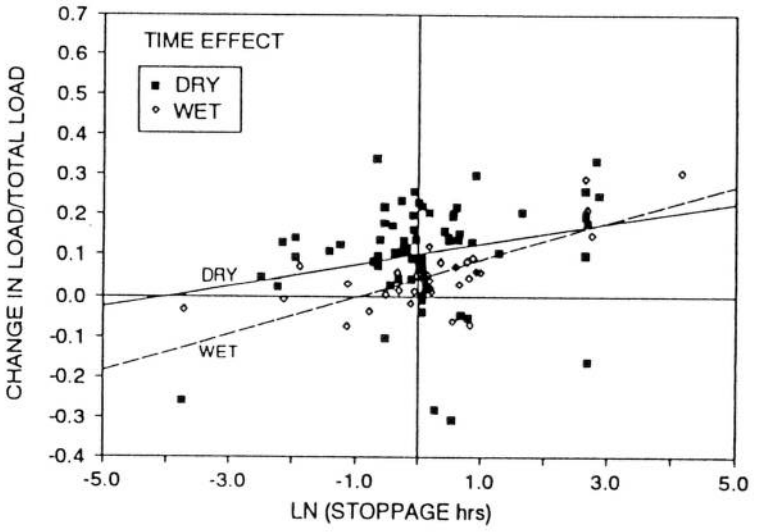

b) Scheme 1

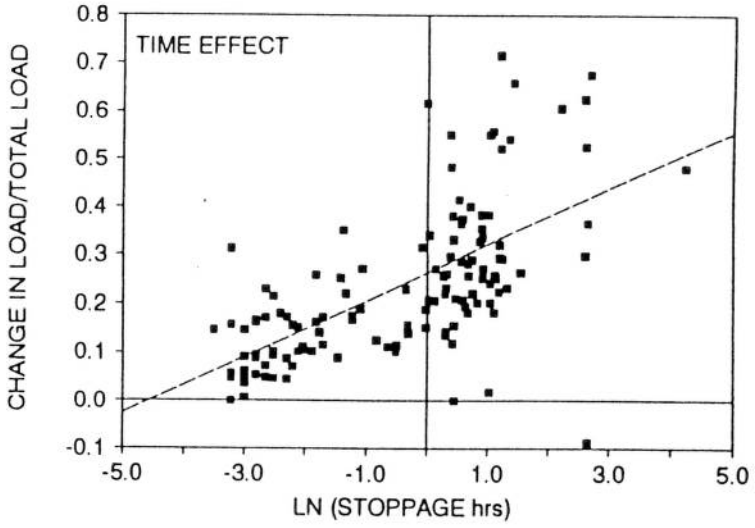

a) Scheme 3

Figure 4.9 Time factors for schemes 1 & 3 (Norris 1992b)

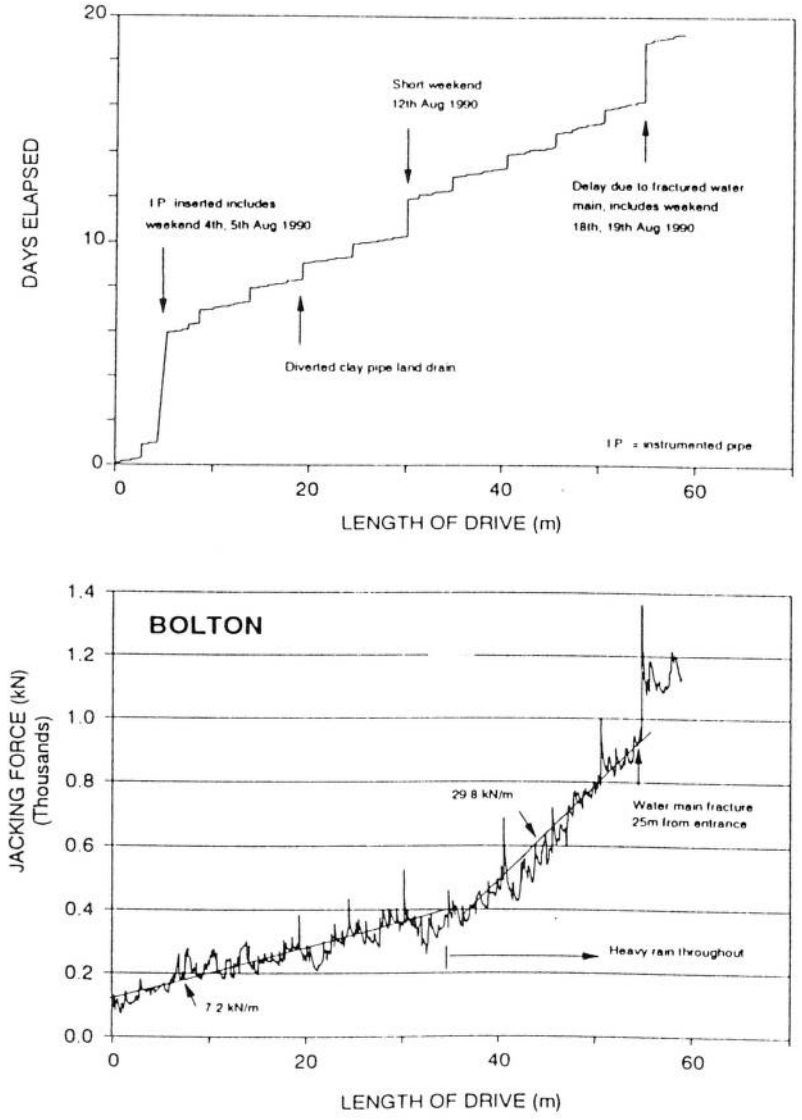

Figure 5.1 Jacking records for scheme 1 (Norris 1992b)

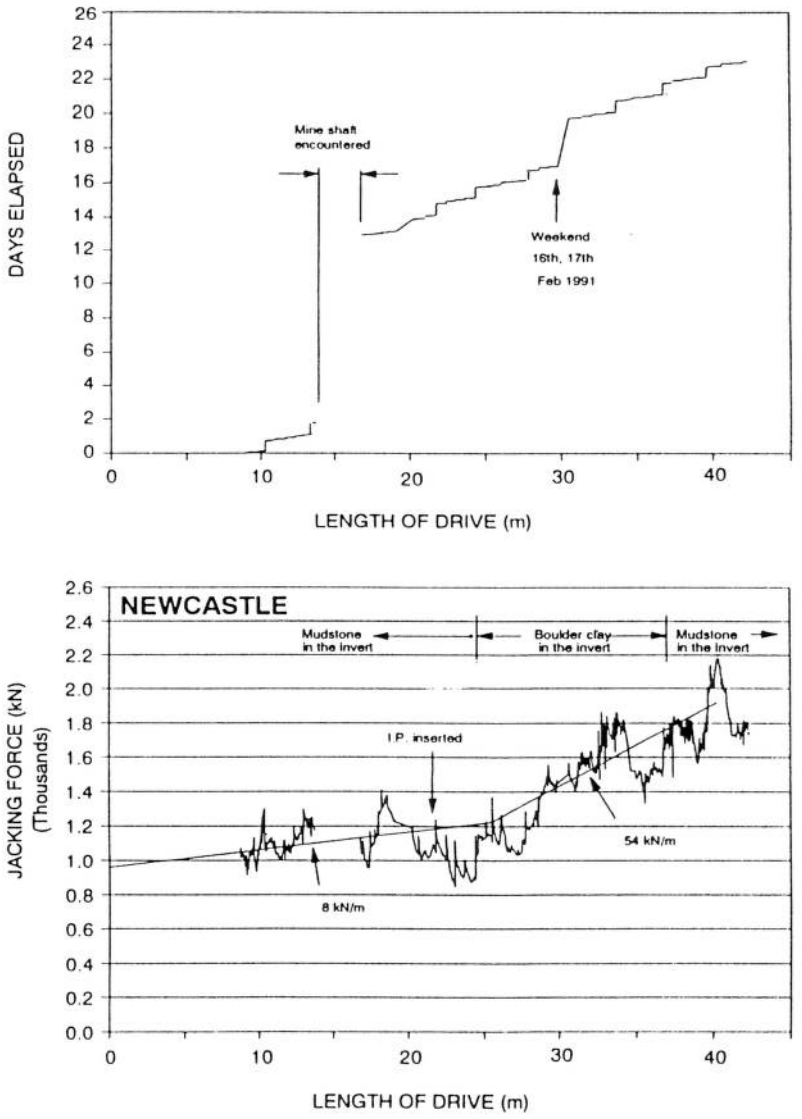

Figure 5.2 Jacking records for scheme 2 (Norris 1992b)

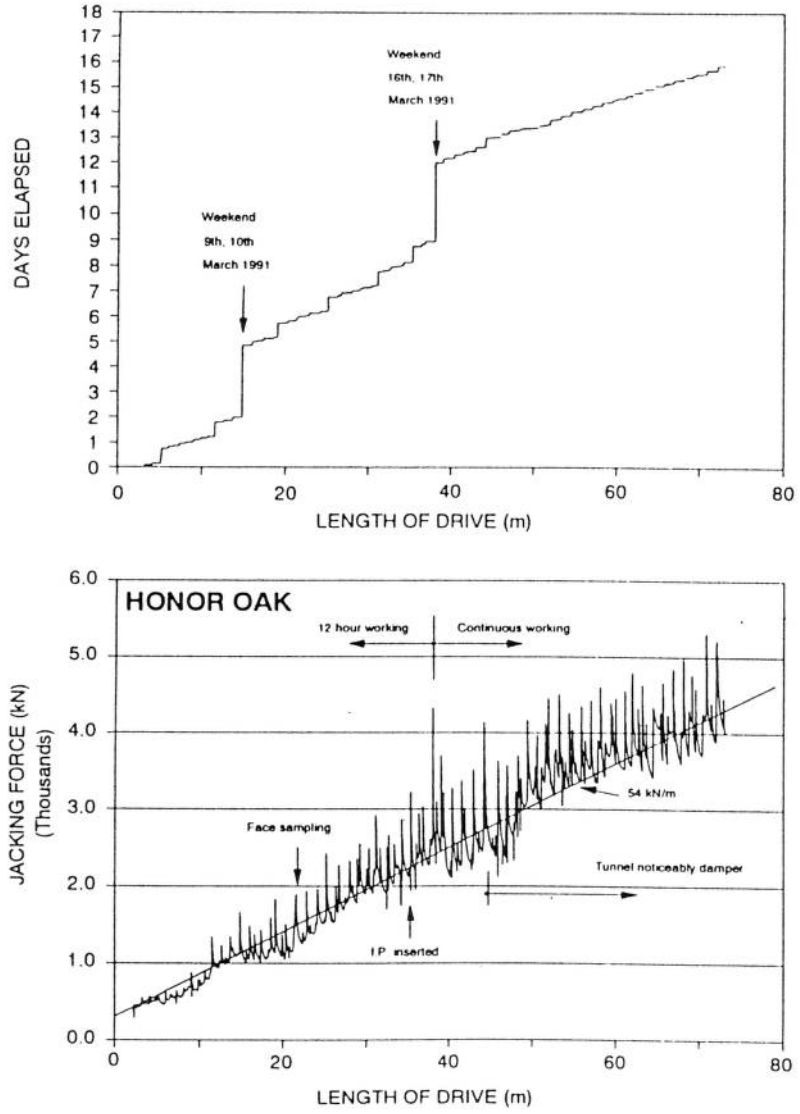

Figure 5.3 Jacking records for scheme 3 (Norris 1992b)

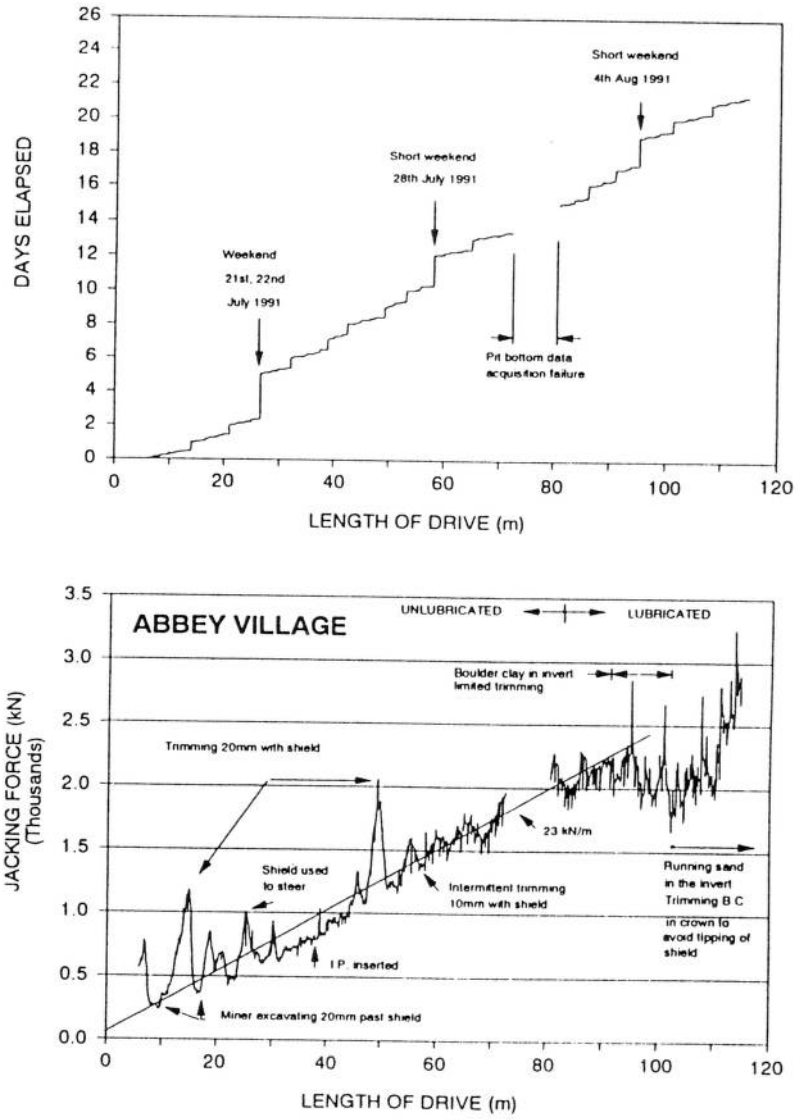

Figure 5.4 Jacking records for scheme 4 (Norris 1992b)

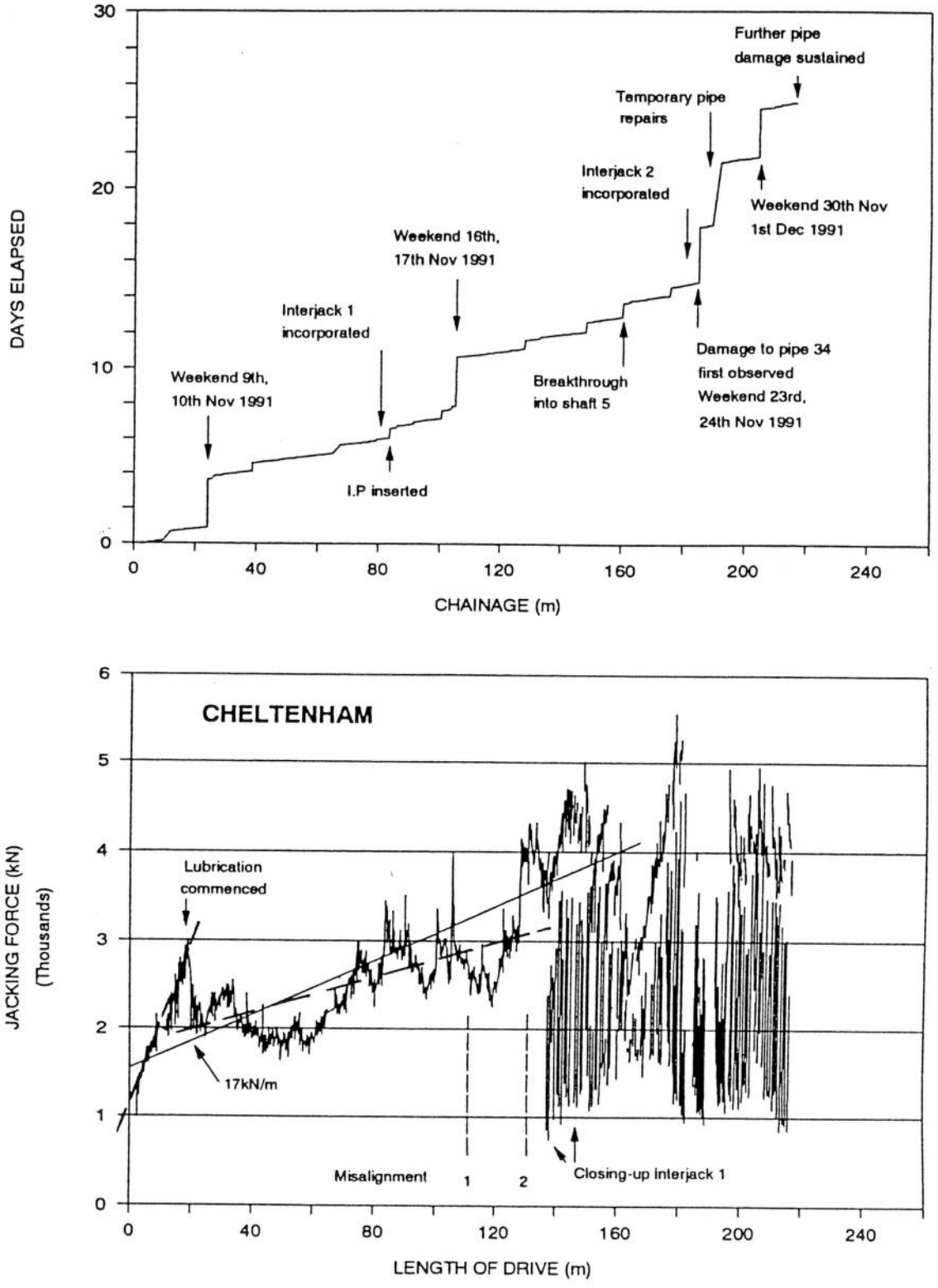

Figure 5.5 Jacking records for scheme 5 (Norris 1992b)

Cohesive with a stable bore
Haslem (1986)

$F = \alpha.s_u\ b$

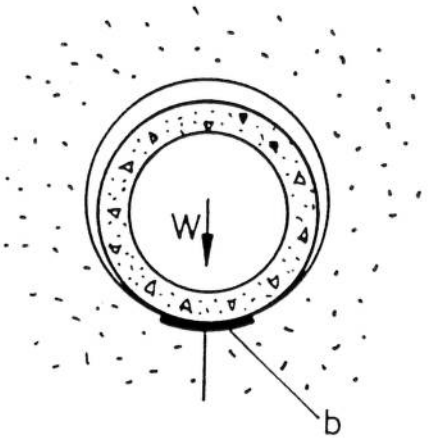

where $\alpha.s_u$ is the "adhesion" between the pipe and clay.
b is the contact width.

$b = 1.6(Pu*kd*Ce)^{1/2}$

where
Pu = contact force per unit length
$kd = D_1*D_2/(D_1-D_2)$
D_1 = internal diameter of the cavity
D_2 = external diameter of the pipe
$Ce = (1-n_1^2)/E_1+(1-n_2^2)/E_2$
E_1 = elastic modulus of the soil
E_2 = elastic modulus of the concrete pipe
n = Poisson's ratios as for E

Scheme	γ	h	E_1	E_2	n_1	n_2	P_u	D_1	D_2
	(kN/m^3)	(m)	(MPa)	(GPa)			(kN/m)	(m)	(m)
1	22	1.5	48	40	0.2	0.2	17.7	1.554	1.530
2	22	11	120	40	0.2	0.2	23.0	1.724	1.700
3	21	16av	96	40	0.2	0.2	35.3	2.304	2.280
4	18	7	144	40	0.2	0.2	24.2	1.804	1.780
5	19	6	144	40	0.2	0.2	-2.2*	1.450	1.430

For scheme 1, b = 0.30m and, from Figure 4.3c, $\alpha.s_u$ = 80kPa approximately.

Then $F = \alpha.s_u.b$ = 24kN/m, compared with a measured value of 29.8kN/m.

Figure 5.6 Model for ground loading in cohesive soil, after Haslem (1986)

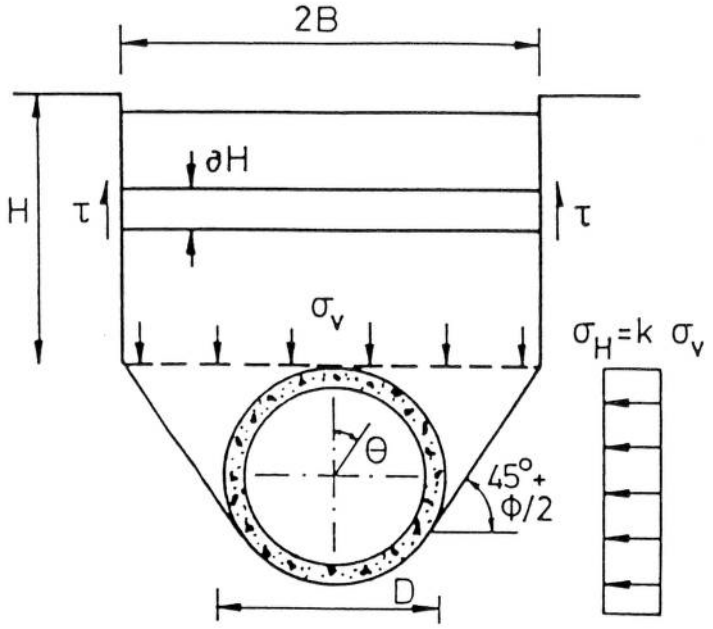

$$\sigma_v = \frac{\gamma . B}{k.\tan\phi}(1 - e^{-k.\tan\phi . H/B})$$

$$\sigma_h = k(\sigma_v + 0.5\gamma . D)$$

The radial stress around the pipe is

$$\sigma_p = \frac{(\sigma_v + \sigma_h)}{2} + \frac{(\sigma_v - \sigma_h)}{2}\cos 2\theta$$

and the total frictional resistance is

$$F = \frac{\pi D}{2}(\sigma_v + \sigma_h).\tan\delta$$

where ϕ is the angle of internal friction of the soil, and
δ is the angle of friction between the pipe and the soil.

For scheme 5:-

$\phi = 32°$, D = 1.45m, B = 1.23m, H = 4.675m, γ =19 kN/m^3

Then k = (1 - sin ϕ)/(1 + sin ϕ) = 0.307

and total jacking force F = 104kN/m

taking $\delta = 0.87\phi$

In addition, weight of pipe is 11.9kN/m, giving friction due to selfweight = 6.3 kN/m

Total calculated frictional resistance is 110kN/m, compared with measured resistance of approximately 2000kN over first 20m, or 100kN/m.

Figure 5.7 Model for ground loading in cohesionless soil, after Auld (1982), Terzaghi (1943).

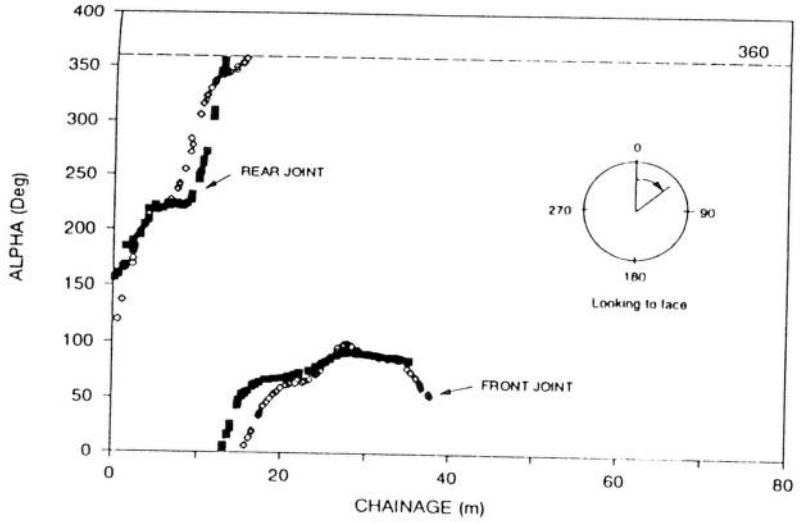

Comparison of the points of maximum compression in the front and rear joints at similar chainages throughout scheme 3.

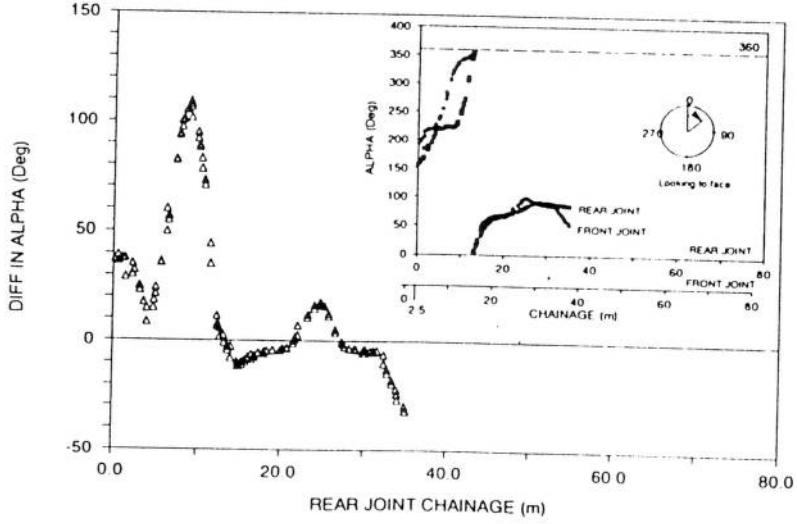

Figure 6.1 Angular difference between the front and rear points of maximum compression; scheme 3 (Norris 1992b)

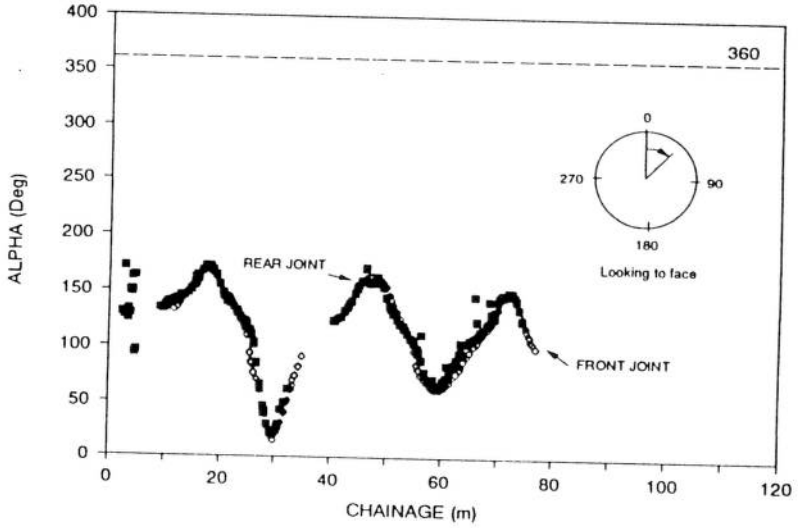

Comparison of the points of maximum compression in the front and rear joints at similar chainages throughout scheme 4.

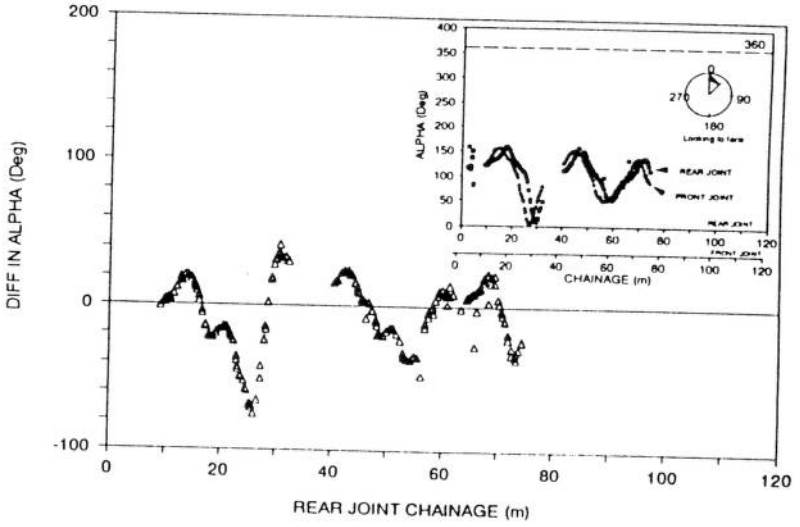

Figure 6.2 Angular difference between the front and rear points of maximum compression; scheme 4 (Norris 1992b)

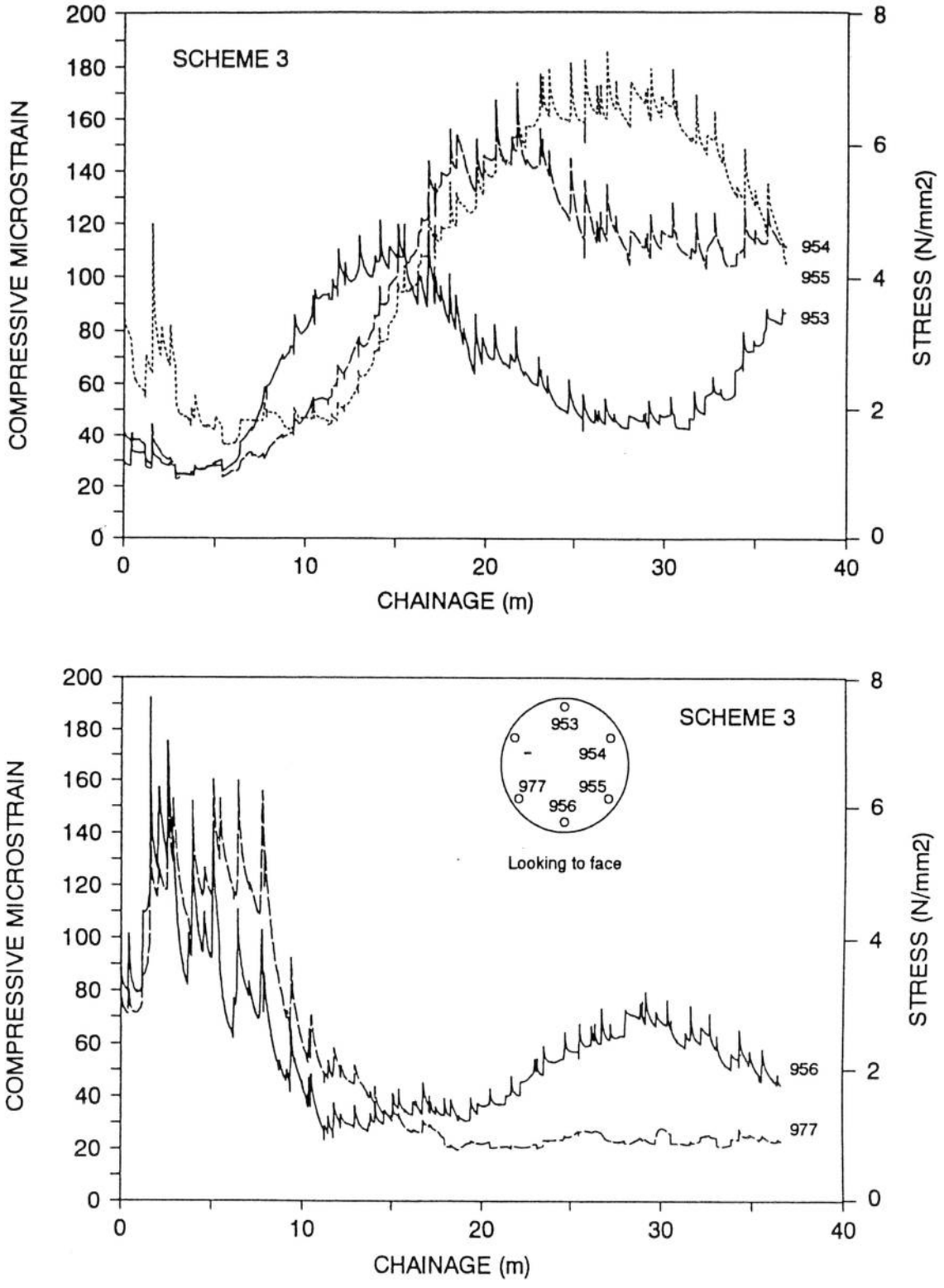

Figure 6.3 Average longitudinal pipe strains during jacking on scheme 3 (Norris 1992b)

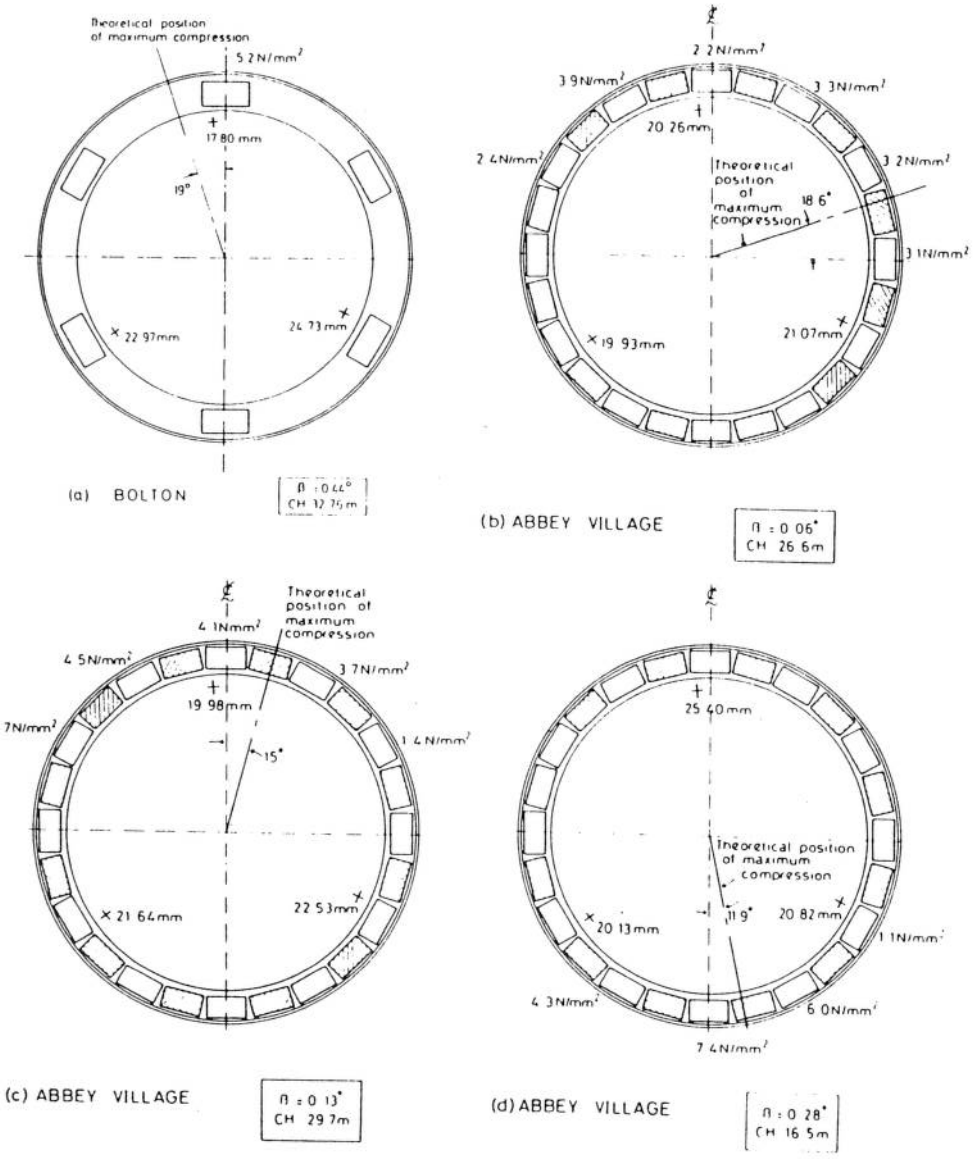

Figure 7.1 Relation between measured joint angle and pressure distribution; schemes 1 and 4 (Norris 1992b)

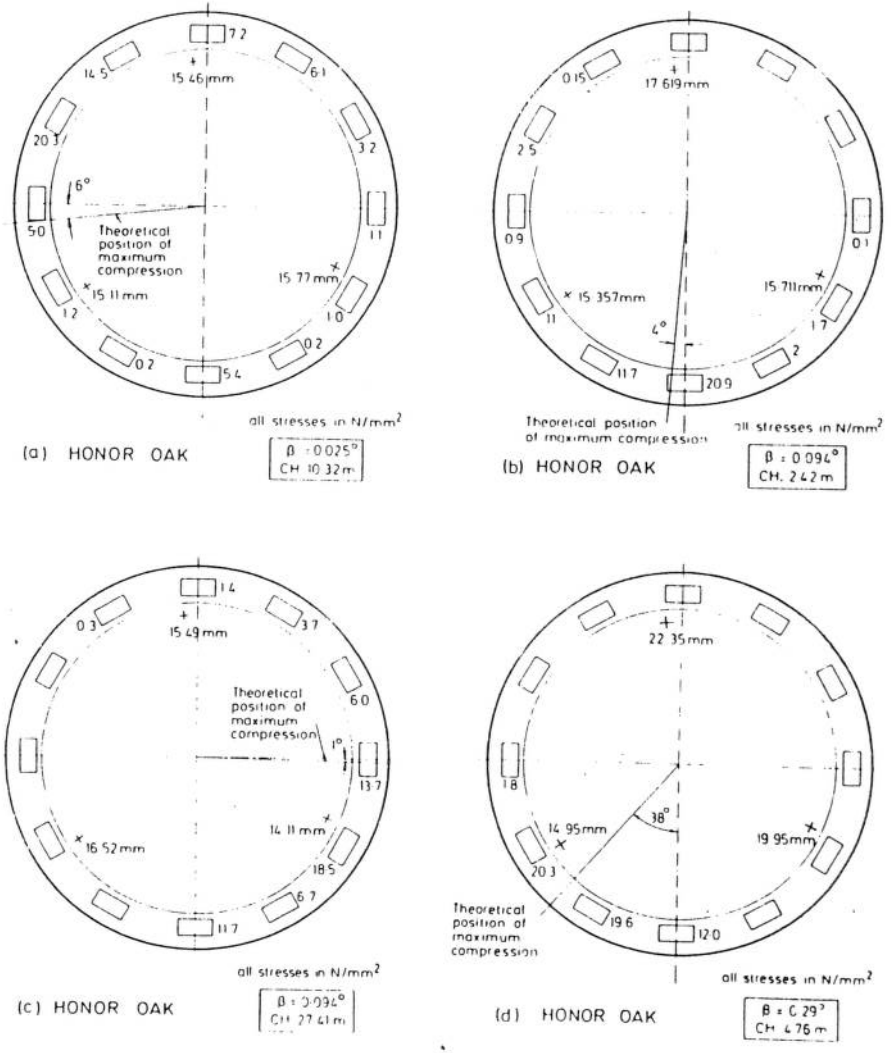

Figure 7.2 Relation between measured joint angle and pressure distribution; scheme 3 (Norris 1992b)

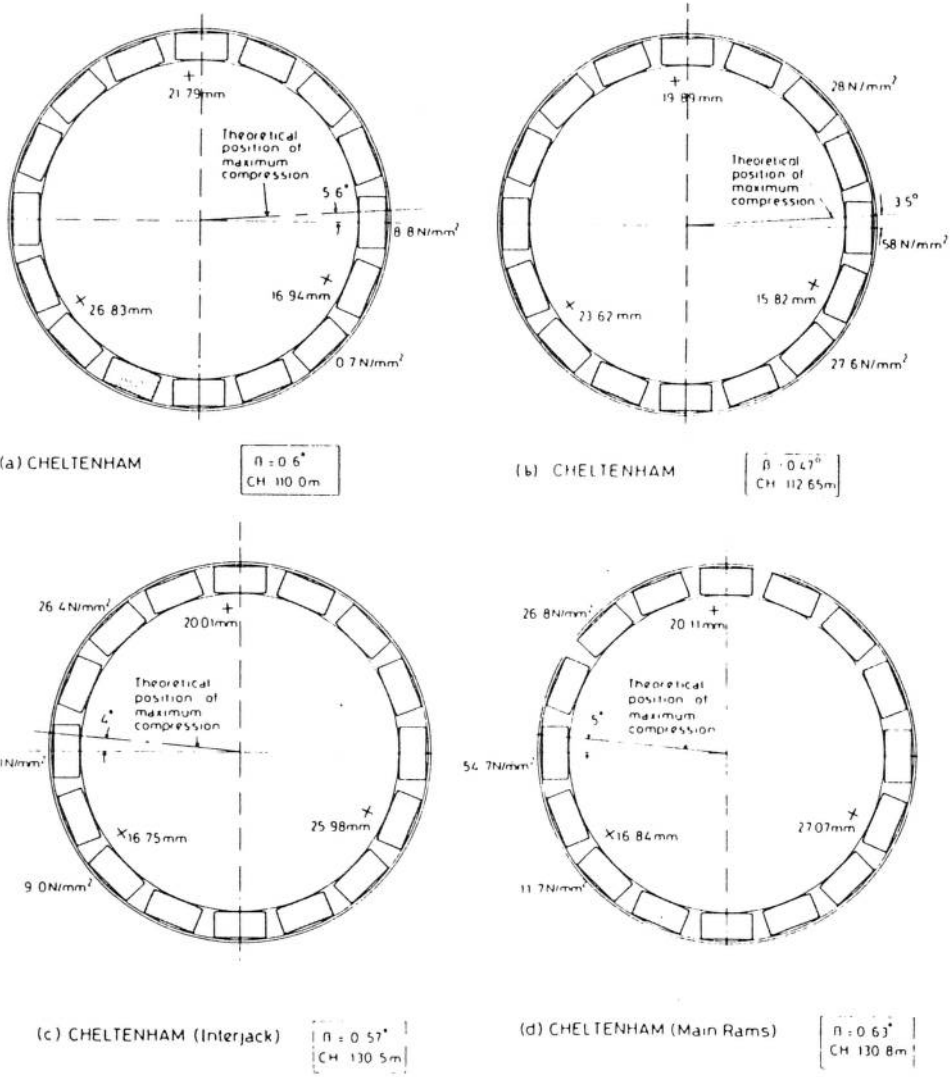

Figure 7.3 Relation between measured joint angle and pressure distribution; scheme 5 (Norris 1992b)

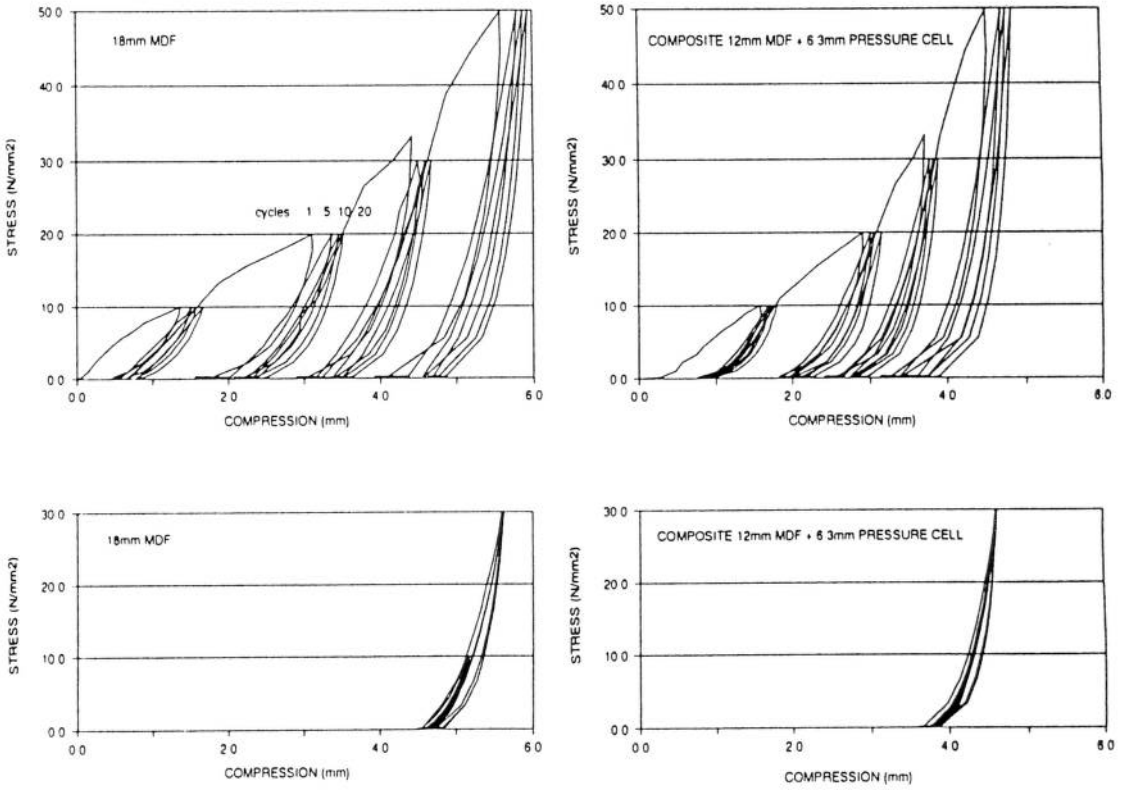

Figure 7.4 Uniaxial compression tests on joint packer material (Norris 1992b)

From the Australian Concrete Pipe association linear stress approach

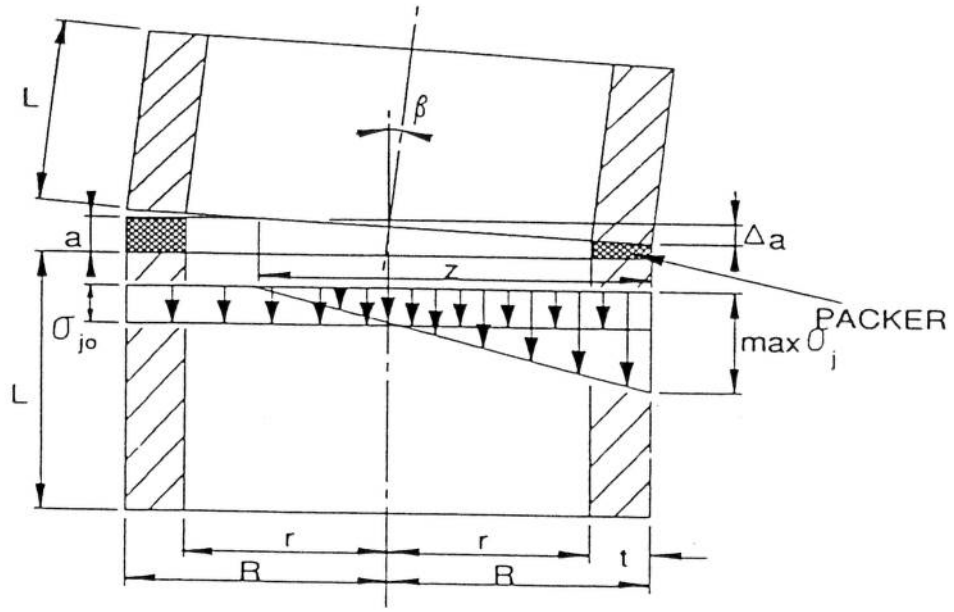

$$z = \frac{180}{\pi} \frac{a}{E_p} \frac{\max \sigma_j}{\beta}$$

Total force over hatched area for linear distribution of stress

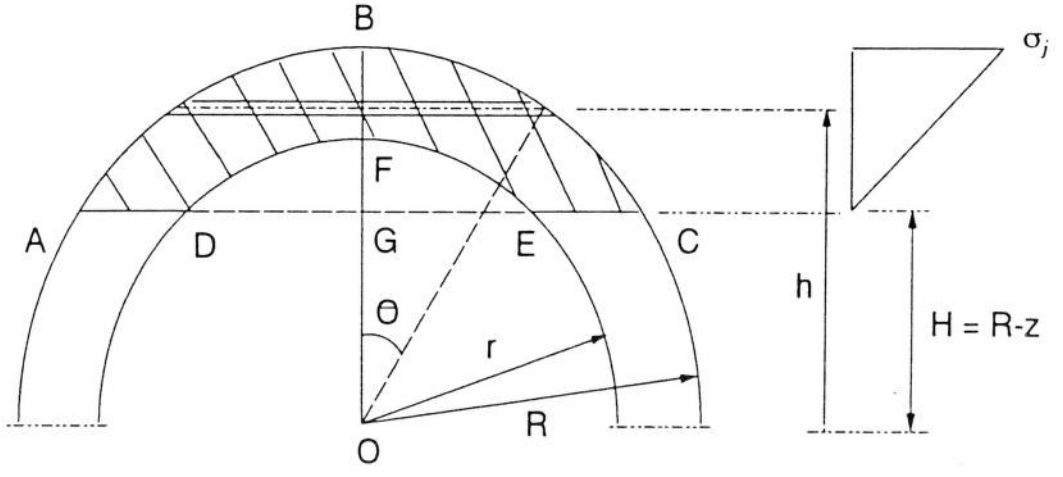

When H > r $F_{permissible}$ =

$$\frac{\sigma_j}{(R-H)} \left\{ 2/3[\,(R^2-H^2)^{3/2}\,] - H\left[R^2 \cos^{-1}\left(\frac{H}{R}\right) \right] + H^2 (R^2-H^2)^{1/2} \right\}$$

Figure 7.5 Jacking forces from linear joint stress model (Norris 1992b)

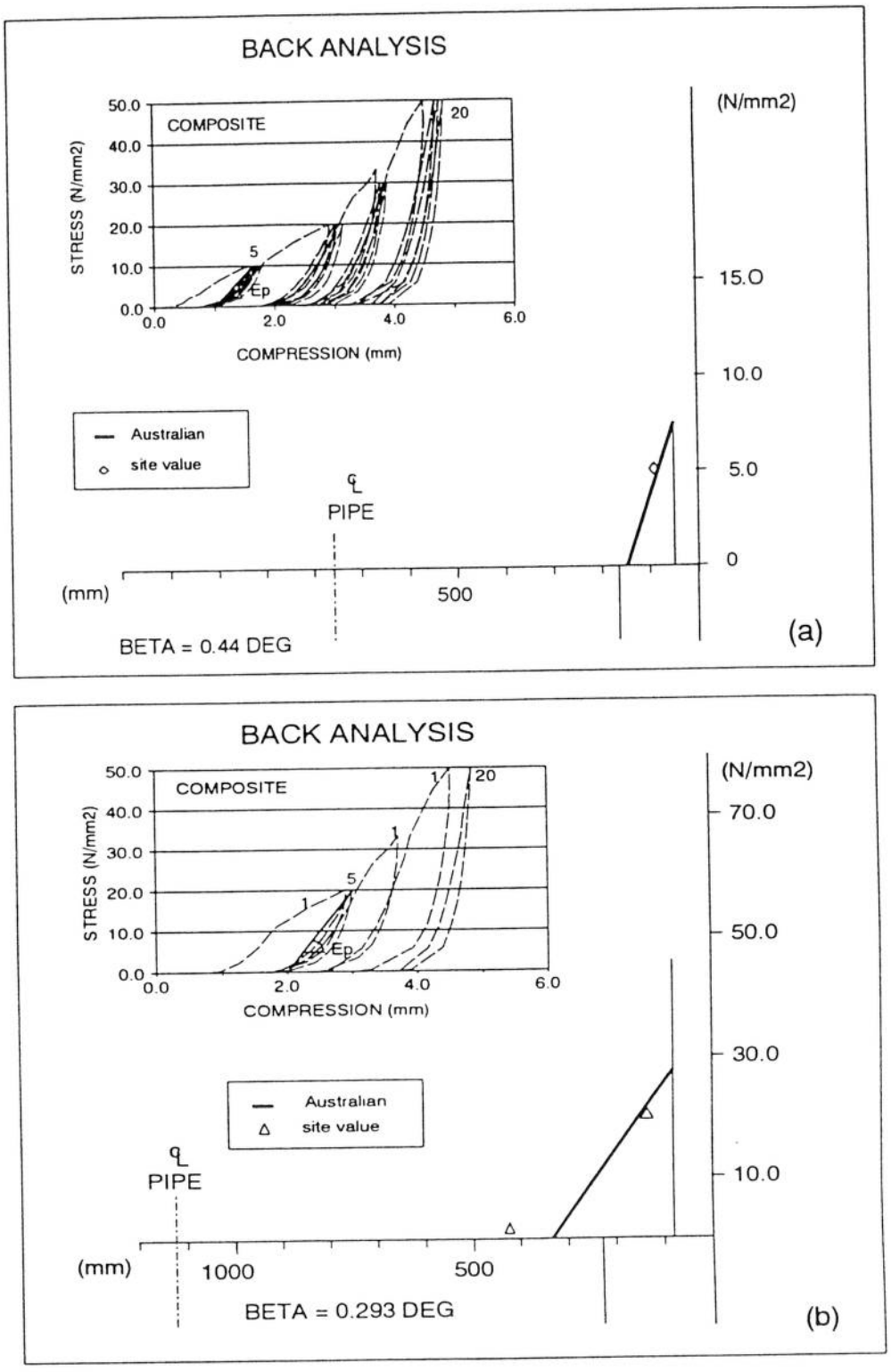

Figure 7.6 Comparison of measured joint stress distribution to predicted using a linear stress model based on the Australian Concrete Pipe Association method. (a) scheme 1 rear joint subject to a β value of 0.44°, and (b) scheme 3 rear joint subject to a β value of 0.29°.

(Norris 1992b)

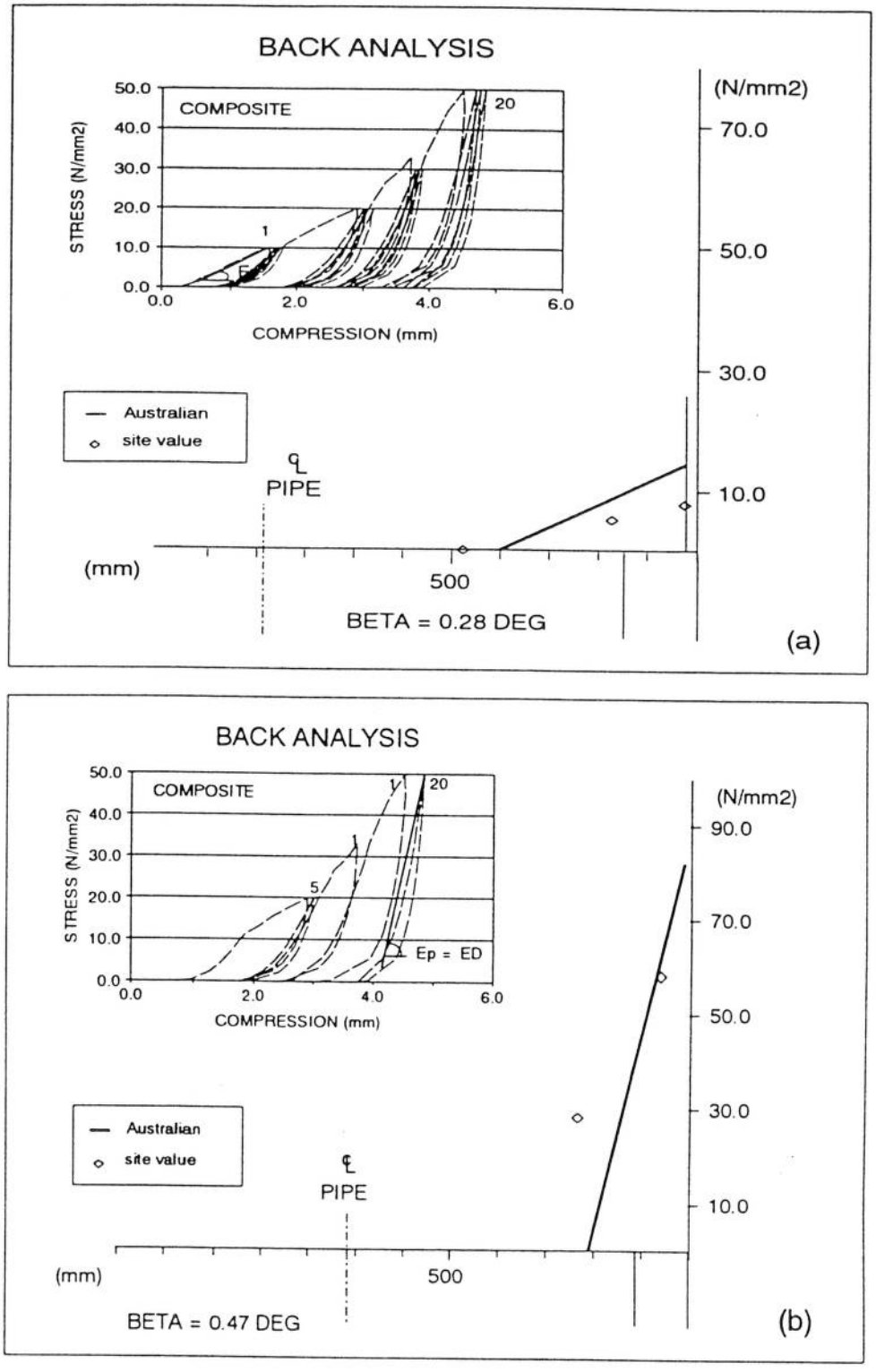

Figure 7.7 Comparison of measured joint stress distribution to predicted using a linear stress model based on the Australian Concrete Pipe Association method. (a) scheme 4 rear joint subject to a β value of 0.28°, and (b) scheme 5 rear joint subject to a β value of 0.47° and pipe damage.

(Norris 1992b)

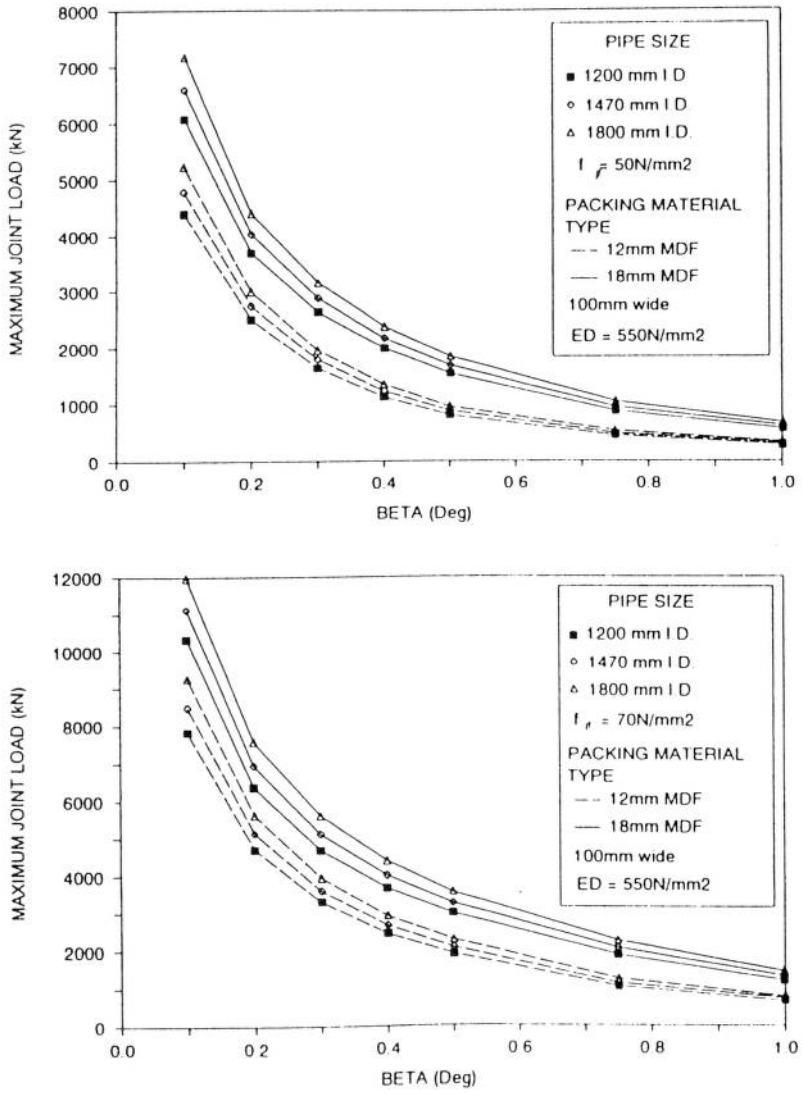

Figure 7.8 Permissible pipe end loading at various angular misalignments; 100mm wide medium density fibreboard (Norris 1992b)

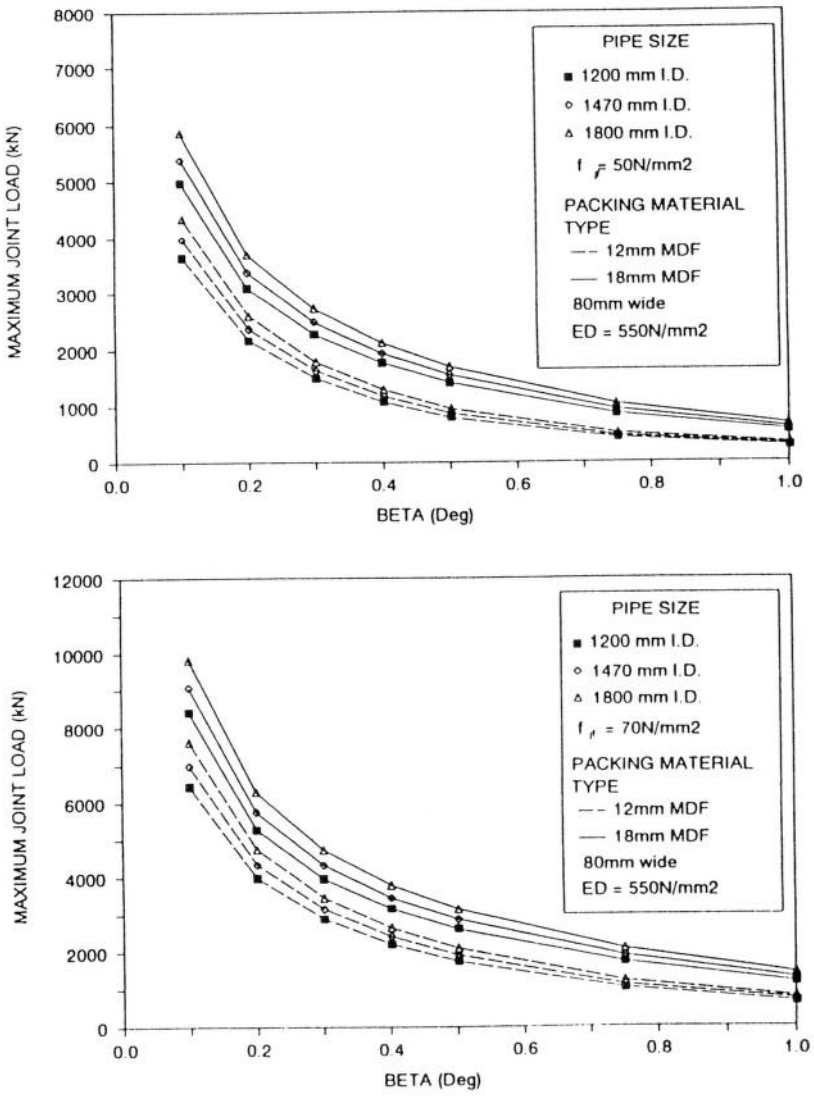

Figure 7.9 Permissible pipe end loading at various angular misalignments; 80mm wide medium density fibreboard (Norris 1992b)

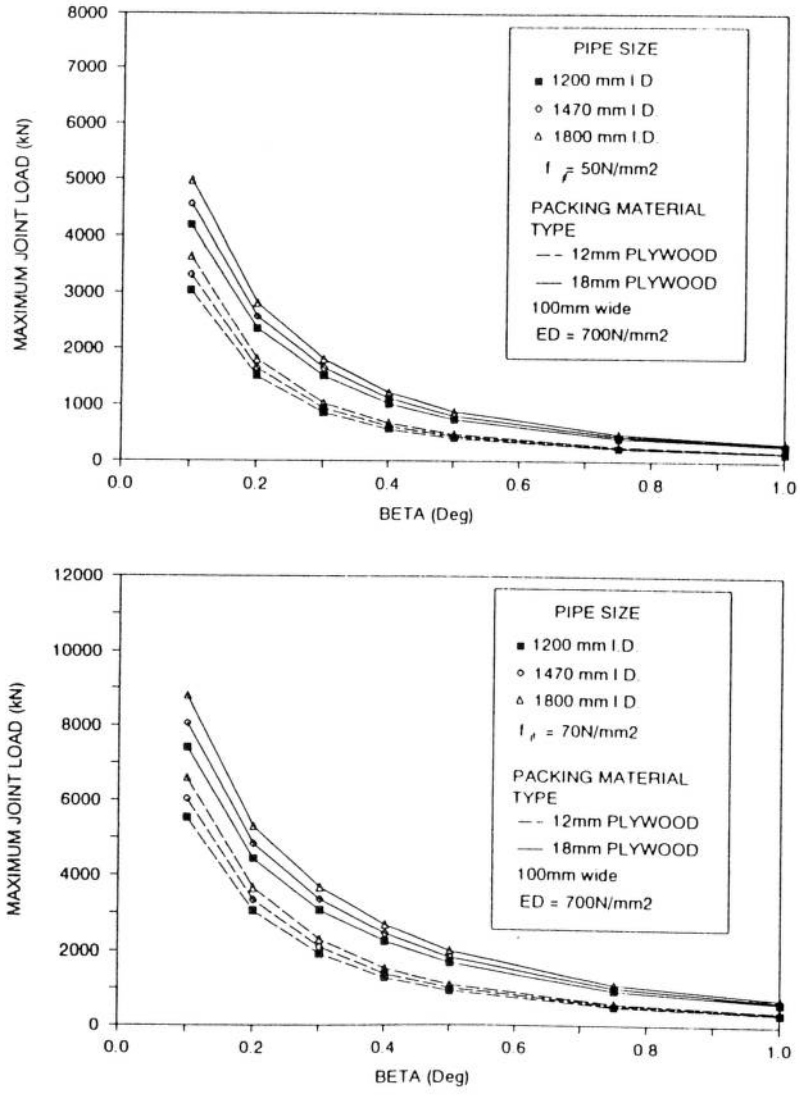

Figure 7.10 Permissible pipe end loading at various angular misalignments; 100mm wide exterior grade plywood (Norris 1992b)

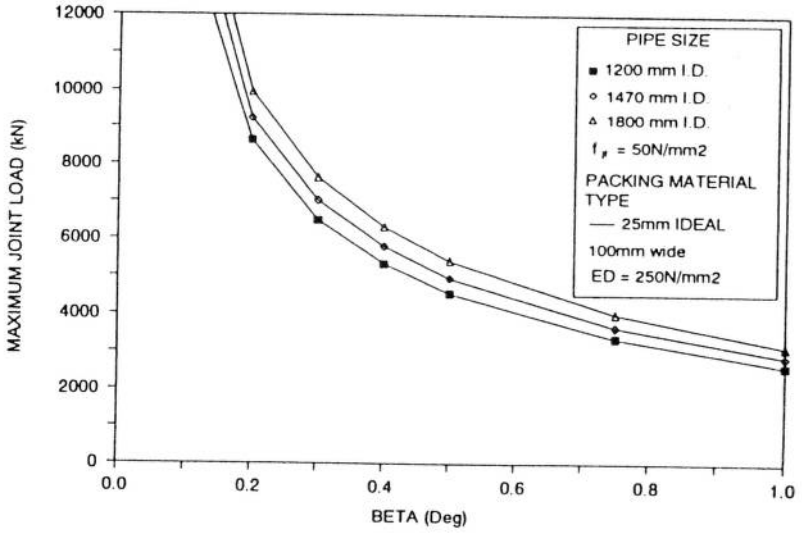

Figure 7.11 Permissible pipe end loading at various angular misalignments; 100mm wide idealised packing material (Norris 1992b)

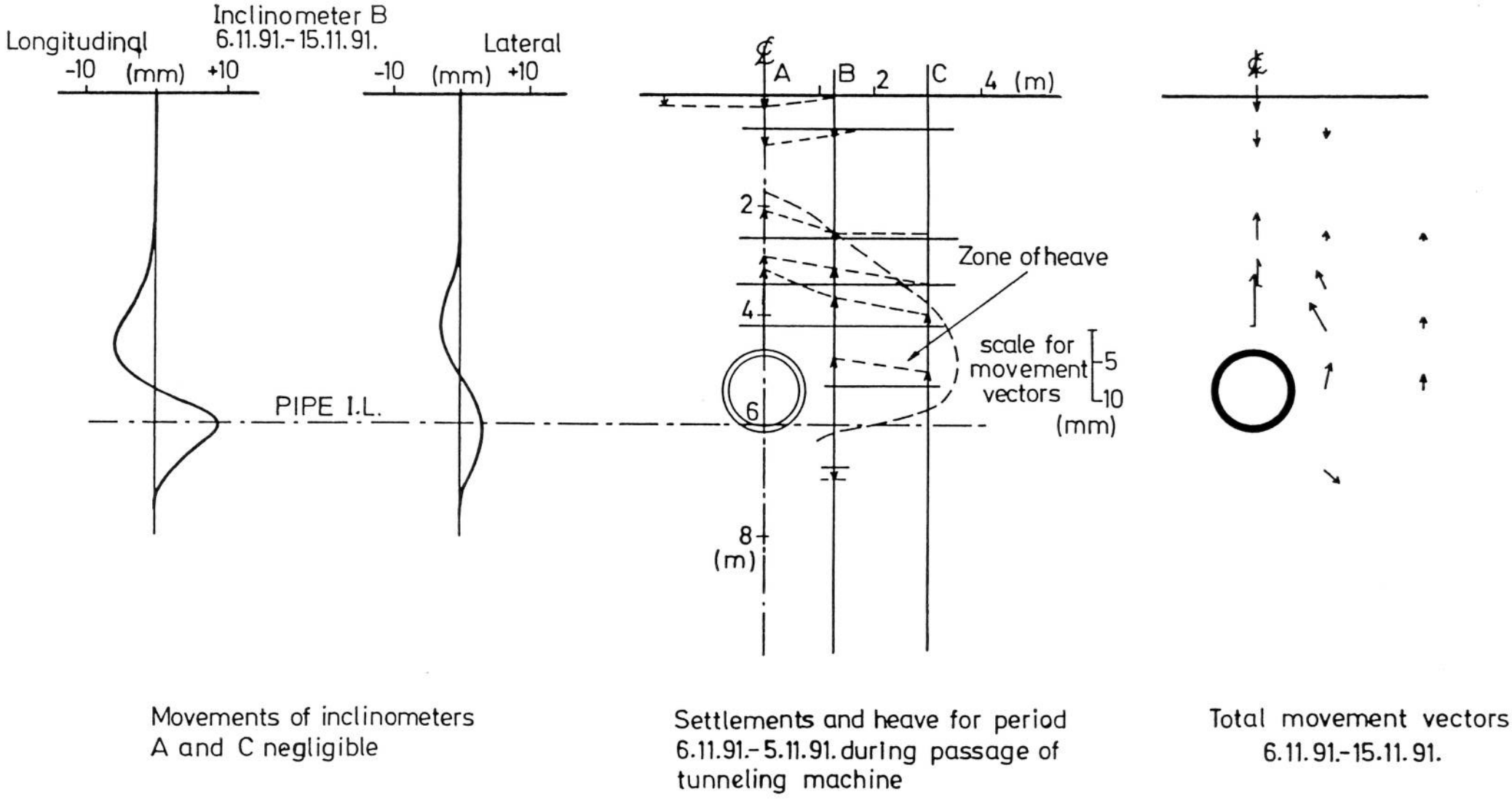

Movements of inclinometers
A and C negligible

Settlements and heave for period
6.11.91.-5.11.91. during passage of
tunneling machine

Total movement vectors
6.11.91.-15.11.91.

Figure 8.1 Measured ground movements due to passage of tunnelling machine; scheme 5

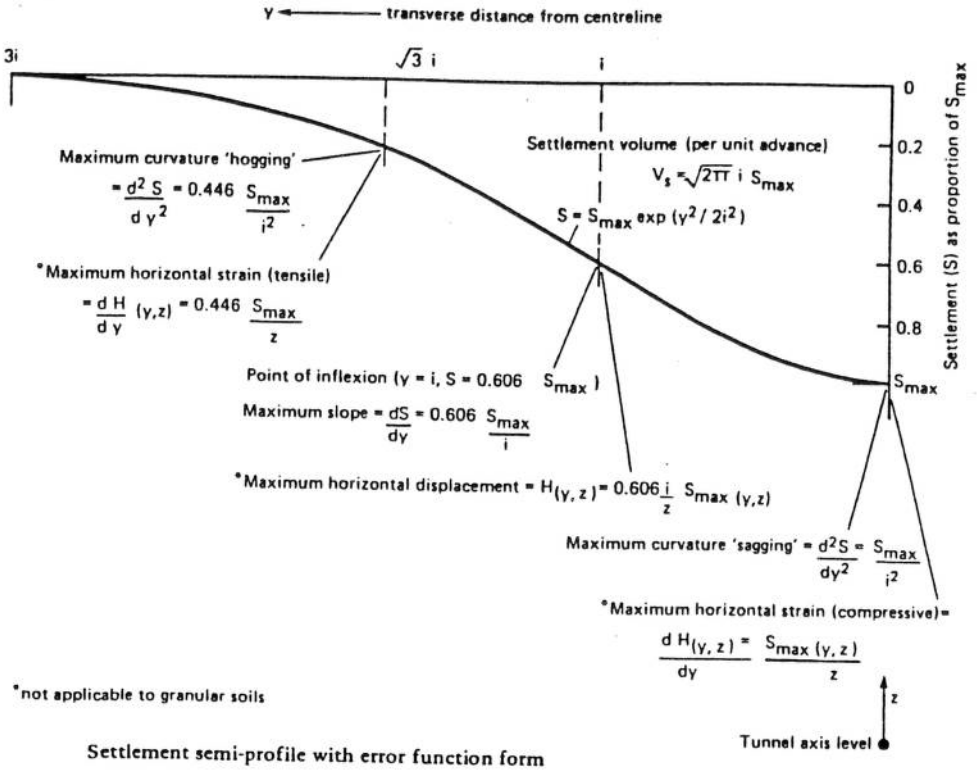

Settlement semi-profile with error function form

From O'Reilly and New (1982)

Surface settlement s is given by

$$s = s_{max} . e^{-y^2/2i^2} = \frac{V_s}{\sqrt{2\pi}.i} . e^{-y^2/2i^2}$$

where V_s = volume loss/unit length.

For scheme 5 instrumented section
depth to tunnel axis z = 5.4m
from plot b) i = 1.4m

Volume of overbreak

$$V_s = \frac{\pi}{4}(1.45^2 - 1.43^2) = 0.045 m^3/m$$

giving s_{max} = 12.8 mm

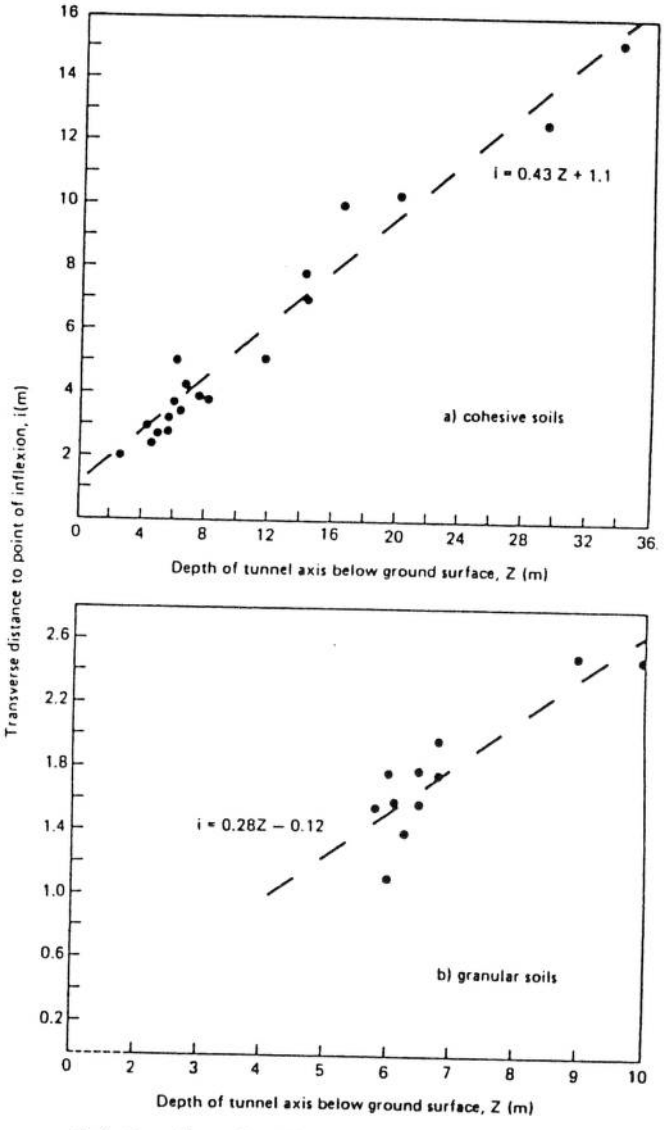

Variation of trough width parameter, i, with tunnel depth

Figure 8.2 Calculation of long-term settlements

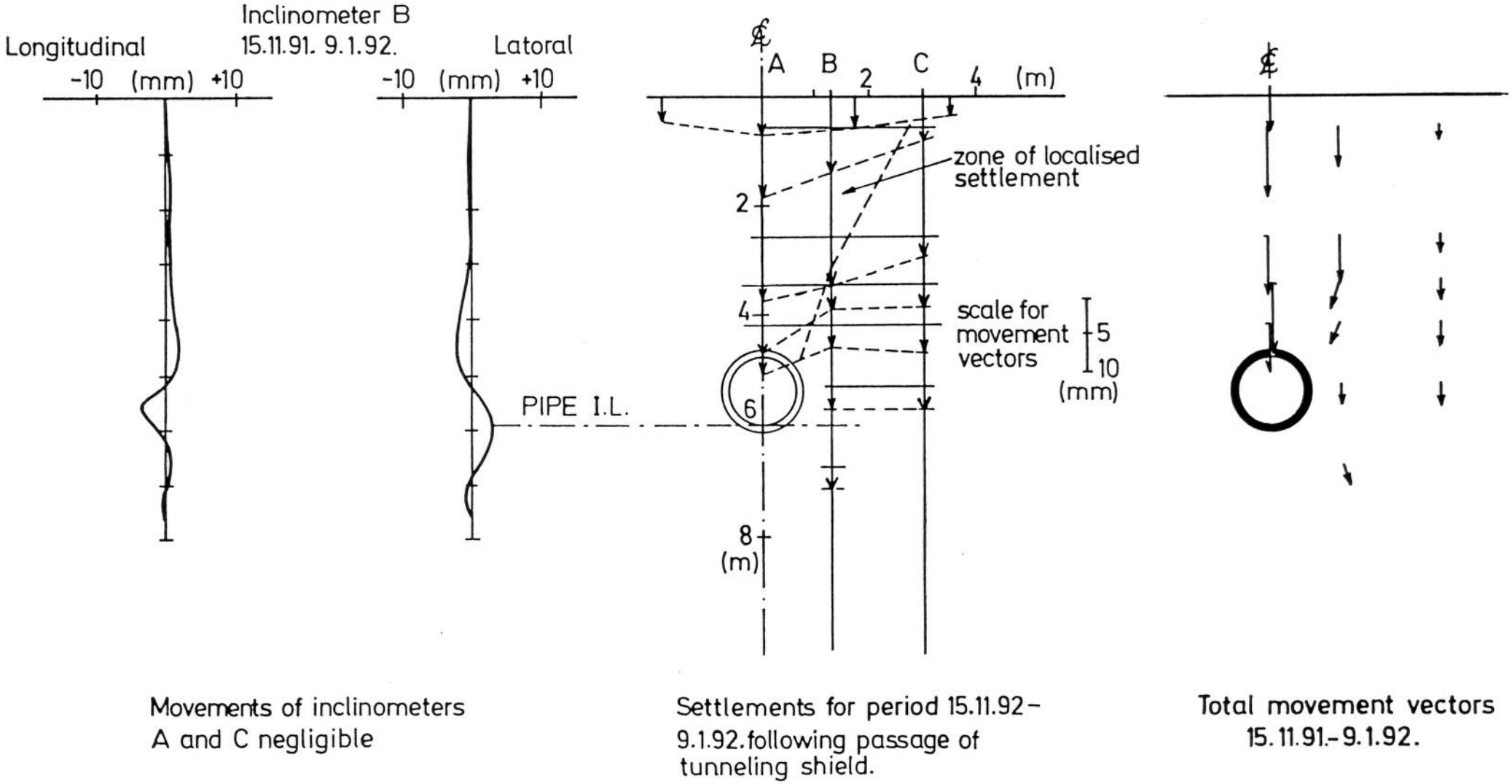

Movements of inclinometers A and C negligible

Settlements for period 15.11.92 – 9.1.92. following passage of tunneling shield.

Total movement vectors 15.11.91.–9.1.92.

Figure 8.3 Measured long-term settlements; scheme 5

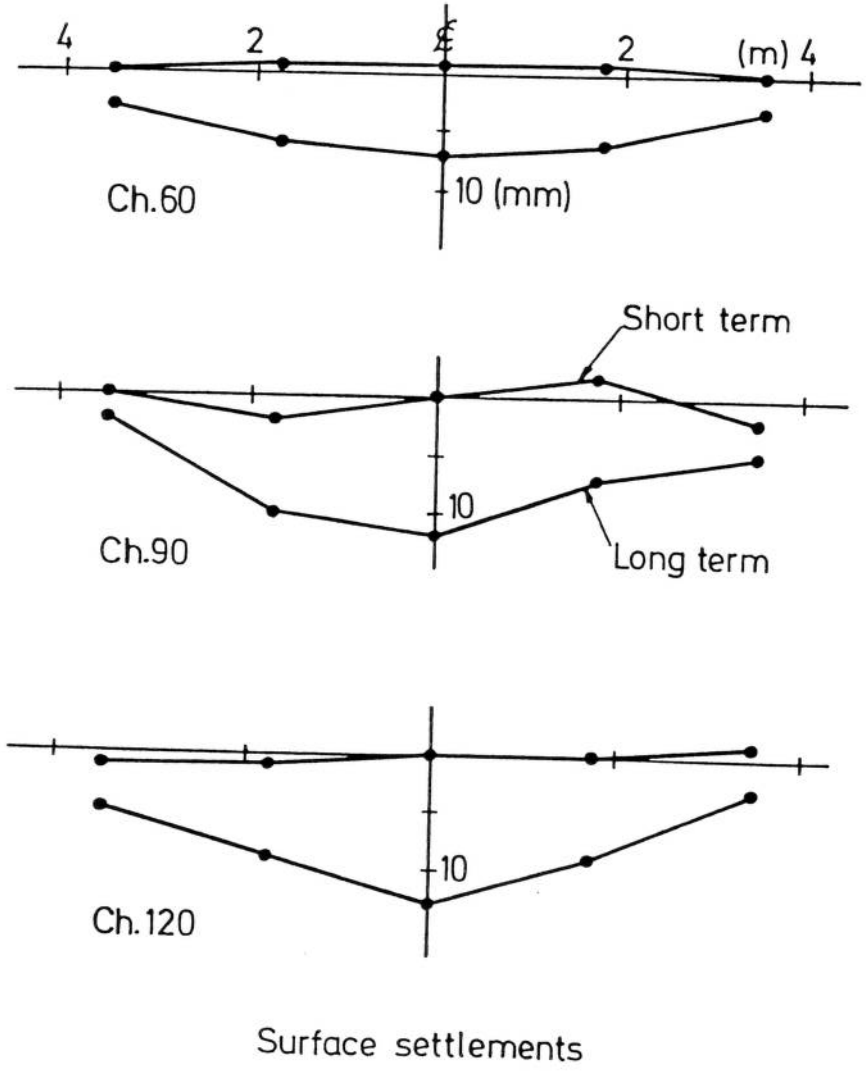

Figure 8.4 Measured surface settlements at three cross-sections; scheme 5

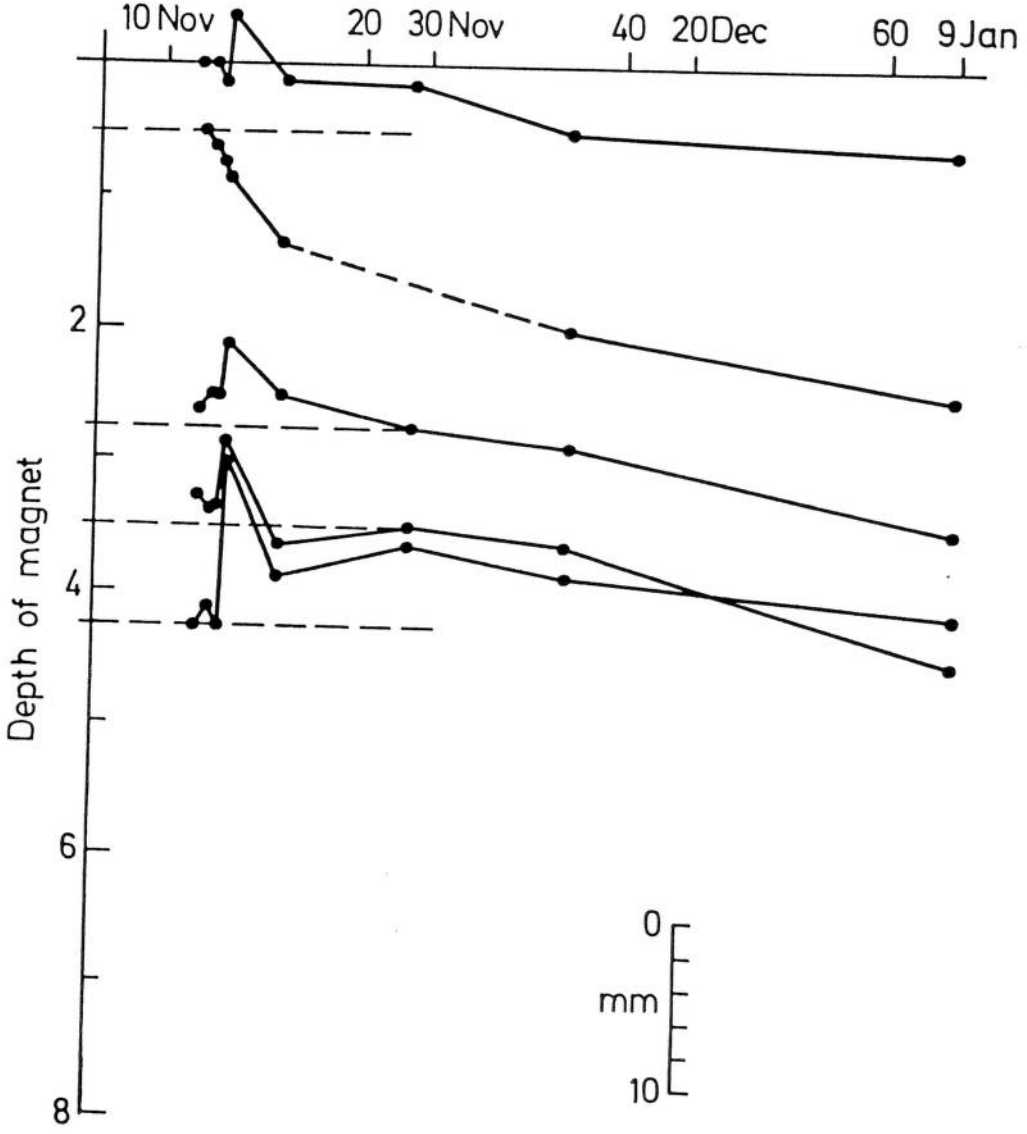

Figure 8.5 Variations with time of ground movements on tunnel centreline; scheme 5

PIPE JACKING - RESEARCH RESULTS AND RECOMMENDATIONS: **Additional notes**

George Milligan, Mark Marshall and Paul Norris

S1. Introduction

These notes have been written as a supplement to the report Pipe Jacking - **Research Results and Recommendations** by Milligan and Norris, published by the Pipe Jacking Association (PJA) on behalf of the Pipe Jacking Research Group. This group is a consortium of the PJA and five water service companies: North West, Northumbrian, Severn Trent, Thames and Yorkshire. With additional funding from the Engineering and Physical Sciences Research Council (EPSRC), formerly the Science and Engineering Research Council (SERC), it has promoted and financially supported a programme of research in pipe jacking and microtunnelling. The work has been in progress through four stages over a period of some ten years, under the direction of George Milligan of Oxford University. The overall objectives remain unchanged, and are set out in the foreword to the report.

Milligan and Norris summarised the principal results from stages 1 and 2; these notes provide a preliminary updating to include the results of stages 3 and 4. Stage 3 has been essentially a continuation of the site monitoring work of stage 2, while stage 4 has involved finite element computer analyses and further laboratory model testing of concrete jacking pipes. Brief details of the four stages are given in Table S1.1.

Most of the new results presented here are from the site monitoring of stage 3. So far, four pipe jacks have been monitored and a fifth is planned for summer 1996; details are given in Table S1.2. In each case instrumentation similar to that used in stage 2 has been employed. However increased numbers of contact stress and pore pressure transducers have been incorporated in the instrumented pipe, to provide more detailed information on pipe-soil interaction, with a reduction in the instrumentation of the pipe joints in comparison with stage 2. In addition, ground movements due to the pipe jacks have been measured on all four sites of stage 3, but only on site 5 of stage 2.

Stage	Dates	Project	RA	Cost - £1000	Sponsors
1	1986-1989	Laboratory testing of model pipes	Kevin Ripley	60	SERC, PJA, CPA
2	1989-1992	Site monitoring of full-scale pipe jacks	Paul Norris	220	SERC, PJA, and 5 water companies
3	1992-1995	Further site monitoring, including ground movements	Mark Marshall	300	As stage 2
4	1993-1996	Finite element analysis and pipe design	Jian Qing Zhou	95	SERC/EPSRC

Table S1.1 Pipe jacking research project stages

Scheme	1	2	3	4	5
Location	Leyton, East London	Southport, Lancs.	Seaham, Co. Durham	Thurrock, Essex	Orpington Kent
Date	Nov.1993	Feb.1994	July 1994	Jan.1995	? 1996
Client	Thames Water	North West Water	Northumb-rian Water	Anglian Water	Thames Water
Contractor	Clancy	Miller	Donelon	Amec	Murphy
Pipe supplier	ARC	Spun concrete	Buchan	Buchan	Spun concrete
Pipe I.D. (mm)	1500	1000	1800	1500	1600
Ground type	London clay	Dense silty sand	Glacial till	Very soft clay	Chalk/ gravel
Cover depth (m)	6 - 8	5 - 8	6	5.5 - 6	4.5 - 5
Drive length (m)	75	160	310	260	305
Test pipe	11	2	74	19	
Excavation method	Hand	Slurry TBM	TBM	Slurry TBM	Slurry TBM
Lubric-ation	No	Yes	No/yes	No/yes	Yes
Packer material	MDF*	MDF	MDF	MDF	MDF

* MDF = medium density fibreboard

Table S1.2 Details of stage 3 sites

S1. Instrumentation

S1.1 Pipe jacking instruments

A typical research instrumentation scheme used during Stage 3 is depicted in Figure S1.1. Instruments in the thrust pit record jacking forces and forward movement of the pipe string. The special instrumented pipe (I.P.) contained the following instruments:

a) Twelve contact stress cells (CSCs) to record localised normal and shear stresses and pore water pressures at the soil-pipe interface. The active face of these instruments have frictional similitude with the concrete of the jacking pipes.

b) Three joint movement indicators positioned equidistantly to measure movements across the joint gaps.

c) The data acquisition hardware with power supply.

d) Where pipe wall thickness and type of joint allowed, joint pressure cells on the pipe end.

Where man-entry was frequent and/or muck removal was by skip, pipe instrumentation was protected by a steel liner (Figure S1.2), as with Stage 2

To assist in interpretation of the huge amount of data, a comprehensive site diary was kept detailing shift progress, times of lubrication and line and level surveys.

S1.2 Ground instruments

Surface settlements above the tunnel were measured using precise levelling techniques on a series of studs and surface monitoring stations (Figure S1.3). Sub-surface movements were monitored by installing on each site inclinometer access tubes with magnetic settlement plates at the locations shown in Figure S1.4. Change in tube profile was monitored frequently during and after construction using a uni-axial inclinometer torpedo with an automatic logger. Vertical movements around the access tubes were monitored using a reed probe triggered by the magnetic plates. Depths to the plates were recorded relative to the top of the tubes so levels were taken on the tube tops at about the same time. In addition to the inclinometers, on Site 3, a set of electro-levels was used, in a near horizontal tube grouted into a borehole just above the crown of the tunnel at the reception shaft (Figure S1.5). The electro-levels operate like a series of short, continuously reading inclinometers, giving settlements by integration of the slopes measured at intervals along the tube.

S2. **Pipeline alignment**

S2.1 **Specification**

The normal practice of specifying limits to allowable errors in line and level, of typically 50 or 75mm, is widely use. However it has been shown that large angular deviation between successive pipes, causing highly localised stresses in the joint, can result from pipe wriggle still within the above limits. Stage 2 research showed typical joint angles of between 0.0° and 0.3° in reasonably well-controlled drives, with maximum values up to 0.5°.

S2.2 **Alignments achieved during Stage 3 monitoring**

Figures S2.1 to S2.4 show the pipe wriggle surveys and measured joint angles as constructed for the four instrumented schemes of Stage 3. Successive line and level surveys again revealed local curvatures once established remain throughout the drive. Joint angles were accurately measured by instrumentation at the joint between I.P. and neighbouring pipe using the analysis presented in Figure 2.8.

The lead miner on the hand-drive of Site 1maintained very good control over level, but deviated considerably from line. In trying to correct the line over a relatively short length, maximum joint angles of about 0.8° were generated (Figure S2.1). Very good control over line and level during the mechanised drive on Site 2 (Figure S2.2) resulted in joint angles of typically less than 0.1°. Although line and level deviated from axis by over 100mm during the early stages on Site 3, corrections were made gradually and joint angles did not exceed 0.35° (Figure S2.3). In the soft clay of Site 4 steering difficulties were experienced (due to machine roll) resulting in the erratic line and level control shown in Figure S2.4. At about distance 120m, where deviation from axis is at a maximum, joint angle measurements were missed due to a prolonged signal failure from the I.P. - the joint angle calculated using line and level information (analysis shown Figure 2.5) is about 0.95°. A bit further into the drive, at about distance 140m, where the deviation is still large, the measured joint angle increases to over 0.4 °.

S2.3 **Alignment control using joint angles**

Section 2.3 and Figure 2.9 detail how steering adjustments might be made to keep angular deviations to within acceptable limits. To illustrate this method, the example from Site 4 above, where the rate of increase in joint angle is large, will be used. At distance 134m, the line and level errors X_1, Y_1, plotted as point A_0 are -85mm and 178mm respectively (Figure S2.5). Advancing the tunnel by one pipe now moves the front of the tunnel to B_0 at X_2, Y_2 (-115, 166). If the tunnel were advanced by a further pipe and there was no angular deviation at the pipe joint located at B_0, the front end of the tunnel would end up at C_0. The co-ordinates at C_0 are given by X_3, Y_3, where:

$X_3 = X_2 + (X_2 - X_1) = -145$mm, and

$Y_3 = Y_2 + (Y_2 - Y_1) = 154$mm.

If there is angular deviation at the joint, the front end of the tunnel would lie anywhere on a circle, centre at C_0, of radius R given by:

$R = L\beta$.

Converting β to degrees and putting L as 2500mm gives:

$R = 43.6\,\beta$.

In this example an angular deviation of 0.2° has been chosen (R = 8.7mm) with point D_0 being chosen, for illustrative reasons only, to be adjusted only in the horizontal plane from C_0. Steering jacks should then be used to change direction from line B_0C_0 to B_0D_0. Repeating this

procedure, using $\beta = 0.2°$ and adjusting points D_n relative to C_n horizontally only, gives the projected line correction (I) as shown. In order to converge towards X=0 and Y=0 some adjustment in the vertical plane is required - also illustrated (II). Corrected line II is compared to the actual line and level in Figure S2.6 (assuming that it might have been possible to apply the angular adjusted line on site) . The angular corrected line is almost identical to the site corrected line until about axis; the angular adjusted levels however, in this case, differ from the actual levels and are brought to axis sooner; also angular deviation, in theory, should be 0.2° or less for the theoretical corrected line.

S4. **Stage 3 Contact stresses**

Due to the extremely large amount of data generated by twelve contact stress cells, it is both impractical and unnecessary to present all the results in this document. Marshall (1996) will provide full details on interface stresses; summarised results along with the main findings will probably be documented in a revised version of Milligan and Norris (1994).

S4.1 **Site 1- London Clay**

Contact between the pipe and ground only occurred along the tunnel invert - little or no contact was measured along the pipe sides and top. A plot of the contact stresses recorded along the bottom at the front of the pipe is shown in Figure S4.1a. The nature of the hand excavation resulted in an uneven and sometimes large overbreak, up to 50mm in places, particulary at the shoulders of the bore, which would account for the lack of contact along the side and top. Shear stresses at the start of the drive (before distance 10m) are very low. This is probably due the pipe being inserted wet - water was falling onto the pipes from a leaking diverted drain in the jacking pit over the tunnel entrance. As the pipe progresses and probably dries, the measured shear stresses increase. Measured pore pressures and radial stresses are a little more difficult to interpret and are not fully understood at this time, they do however indicate some suction taking place during the pushing.

Lubricant was infrequently pumped and was not pressurised. The only injection point was in the top of the shield and directed slurry back over and around the front pipes - injection points were not provided in the pipe string. It is very unlikely that the pumped slurry would flow back as far as the I.P., placed at pipe 11, 25m behind the shield, but some would inevitably find its way to the tunnel invert and assist in any remoulding and softening of the soil which probably kept shear stresses quite low. The undrained strength of the intact clay, is about 120kPa; data from individual pushes - an example of which is also shown in Figure S4.1b - suggests a limiting value was reached at about 45kPa, resulting in an apparent alpha-value (ratio of undrained adhesion to undrained soil strength) of 0.38.

S4.2 **Site 2 - Fine sand**

In the fine sand of this site, contact occurred mainly between the crown and left side of the pipe and ground. Along the right and bottom of the pipe, contact stresses and pore pressures mostly measured fluid pressure, equal to ground water pressure and lubricant pressure when pumping slurry. Figure S4.2 shows data from the contact stress cell array at the pipe rear - the contrast between top and left stresses, to bottom and right stresses is clearly evident. It appears that the pipe was floating in the bentonite lubricant filling the tunnel bore - the data suggest a non-uniform gel around the pipe as illustrated in Figure S4.3.

The relationship between local shear and effective radial stresses on the pipe is clearly frictional (Figure S4.4). Over the greater stress range, recorded on the pipe left, centre and rear, the friction angles of 39° and 35° respectively are reasonable for a dense sand. From the Client's site investigation, the internal angle of friction for the sand is 43 °which, taking the above angles, gives skin friction coefficients of 0.90 and 0.81; again, reasonable friction coefficients between sand and concrete.

The I.P. was inserted at pipe 2, the nearest lubricant injection points were placed on the right both in the shield and pipe 4. The change in measured fluid pressures due to lubricant pumping with respect to time, varied around the pipe - an example is shown in Figure S4.5. At the front of the pipe the pressure increase above hydrostatic is almost immediate and rises gradually to a steady state of about 70kPa; at the centre, there is a very small linear increase after commencement of pumping until about 15:35:30 when a sudden increase takes place; fluid pressure at the rear follows a similar curve to the centre but with a time lag of about 1 minute.

Figure S4.6 shows the effect lubricant pumping on shear and effective stresses measured at the left-rear stress cell. After the start of pumping the stresses decrease, somewhat erratically, until the increase from about 15:35:30 to 15:36:30. This is may be due to lubricant pressure from the right of the pipe pushing it against the soil on the left. As fluid pressures begin to rise sharply from 15:36:30, contact stresses fall dramatically to zero. When the fluid pressure reaches a steady state, indicating the formation of an effective lubricant zone, there is no further contact between pipe and soil.

S4.3 **Site 3 - Boulder clay**

Contact stresses recorded around the rear of the I.P. are illustrated in Figure S4.7. Pore pressure readings closely match total radial stress readings resulting in low effective stresses; shear stresses are also very small. On the bottom of the pipe, both shear stress and effective radial stress are close to zero suggesting pipe buoyancy. Along the sides and top of the pipe, the effective stress plots indicate erratic contact between the pipe and soil but the corresponding shear stresses, typically limited to less than 10kPa, might suggest contact between pipe and soil/bentonite filter cake. It is clear the lubricant was effective, certainly around the I.P., and probably the whole pipeline. The I.P. was placed at pipe 74, injection points were provided in the top and both sides of pipes 73 and 76; slurry was pumped at regular intervals and was kept pressurised.

The contact stresses measured on the rear-right during several pushes are shown in Figure S4.8. The data show very low shear stresses, the limiting value being about 7kPA, perhaps representing the undrained shear strength of a bentonite filter cake, and erratic but small effective radial stresses.

S4.4 **Site 4 - Soft clay**

Local contact stresses recorded around the front of the I.P., except the front-left location where the cell glue line failed, are depicted in Figure S4.9. The stresses show relatively uniform contact around the pipe, which is also true of stresses measured at the centre and rear cell arrays. The pattern again is one of very low shear and effective radial stresses.

Figure S4.10 shows contact stresses around the rear of the I.P. (placed at pipe 19), soon before and soon after lubrication. Before lubrication commenced, effective stresses around the pipe circumference are almost uniform at about 20kPa (except along the left, where they are slightly larger), similarly the shear stresses are relatively uniform at about 10 to 15 kPa. Following lubrication, the most notable result is the reduction in contact stresses on the right - effective stresses fall to zero, while shear stress falls by about 50%. This is a similar situation to Site 2, but in very different ground conditions, where the effect can probably be attributed to a lubricant injection points on the right of pipe 18.

The radial stress, shear stress relationship for contact stresses recorded on the bottom of the pipe, during several pushes after lubrication commmenced, is illustrated in Figure S4.11. As with the example shown for Site 3 above, the pattern is one of very low shear stresses (the limiting value is about 8kPa) over a low range of effective stresses.

S5. **Total jacking forces**

The jacking records for the four stage 3 sites are shown in Figures S5.1 to S5.5, and the measured face resistance and line friction values tabulated in Table S5.1.

In scheme 1, in London clay, the face was hand-excavated with quite a generous overcut around the shield; as a result the face resistance was negligible. The jacking force increased linearly overall, but at a low rate, much lower than for the drive through London Clay at Honor Oak in scheme 3 of stage 2. The latter was at greater depth and the ground closed on to the pipes. Here the contact stress cell readings showed that the bore remained open and the pipes were simply sliding along the base. The simple selfweight sliding model using a residual friction angle of 13° gives a calculated resistance of only 5.4 kN/m (see Table S5.1). The average measured resistance is 12.7 kN/m, but the lower bound is about 6.7 kN/m, some 25% higher than calculated. However there is some evidence from the stress cell readings that, due to the presence of water from a leaking drain, a layer of softened clay formed in the base of the bore, with a shear strength of about 35 kPa. In this case the Haslem model (Figure 5.6) may be more appropriate, as in the later stages at Bolton in scheme 1 of stage 2.

As expected, the jacking force showed significant peaks after stoppages between pushes, between shifts and due to overnight and weekend breaks. The behaviour is very similar to that at Honor Oak, as shown in Figure S5.2.

Site 2 at Southport produced a very erratic jacking record, despite its almost perfect alignment (Figure S5.3). The variations in line friction have been related closely to the lubrication procedures recorded in the site diary. Where lubricant was being supplied continuously under pressure to the overbreak annulus around the pipes, very low jacking resistances were measured, while resistances twenty times higher were recorded when the lubricant pump was out of action. It is noticeable that it was not possible to reduce previously generated frictional force once lubrication restarted. The "selfweight sliding" resistance based on the buoyant (negative) pipe weight provided a reasonable estimate for the fully lubricated condition, while the Terzaghi analysis (Figure 5.7) modified for the presence of the water table (see Guide to Best Practice) provided an upper bound prediction for the frictional resistance without lubrication.

Scheme 3 started without lubrication, and the jacking load increased very rapidly; the magnitude of the frictional resistance is much greater than predicted by the selfweight sliding resistance, suggesting that a cohesive "Haslem" mechanism was operating. Introducing lubrication reduced the line friction to less than a third of the unlubricated value, but still much higher than predicted by a frictional model based on buoyant weight. The pressure cells show contact between pipe and soil at the sides as well as the top of the pipe; the pipe line is probably being forced against the sides of the tunnel bore due to its fairly erratic line. The rest of the resistance appears to come from the shear stresses in the lubricant layer, of perhaps about 2 kPa.

The very large increases in jacking force after a weekend are probably due in this case to dissipation of the lubrication into sand lenses in the glacial till; the restart forces show a similar rate of increase to the unlubricated pipe line. Note that, because the tunnel bore was stable, lubricant was obviously able to work back into the initially unlubricated length.

The same effect is apparent in scheme 4, in very soft clay and peat. Here the stress cells showed ground contact all round the pipe during the unlubricated stage, with an average shear stress of about 4.5 kPa. After starting lubrication, the average resistance gradually dropped back to about 2.5 kPa.

Scheme		Face load (kN)	Pipe friction (kN/m)	Average shear stress (kPa)	Calc. pipe friction (kN/m)	Notes
Leyton		0	12.7 average 6.7 lower bound	2.24 1.18	5.4 (1)	Cf. 54 kN/m at Honor Oak
Southport	Full lubrication Imperfect lubrication	600	2.6 41.6	0.69 11.0	2.3 (2) 79 (3)	Cf. 10 kN/m at Cheltenham cf. 100 kN/m at Cheltenham
Seaham	Unlubricated Lubricated	300	48 15 2.0 min	7.07 2.21 0.29	9.2 (4) 44 (5)	
Thurrock	Unlubricated Lubricated	750	25 14	4.35 2.44		

(1) Calculated from $F = W\tan\delta$, $\delta = 13°$
(2) Calculated from $F = W'\tan\delta$, $\delta = 37.5°$
(3) Calculated from Terzaghi model, $\phi' = 43°$
(4) Calculated from $F = W\tan\delta$, $\delta = 19°$
(5) Calculated from Haslem model

Table S5.1 Face loads and friction forces for stage 3 sites

7. Improvements to joint design

The stage 4 research work has been concerned with the analysis of pipes and their joints under various different load and restraint conditions, to match those occurring during jacking. This has involved fully three-dimensional modelling with finite elements. These analyses have allowed pipe and joint stresses and deformations to be studied in detail; more importantly they have then allowed various ideas for improving the load capability of pipe joints to be investigated. Following these analyses, a series of tests have been carried out on small scale model concrete pipes, as shown in Figure S7.1. The model pipes were of 200mm O.D., 150mm I.D. and length 250mm; the concrete cube strengths at time of testing had a mean value of about 60 N/mm^2. Uniform loading was applied through a flat loading platen, while use of a platen machined with two 1-degree bevels applied localised non-uniform loading to the pipe ends.

Results of the tests are presented in Table S7.1. Pipes either had a plain square end, or the end face was profiled as shown in Figure S7.2. The latter was intended to reduce stresses near the edge of the pipe under misaligned conditions, and hence prevent local spalling which might affect joint seals or expose reinforcement. Pipes were tested with no packing material, rubber packing (a material with high Poisson's ratio) and packing made of 3mm thick plywood. Ripley's work in stage 1 had shown plywood to be less effective than chipboard or medium density fibreboard, but neither of the latter were available in sufficiently thin sheets for correct scaling. The pipes were unreinforced except where noted; local reinforcement refers to four closely spaced reinforcement hoops in the end of the pipe close to the outer face, while prestressing refers to a steel band tightened on to the outside of the end of the pipe.

For the uniform loading, rubber packing or the profiled end geometry without a packer reduced the failure load significantly. For non-uniform loading the use of plywood packing, the profiled end geometry, and prestressing or local reinforcing were all beneficial. A combination of local reinforcement and the profiled end gave a good failure load and also completely stopped any local joint spalling at lower loads. This combination appears promising and it is hoped to test larger pipes under more realistic loading conditions to confirm the improved performance.

TEST DETAILS	Normalised strength (%) (1)		NOTES
	Uniform Loading	Non-uniform Loading	
Plain ended pipes			
No packing	85	43	Local spalling and cracking of pipe edges at low loads under non-uniform loading:- @<50% failure load for no packing; @<30% failure load for rubber packing; @ late stage only for plywood packing
No packing, with local reinforcement	-	40	
Rubber packing	55	46,42	
Plywood packing	83	54,54	
Plywood packing, with prestressing	77	61,57	Local spalling greatly reduced
Plywood packing, with local reinforcement	79	62,67	
Pipes with profiled end			
No packing, with local reinforcement	52	35,44	No local spalling at loads up to failure load
Plywood packing, no reinforcement	74	61,57	
Plywood packing, with local reinforcement		63	

(1) Normalised strength = pipe failure load/(pipe section area x cube strength)

Table S7.1 Strengths of model pipes

S8. **Ground Movements**

S8.1 **Surface settlements**

The most commonly used method for predicting a surface settlement profile is the Gaussian distribution curve - see Figure S8.1.
The surface settlement, S_0, is described by

$$S_0 = S_{0,max} \exp(-x^2 / 2i^2) \qquad \text{(S8.1)}$$

where $S_{0,max}$ is the maximum settlement over the tunnel centre line and i is the distance from centre line to the point of inflexion. O'Reilly and New (1982) produced the following expressions for the parameter i:
For granular soils,

$$i = 0.28z_0 - 0.12 \text{ (m)} \qquad \text{(S8.2)}$$

and for cohesive soils

$$i = 0.43z_0 + 1.1 \text{ (m)} \qquad \text{(S8.3)}$$

where z_0 is depth to tunnel axis.
The value of $S_{0,max}$ may be obtained by equating the volume of the settlement trough ,V_s, to the volume of estimated ground loss. It can be shown that

$$S_{max} = \frac{V_s}{i\sqrt{2\pi}} \qquad \text{(S8.4)}$$

Ground loss due to tunnelling has two main sources - movements at the tunnel face and closure of the ground between the shield and liner. The calculations here assume that ground movement at the tunnel face is negligible, either because the face was continually supported by slurry pressure or because the excavations are in highly stable stiff clay. The only significant contribution to ground loss is due to the overbreak where the ground is excavated to a larger diameter, D_e, than the pipe diameter, D_p. It is therefore assumed here that

$$V_s = \frac{\pi}{4}(D_e^2 - D_p^2) \qquad \text{(S8.5)}$$

S8.2 **Subsurface movements**

Subsurface movements are important for their effect on existing services, foundations etc in the ground above or close alongside the tunnel, and may be more severe than the surface settlements. For instance, Mair et al (1993) approximated the data for *i* for cohesive soils in Figure 8.2 and extended the analysis to subsurface movements as shown in Figure S8.2. The nearer the crown of the tunnel, the smaller the value of *i* and the greater the maximum settlement, and hence the more serious the local distortions of any existing service pipe crossing the line of the pipe jack.

An alternative approach starts with the theoretical analysis for closure of a cylindrical cavity in elasto-plastic material, with equal horizontal and vertical initial stresses in the ground. The displacements towards the tunnel are critically controlled by the stability ratio N^*; for N^* less than 1.0, movements are entirely elastic, but as its value exceeds 1.0, plastic yielding starts

and displacements increase exponentially (Figure S8.3).

Empirical data is available from measured ground movements around large diameter tunnels at depth in London clay. Mair and Taylor (1993) have plotted the variation with distance from the tunnel of vertical movements above the crown and horizontal movements at axis level (see Figure S8.3). Geometrical scaling suggests that this plot might also apply to 1.5m diameter pipe jacks at about 10m depth, or 0.6m diameter microtunnels at about 4m depth. However the differences in ground stiffness and construction procedures may lead to significantly different patterns of movement, which need to be checked by field measurements.

S8.3 **Results and discussion**

S8.3.1 *Site 1*

The predicted surface settlement profile and measured settlements are shown in Figure S8.4. From O'Reilly and New (1982) the value of i at the surface is 4.76m, assuming the ground to be cohesive (there is in practice a significant layer of sandy gravel above the London Clay), and the maximum predicted settlement is 12mm. The measured values taken soon after completion of the tunnel, indicate a similar settlement profile to the predicted except that the centre line value is rather less than those either side; though all lie within the calculated settlement profile. The final set of measurements on the road studs - taken almost two years after completion - show a consistent profile but with levels slightly higher than expected. This can probably be attributed to local movements in the road pavement, either by traffic damage or temperature and seasonal movement.

Access tube profiles perpendicular to the tunnel axis are plotted in Figure S8.5, showing horizontal movements of 5mm at about the level of the tunnel. The final readings show similar profiles but with slightly greater or lesser movements. This could be attributed to small movements in the assumed fixed datum of the tube tops. Data from the inclinometer and settlement plates have been combined for measurements taken about one month after completion to give the transverse ground movement vectors shown in Figure S8.6.

Inclinometer data of movements in the direction of the drive - taken forty days after completion - indicate maximum movements into the excavation of about 2mm in tubes A and B (over the centre line and offset by 1.5m respectively), and about 1mm for tube C (offset by 3.5m).

Comparison with deeper tunnels

Measurements of sub-surface ground movements during construction of five London Underground tunnels of approximately 4m in diameter, at depths of 20-29m, in London Clay were presented in dimensionless form by Mair and Taylor (1993), as shown in Figure S8.3. The vertical ground movements were measured at different distances above the tunnel centre-line and the horizontal movements were measured at various positions at tunnel axis level. The data are reasonably consistent and are in general agreement with linear plots. Mair and Taylor (1993) show that the gradient of the lines in Figure S8.3, which are almost parallel, is consistent with a G/s_u ratio of about 100; this assumes idealised linear elastic-perfectly plastic soil behaviour.

Figure S8.7 shows observed sub-surface ground movements around the pipe jack plotted in the same dimensionless form as in Figure S8.3). It is interesting to note that the gradient of the lines through the pipe jack data are similar to those for the deeper and larger tunnels. Assuming an undrained shear strength of about 100kPa at the 8.5m depth of the pipe jack (from Self-boring Pressuremeter tests), the stability ratio $\gamma z/s_u$ is 1.7, compared with an average value of about 2.5 for the deeper tunnels. Taking this into account, and assuming a complete unloading of the cylindrical cavity in the case of the pipe jack, a G/s_u ratio of about 80 is implied by the

data in Figure S8.7. This compares favourably with the G/s_u ratio of about 100 deduced from the movements around larger and deeper tunnels in London Clay.

S8.3.2 *Site 2*

Figure S8.8 shows the measured surface settlements and two predicted profiles. The profile with S_{max} = 18mm assumes that the full overbreak of volume between cutter diameter and pipe outer diameter is converted into settlement. Observed movements four days after tunnel completion show a maximum settlement of only 6mm over the centre line but a distance to the point of inflexion close to the predicted value of 1.45m. There are two probable factors accounting for the discrepancy in magnitude of settlement:

i) Shearing of the soil during settlement will cause some dilation of the dense sand resulting in the volume of the settlement trough being less than the overbreak volume.

ii) The bentonite slurry gel - used as a lubricant - prevents the ground completely collapsing onto the pipes.

An alternative calculation, giving S_{max} = 7.8mm, assumes that the difference in diameter between cutter and shield gives the overbreak volume. Allowing for some dilation, this alternative predicted profile is in reasonable agreement with the observations made four days after completion. However, the calculation leaves some doubt over whether settlements continue as the bentonite/soil gel consolidate under pressure from the surrounding soil. In this case, observations made two hundred and eighteen days after completion show a further settlement over the centre line of about 2mm; the profile however, is much flatter than predicted probably due to the stiff road pavement. More recent measurements indicate no further increase in settlement.

Deformation of the inclinometer tubes was negligible - typically less than 1mm - and showed no consistent pattern. The magnetic settlement plates however, did indicate some downward movement around the tubes. The vectors shown in Figure S8.9 illustrate the plate movement.

S8.3.3 *Site 3*

Surface settlement profiles from Site 3 are plotted in Figure S8.10 with two predicted profiles. The value of S_{max} = 13.3mm assumes full closure of the overbreak between cutter and pipes whereas the value of S_{max} = 10mm results from closure between cutter and shield, assuming that the remaining annulus is held open by bentonite slurry pressure. Both profiles are larger than early measurements, though the shape of the settlement trough is well predicted. Surprisingly, the settlements on the road nails were greater than on the settlement monitoring stations founded beneath the pavement. A more recent set of measurements show a less defined trough pattern with settlements close to the predicted profile where full overbreak closure is assumed.

Inclinometer plots for transverse movements in the tubes to the side of the tunnel are illustrated in Figure S8.11. Measured movements towards the excavation were small, reaching a maximum of about 2.5mm at tunnel depth. Deformation over the centre line, and in the direction of the drive, was negligible. Movement vectors in the transverse plane are shown in Figure S8.12. The most recent set of readings cannot be used as the tubes were damaged during site clearance and full of debris.

Figure S8.13 shows settlement profiles along the centre line over the crown of the pipes, plotted from electro-level data. The maximum settlement detected was about 10mm, greater than measured by the settlement plates, but still much less than calculated for this depth. Settlement starts to be detectable about 1.5m ahead of the tunnel face, but most of the settlement occurs after the passage of the cutting head, confirming that ground loss due to inward movement of the tunnel face is negligible. Further settlement after tunnel completion, illustrated in Figure

S8.14, continues for about 10 days at a point some 7m from the shaft wall.

S8.3.4 *Site 4*

Observed surface settlements with predicted profiles are shown in Figure S8.15. As with the calculations for sites 2 and 3, the deeper profile, where S_{max} = 11.5mm, assumes full overbreak closure. With partial closure, S_{max} = 5.8mm, the predicted profile matches almost exactly the observed settlements which might suggest the presence of pressurised slurry is preventing full short-term closure of the overbreak. However, the most significant sub-surface movements measured during Stage 3 (Figure S8.16) may negate this hypothesis. In the transverse direction, tube deformation is an order of magnitude greater than that recorded on the previous sites - the tube closest to the tunnel moving towards the excavation by almost 100mm at about axis level. The tube furthest away also deforms significantly by about 20mm at tunnel level. Movement into the excavation, both transverse and parallel to the drive, began in Tube B with the face still 3m from the instrumentation array (Figure S8.17). Movement towards the tunnel, measured 28 hours after the face had passed the array, is far greater than can be explained by overbreak closure (the full overbreak being 20mm on radius). It is not yet fully understood why the significant sub-surface movements did not translate to greater surface settlements.

Data from the settlement magnets - used in the calculation of transverse vertical movement vectors - is proving difficult to interpret. Because of double shifts on this drive, measurements were taken by two different people and the two sets of readings are not consistent - movement vectors are therefore not presented.

Instrumented Pipe

12 No. Contact stress cells, incorporating pore pressure transducers (6 at axis level, 3 each on the left and right; 3 in the pipe bottom; and 3 in top of the pipe).

3 No. joint movement indicators.

3 No. joint movement indicators.

Jacking Pit

1 No. linear displacement unit.

4 No. jack load cells (or hydraulic pressure transducers).

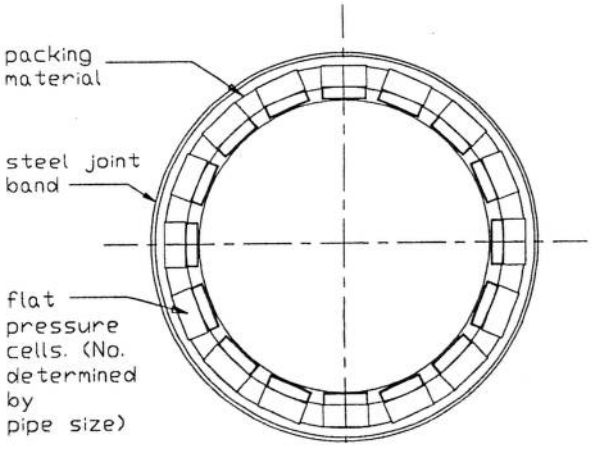

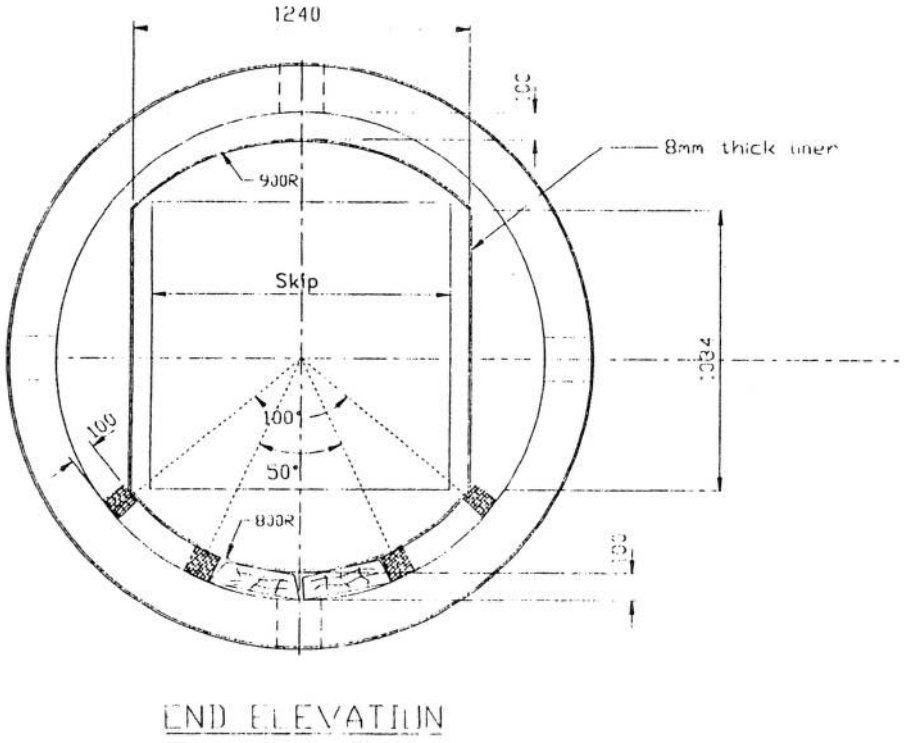

Figure S1.2 Protective liner

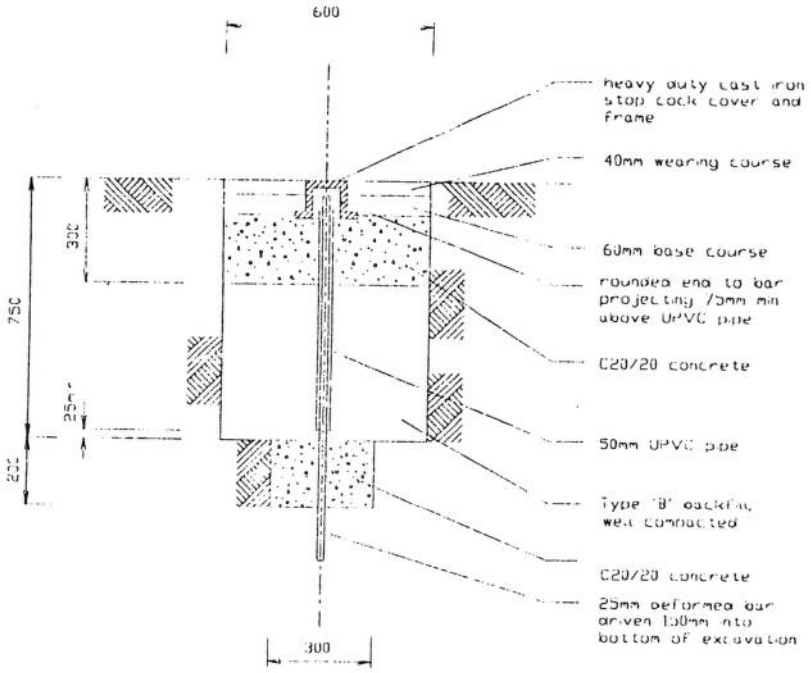

Figure S1.3 Surface level monitoring station

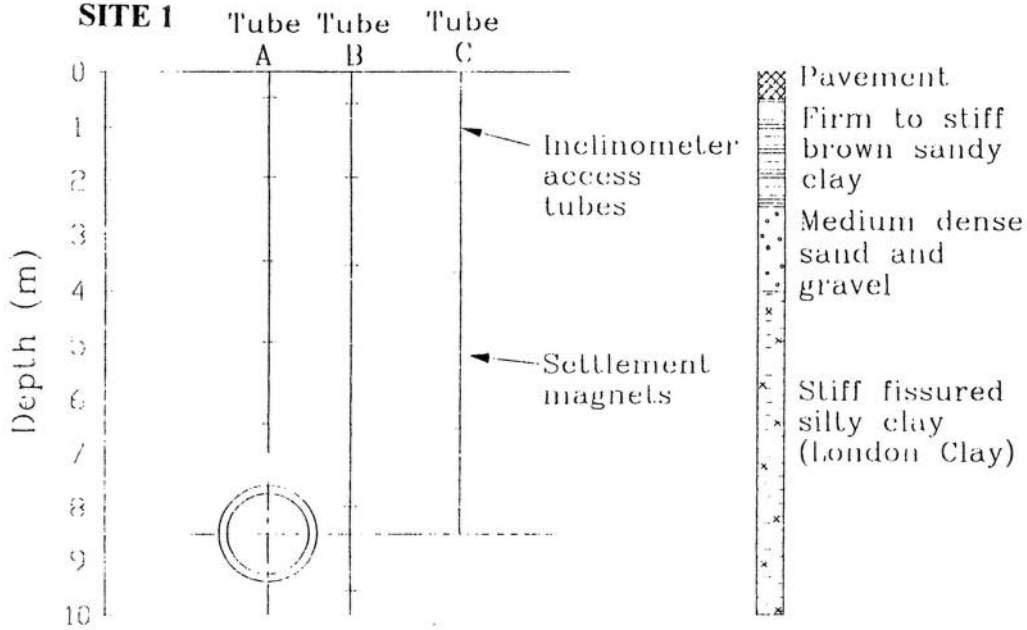
SITE 1
Tube A
Tube B
Tube C
Depth (m)
0
1
2
3
4
5
6
7
8
9
10
Inclinometer access tubes
Settlement magnets
Pavement
Firm to stiff brown sandy clay
Medium dense sand and gravel
Stiff fissured silty clay (London Clay)

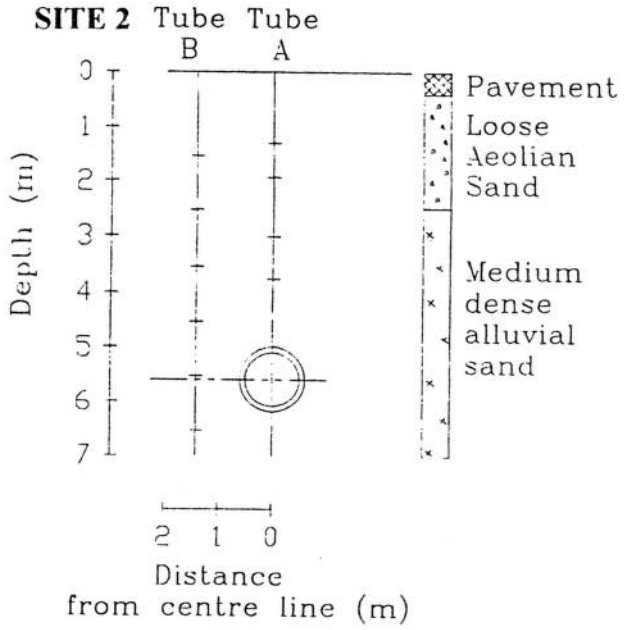
SITE 2
Tube B
Tube A
Depth (m)
0
1
2
3
4
5
6
7
2 1 0
Distance from centre line (m)
Pavement
Loose Aeolian Sand
Medium dense alluvial sand

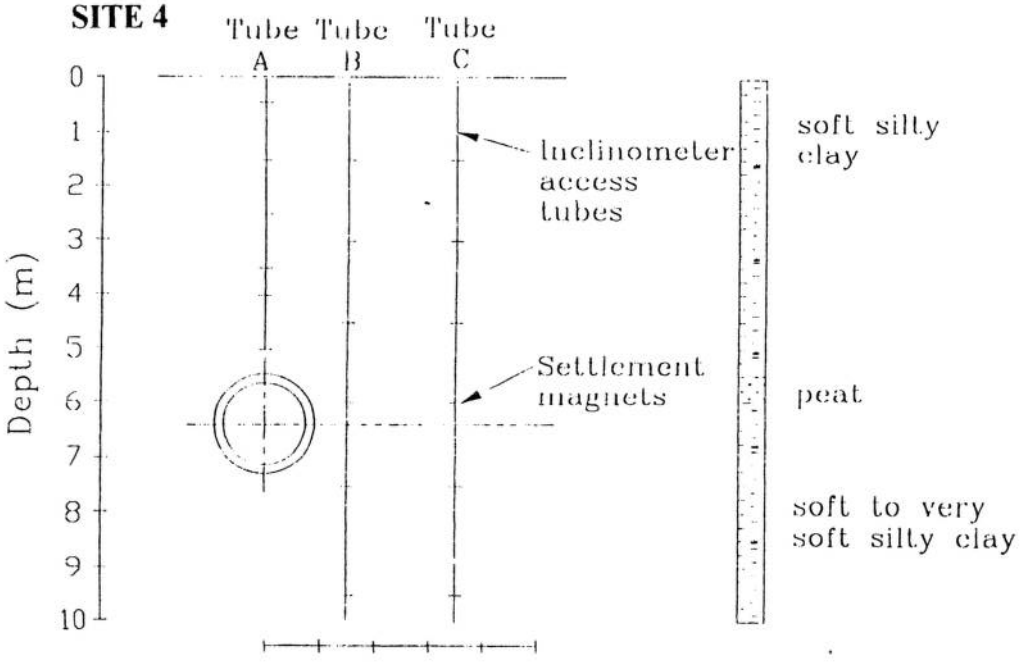
SITE 4
Tube A
Tube B
Tube C
Depth (m)
0
1
2
3
4
5
6
7
8
9
10
Inclinometer access tubes
Settlement magnets
soft silty clay
peat
soft to very soft silty clay

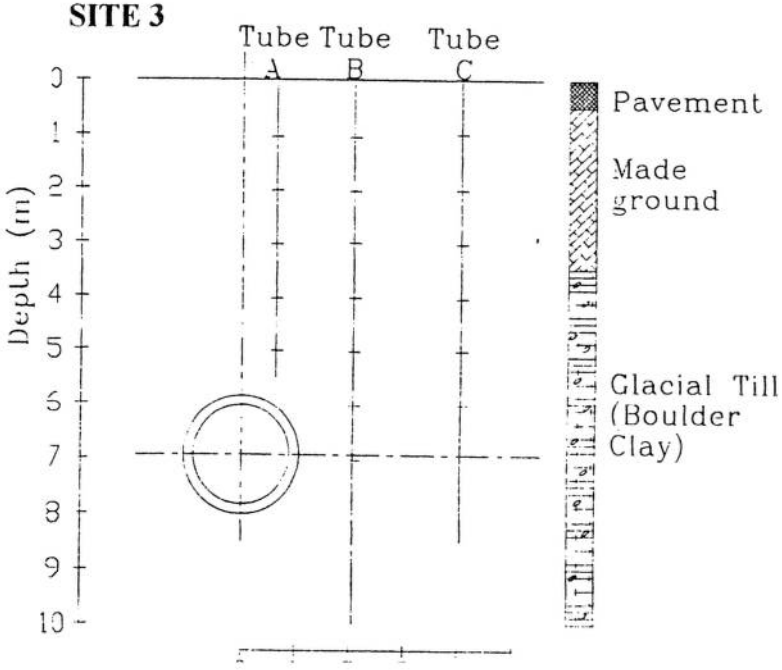
SITE 3
Tube A
Tube B
Tube C
Depth (m)
0
1
2
3
4
5
6
7
8
9
10
Pavement
Made ground
Glacial Till (Boulder Clay)

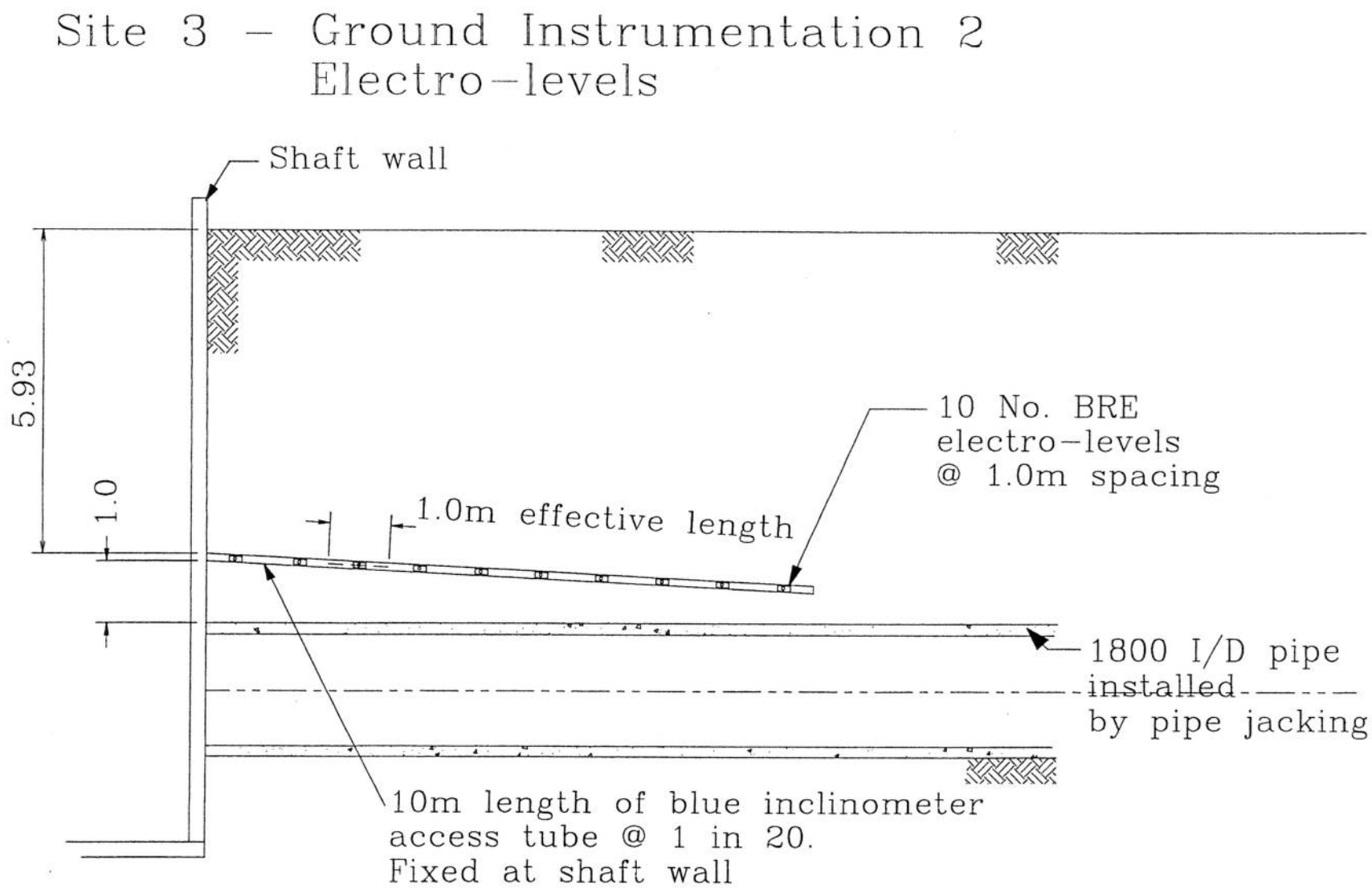

Figure S1.5 Electro-level monitoring

Site 1 - Line & Level Survey

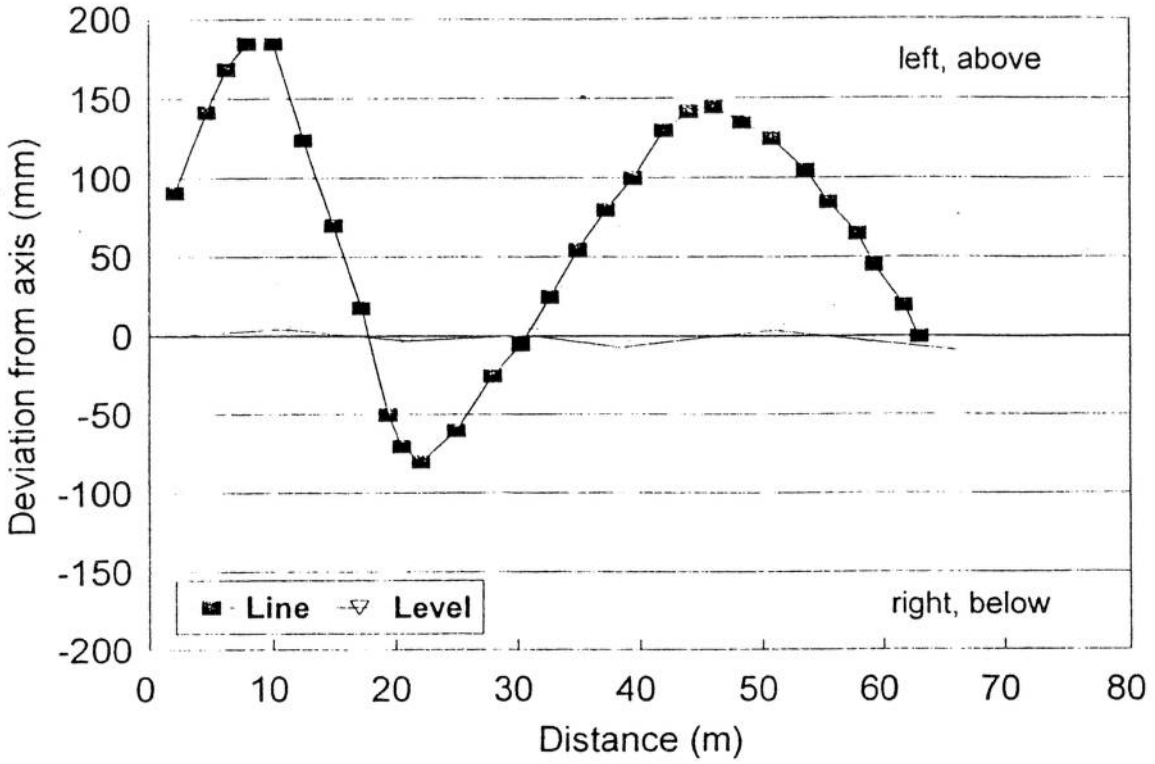

Site 1 - Misalignment angle

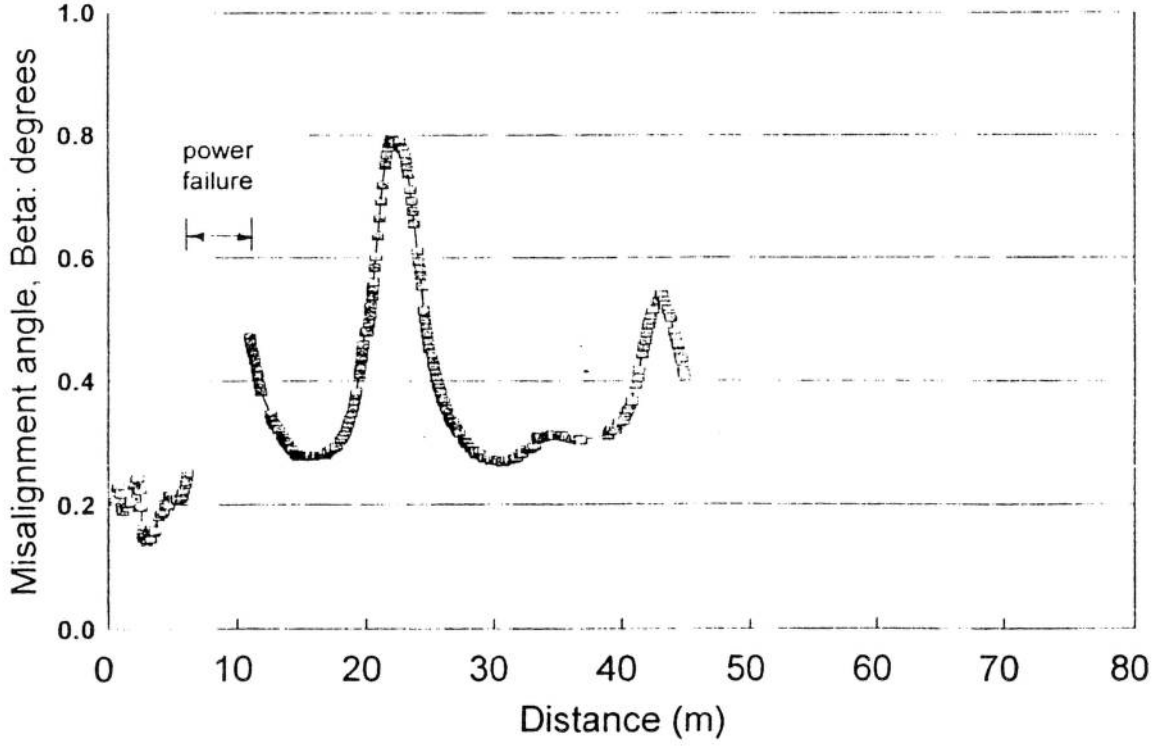

Figure S2.1 SITE 1 - Tunnel alignment

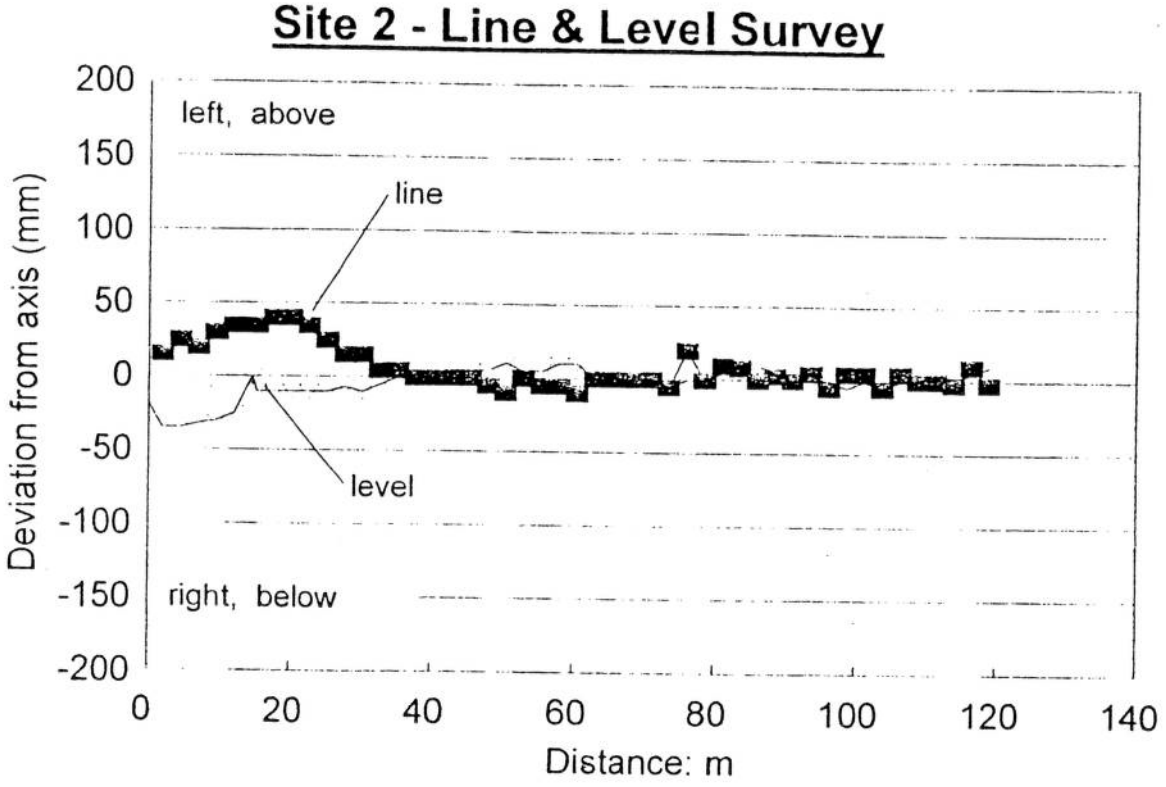

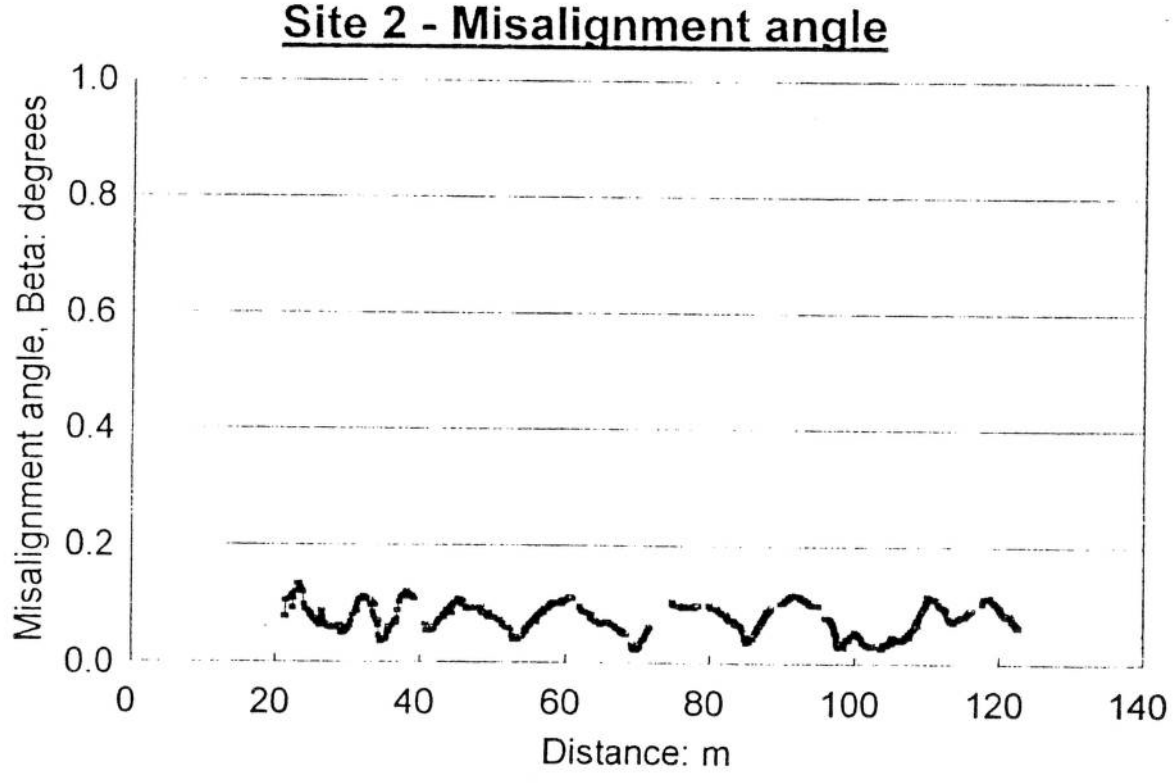

Figure S2.2 SITE 2 - Tunnel alignment

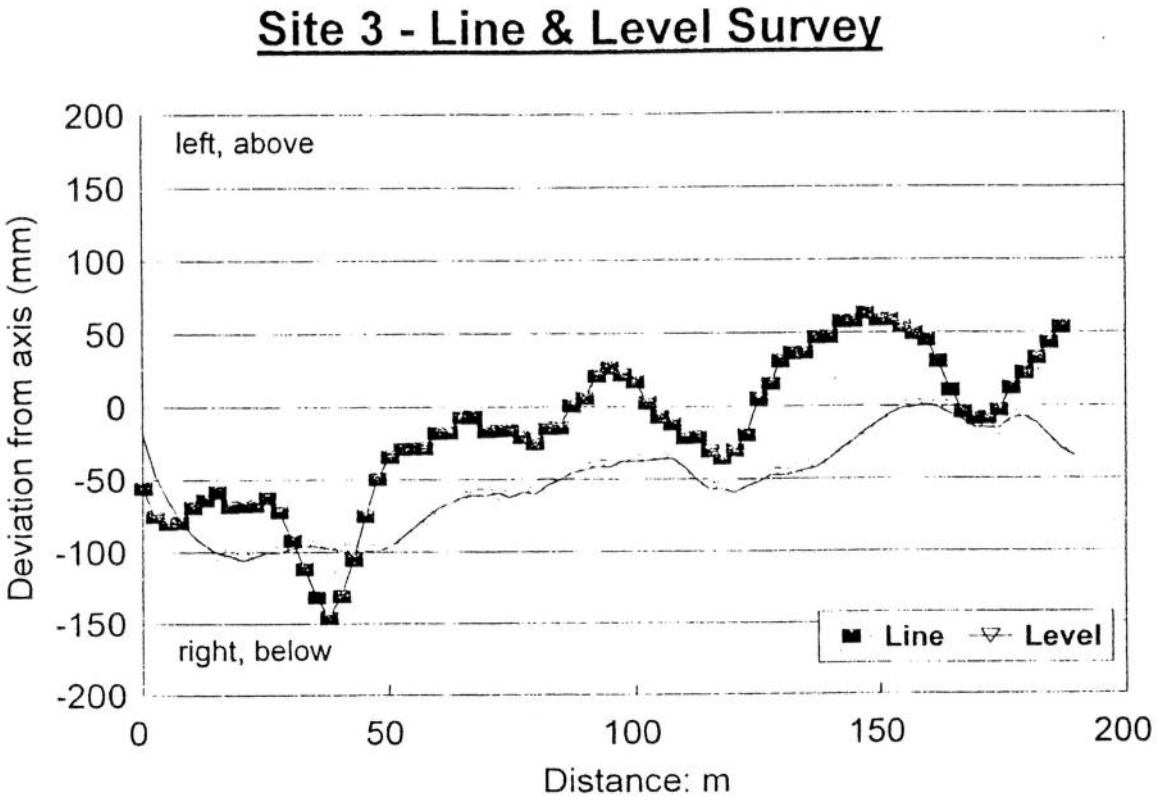

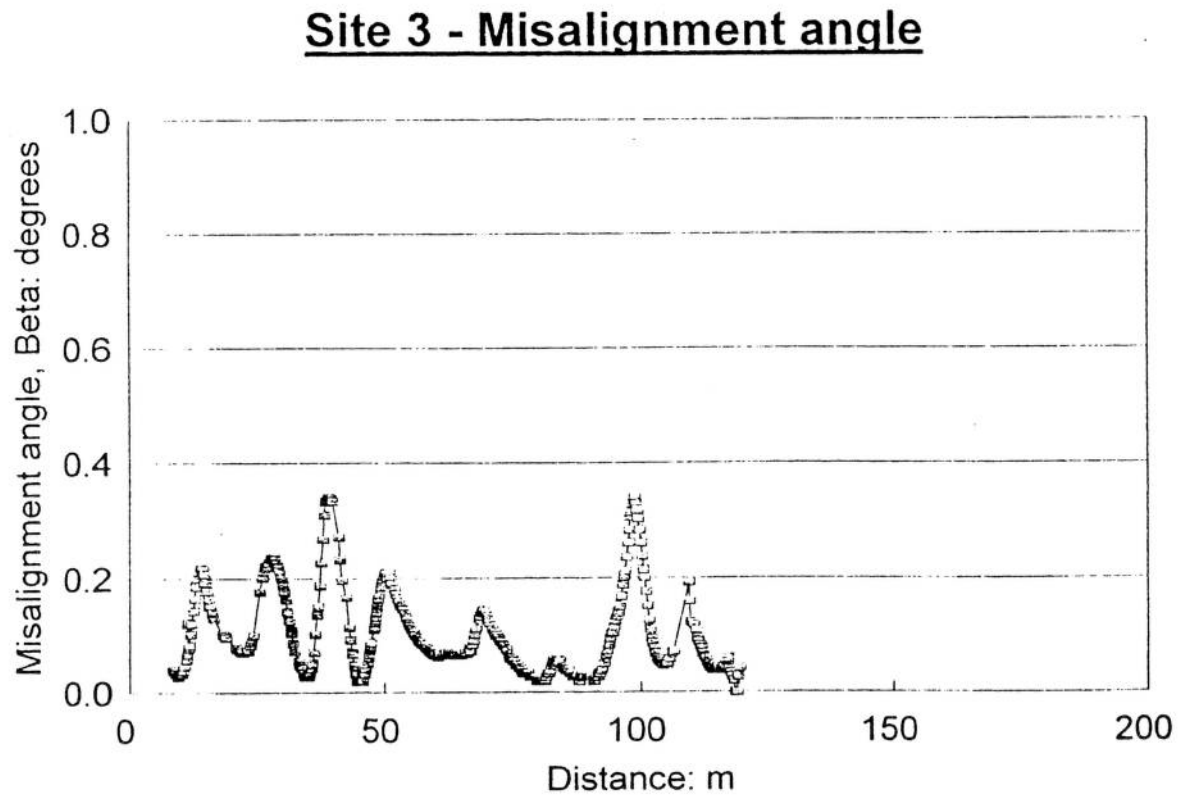

Figure S2.3 SITE 3 - Tunnel alignment

Site 4 - Line & Level Survey

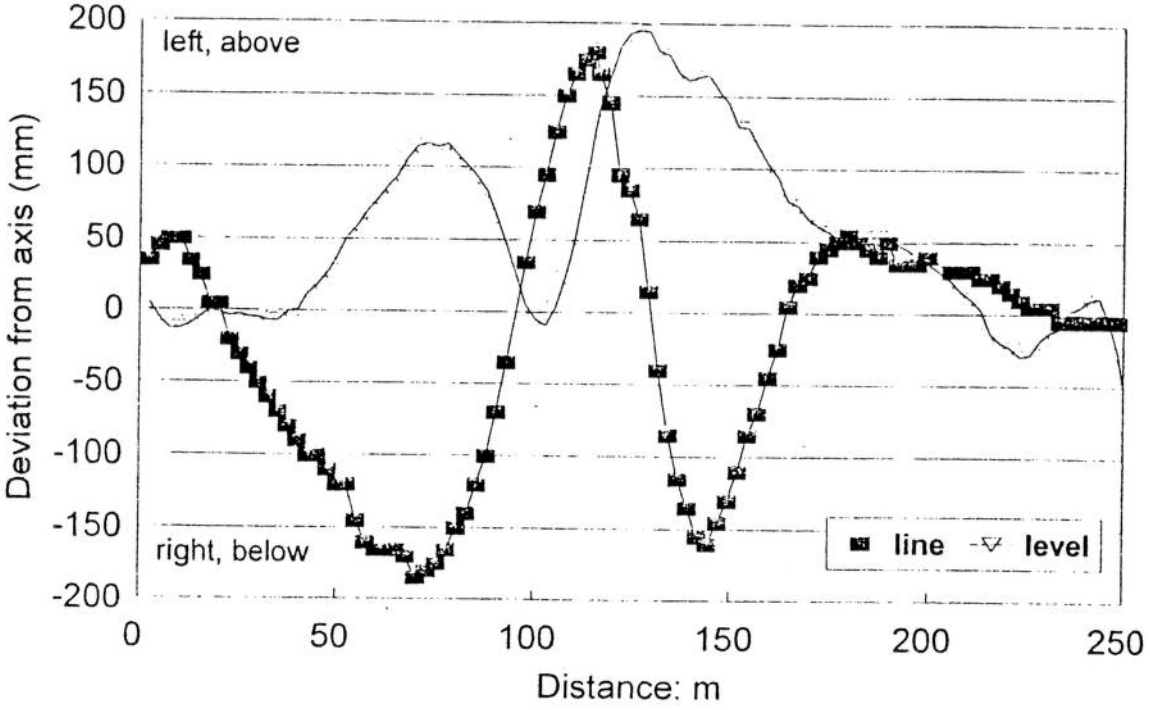

Site 4 - Misalignment Angle

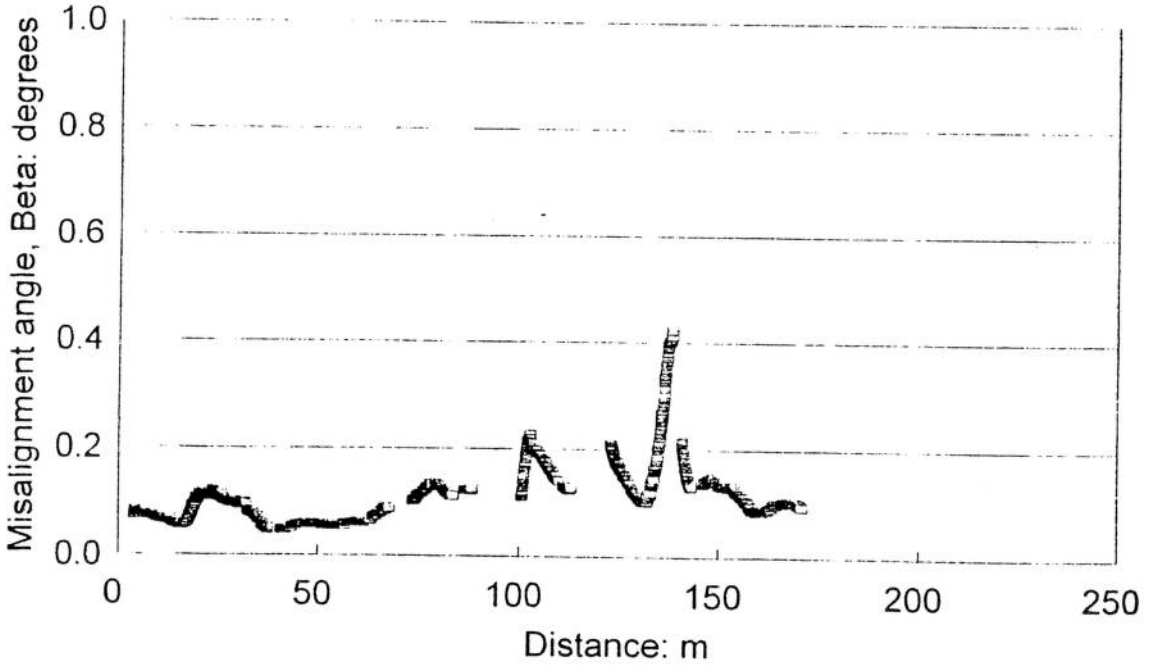

Figure S2.4 SITE 4 - Tunnel alignment

Site 4 - Line & Level Survey

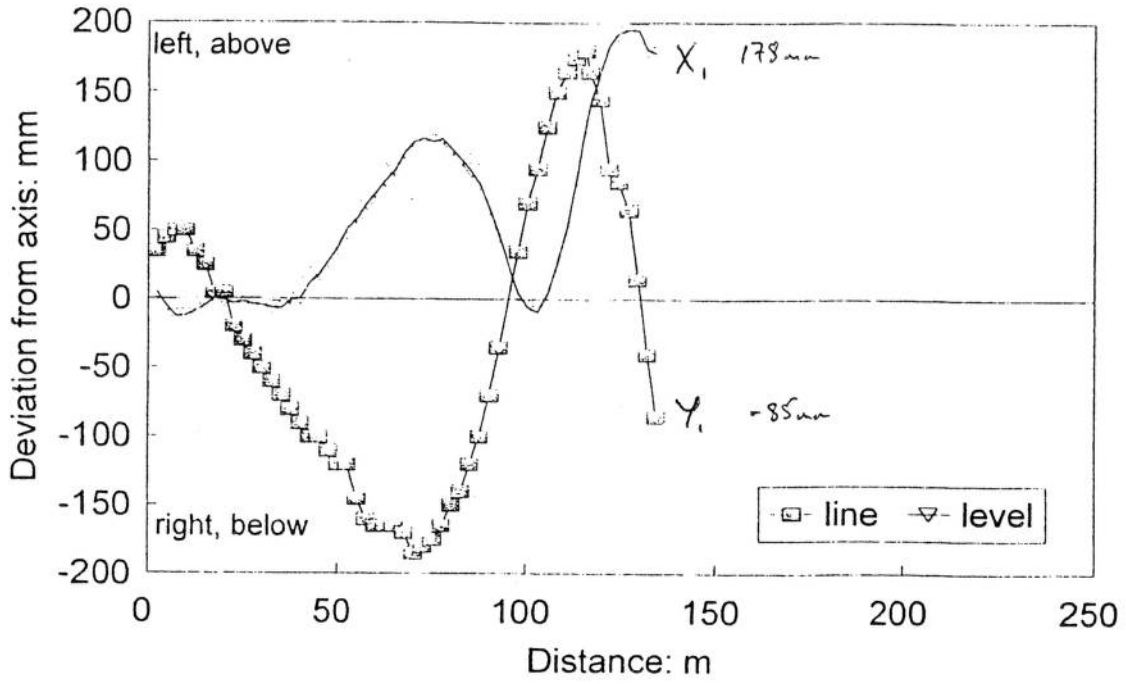

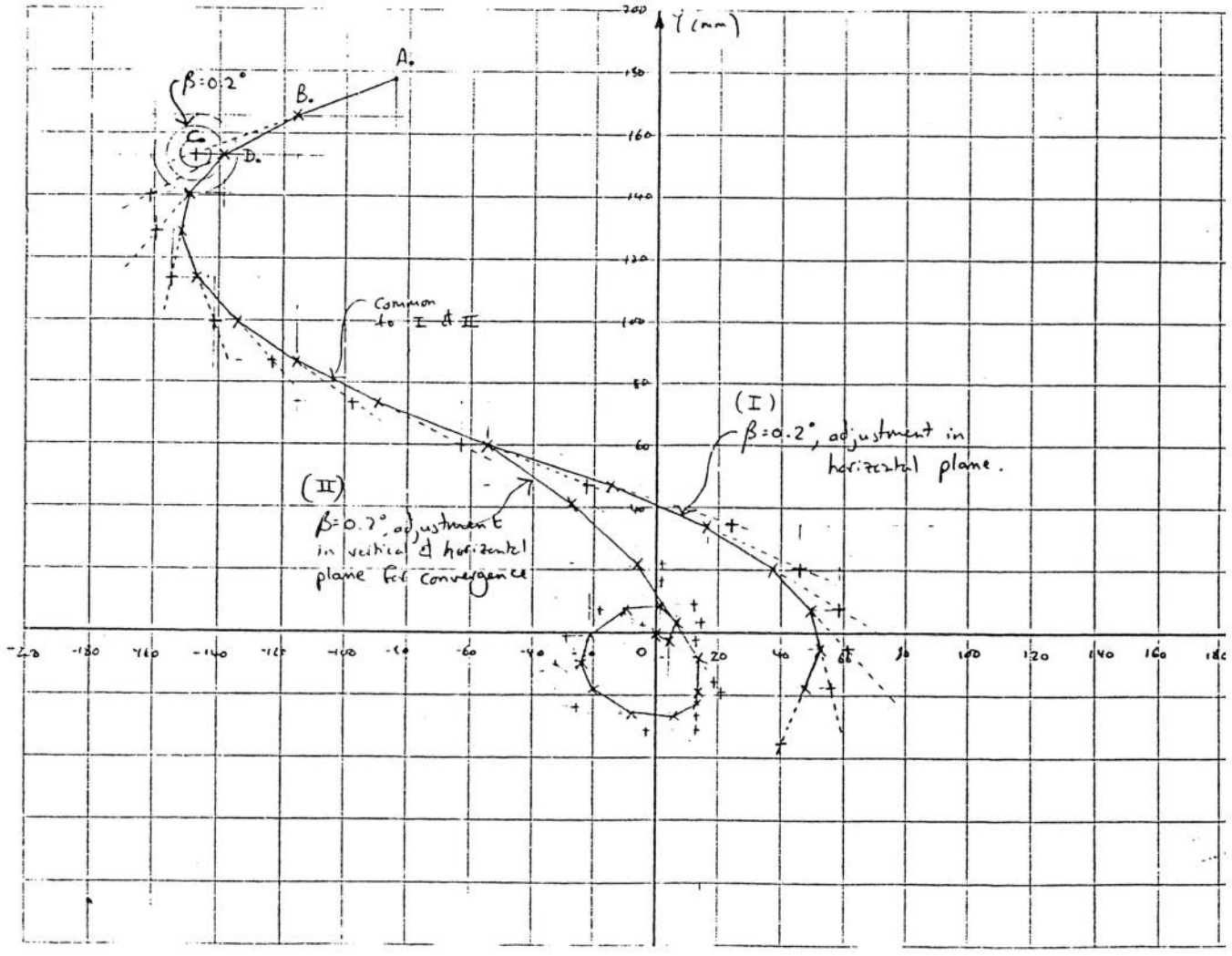

Figure S2.5 Alignment correction using joint angles

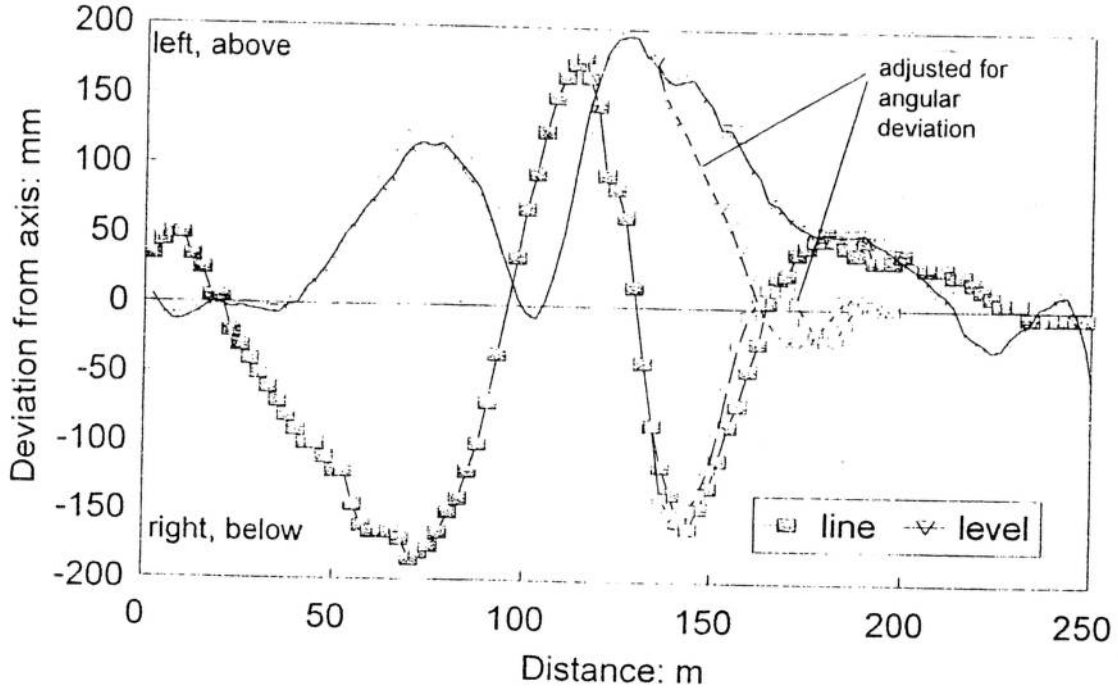

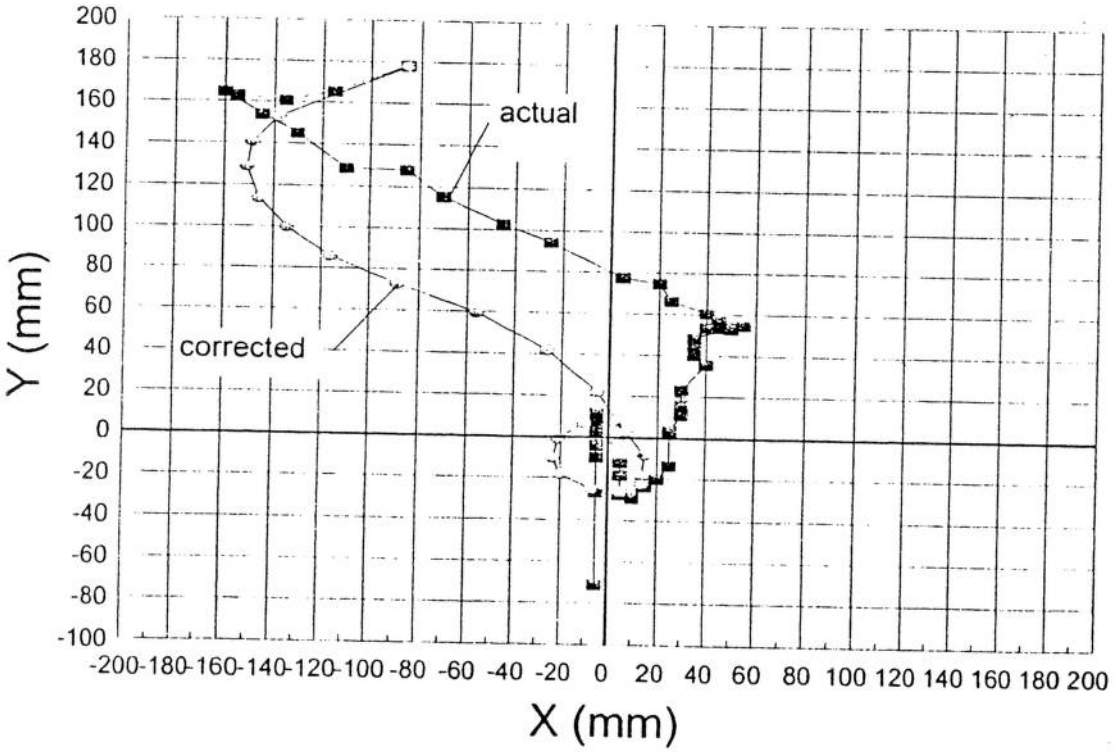

Figure S2.6 Corrected line and level - Site 4 example

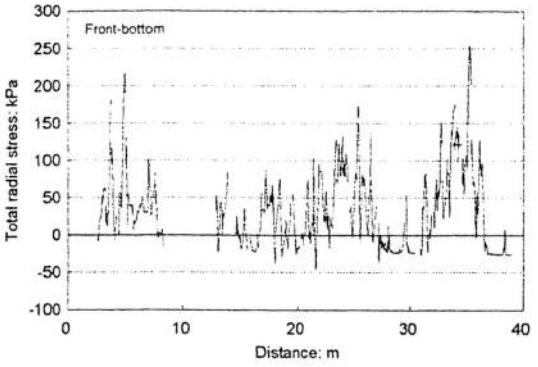

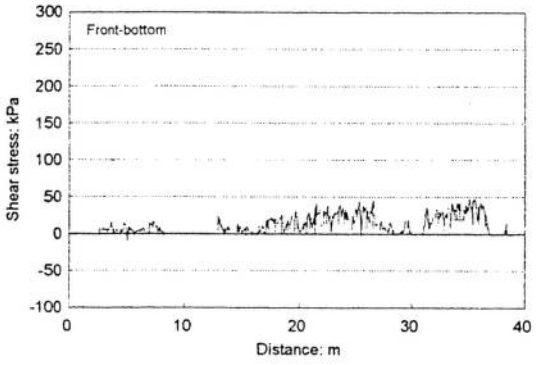

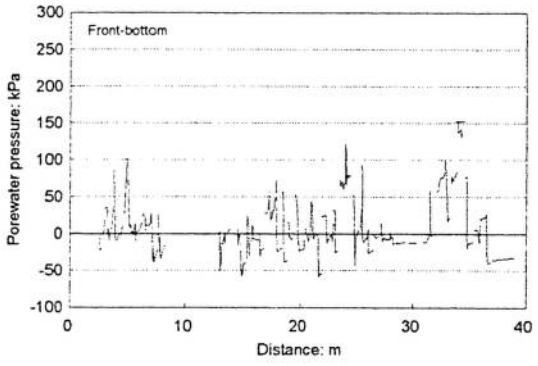

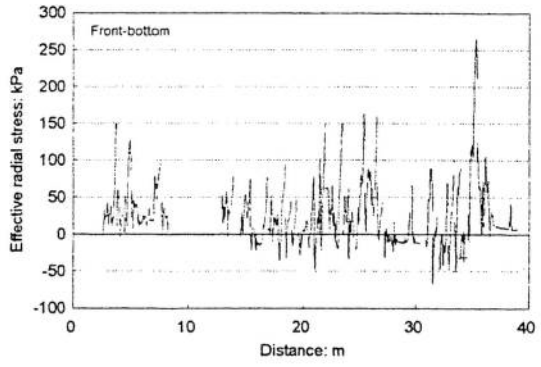

(a) Record of bottom interface stresses

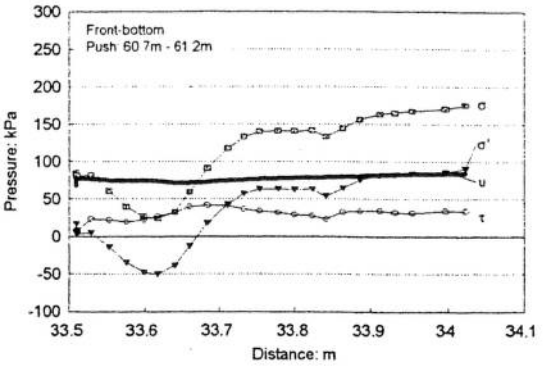

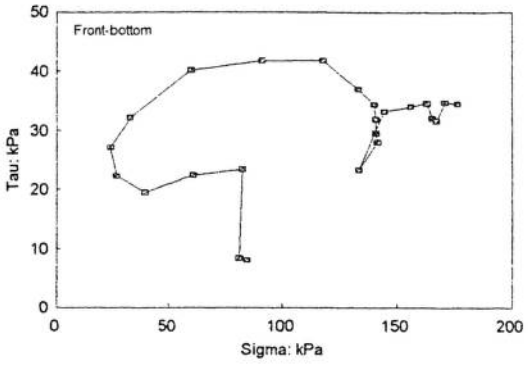

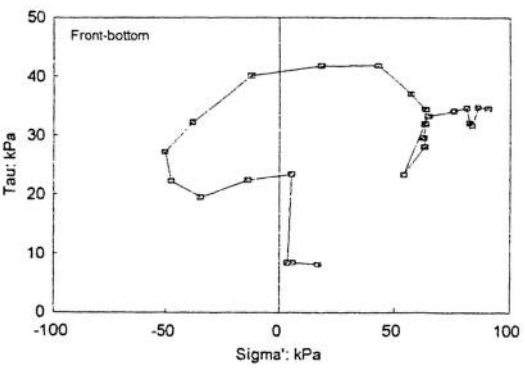

(b) Interface stresses during a single pus

Figure S4.1 - Site 1 contact stresses

Top

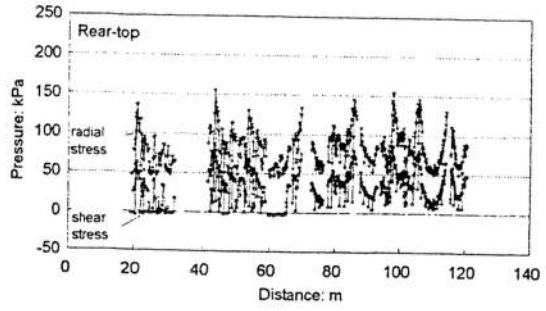

Left

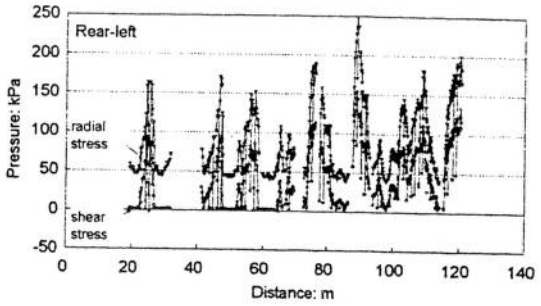

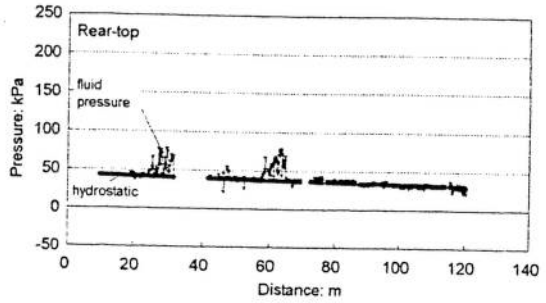

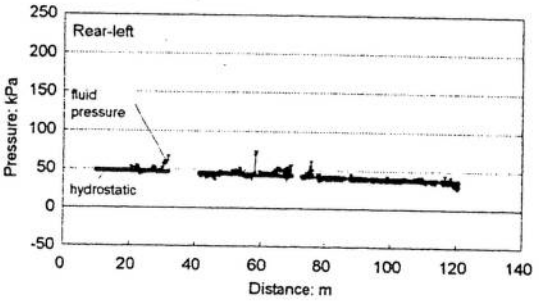

Bottom

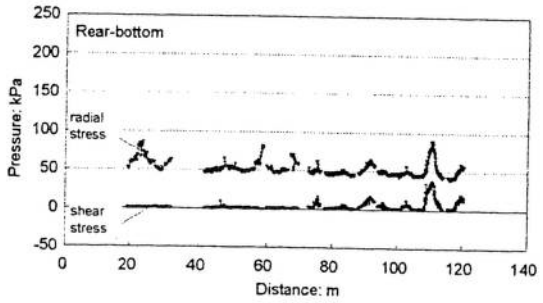

Right

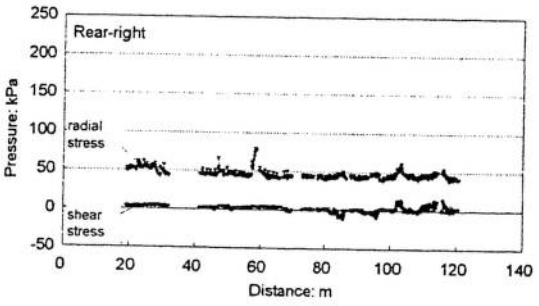

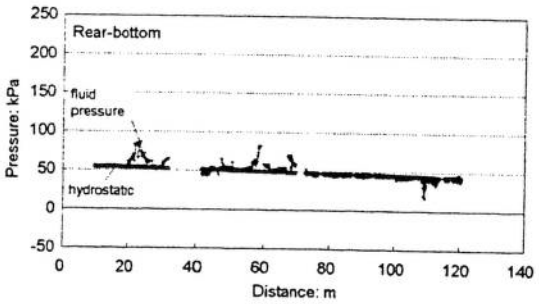

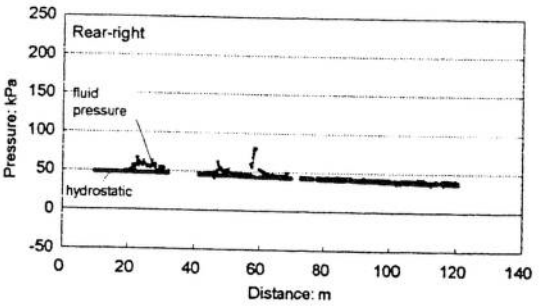

Figure S4.2 - Site 2 contact stresses

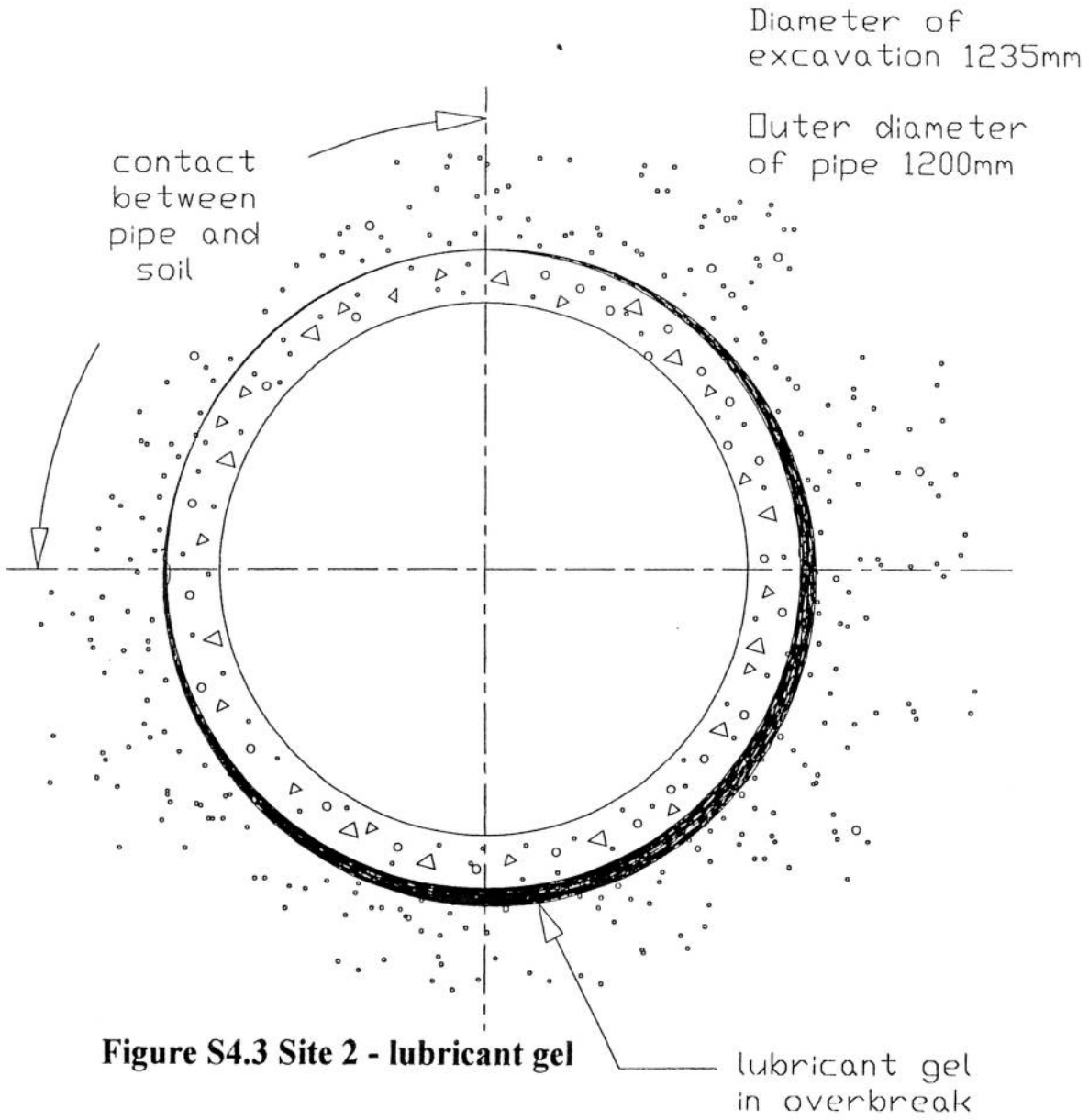

Figure S4.3 Site 2 - lubricant gel

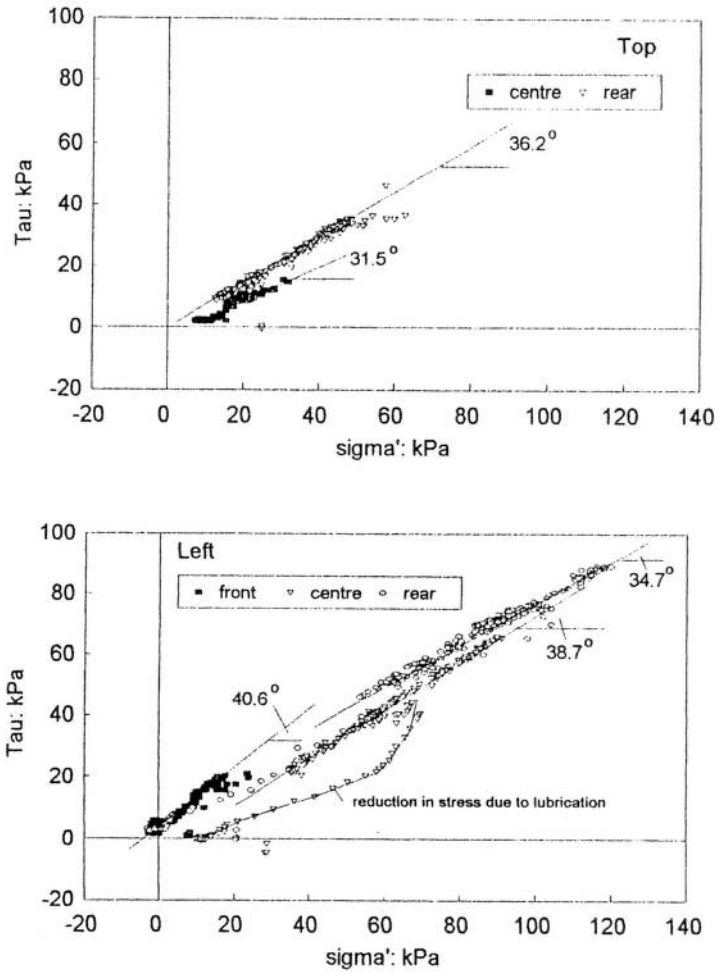

Figure S4.4 Site 2 - effective radial stress /shear stress relationship (single push)

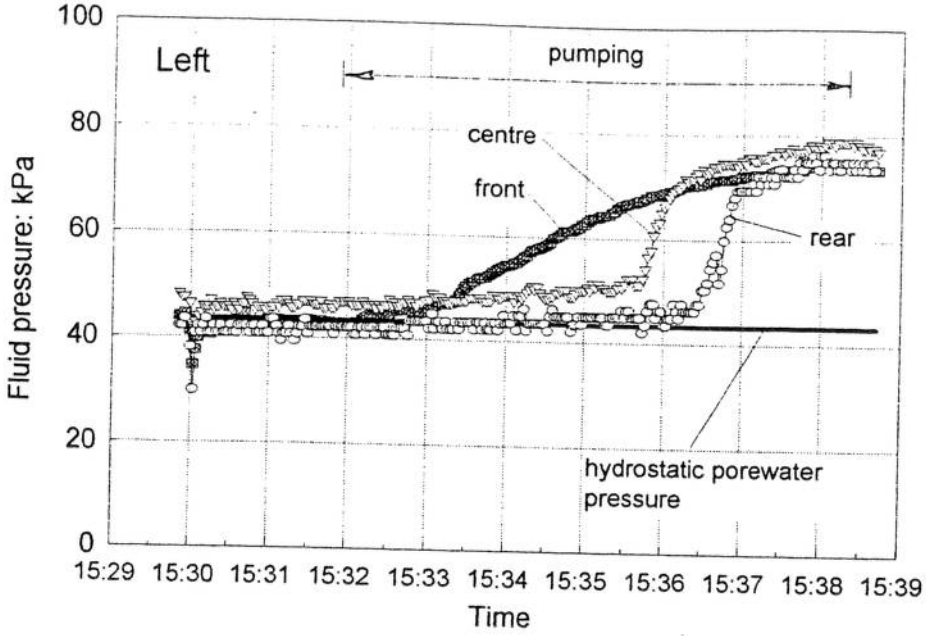

Figure S4.5 Site 2 - Change in fluid pressure during lubrication (single push)

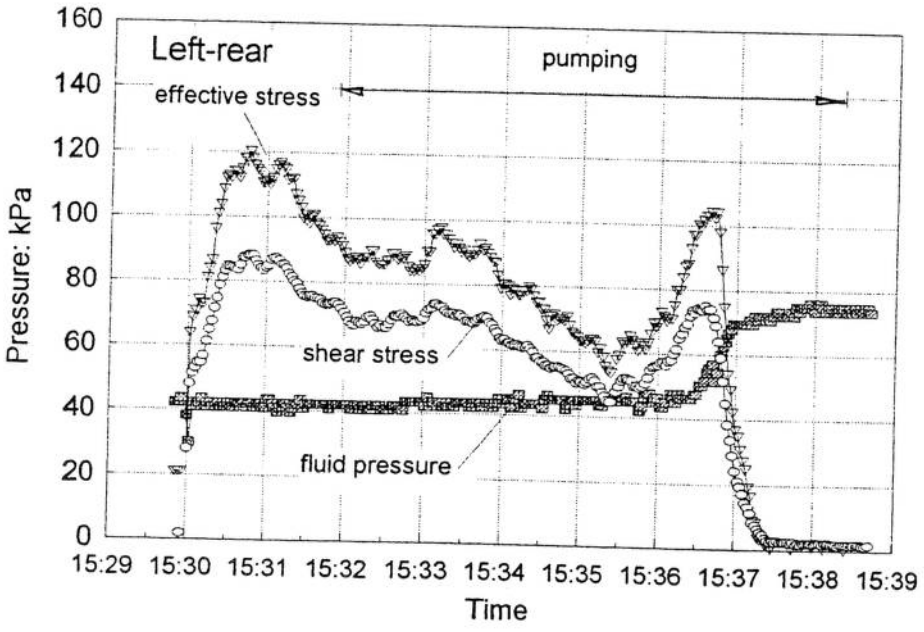

Figure S4.6 Site 2 - effect of pressurised lubricant on interface stresses

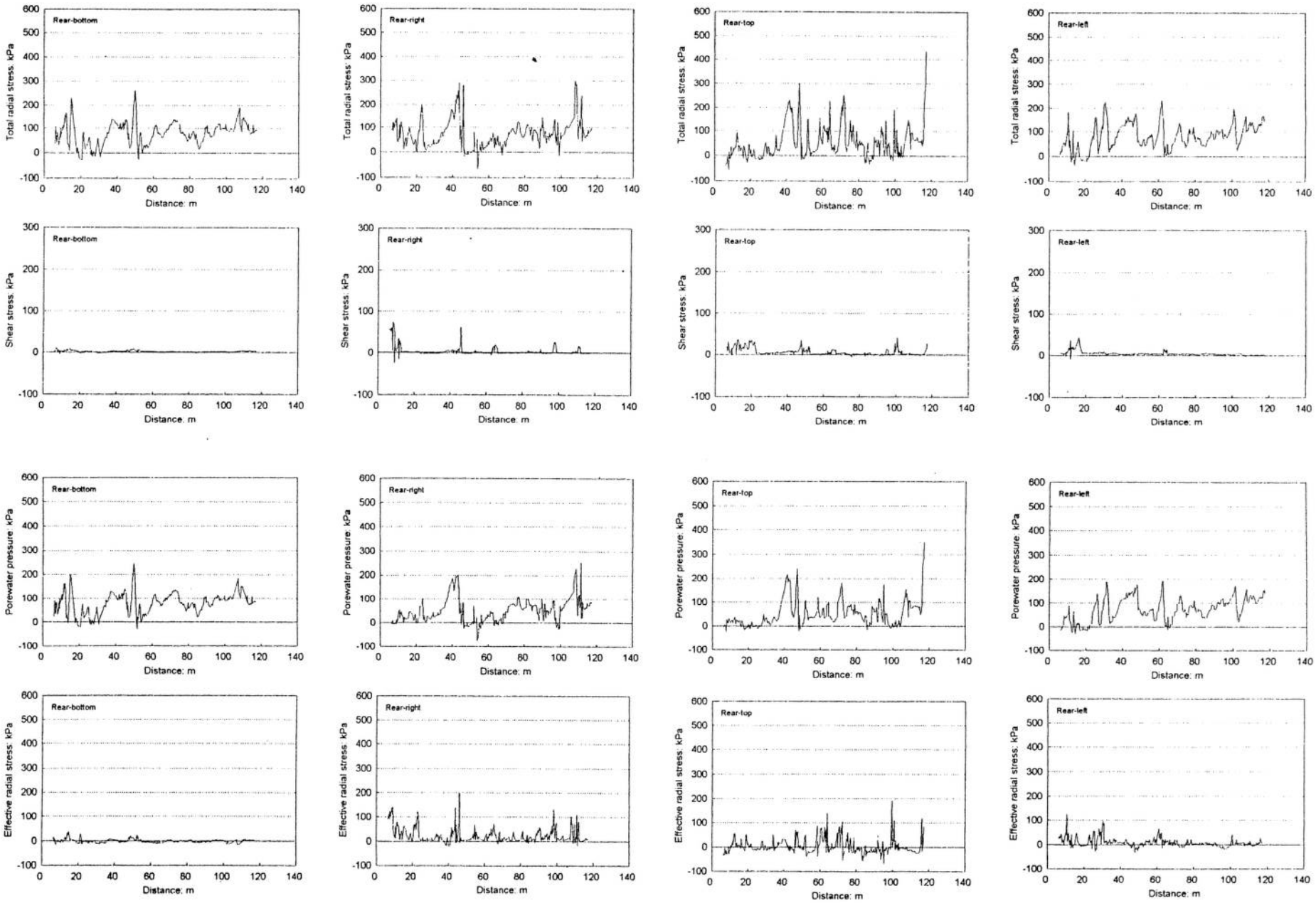

Figure S4.7 Site 3 - Contact stresses

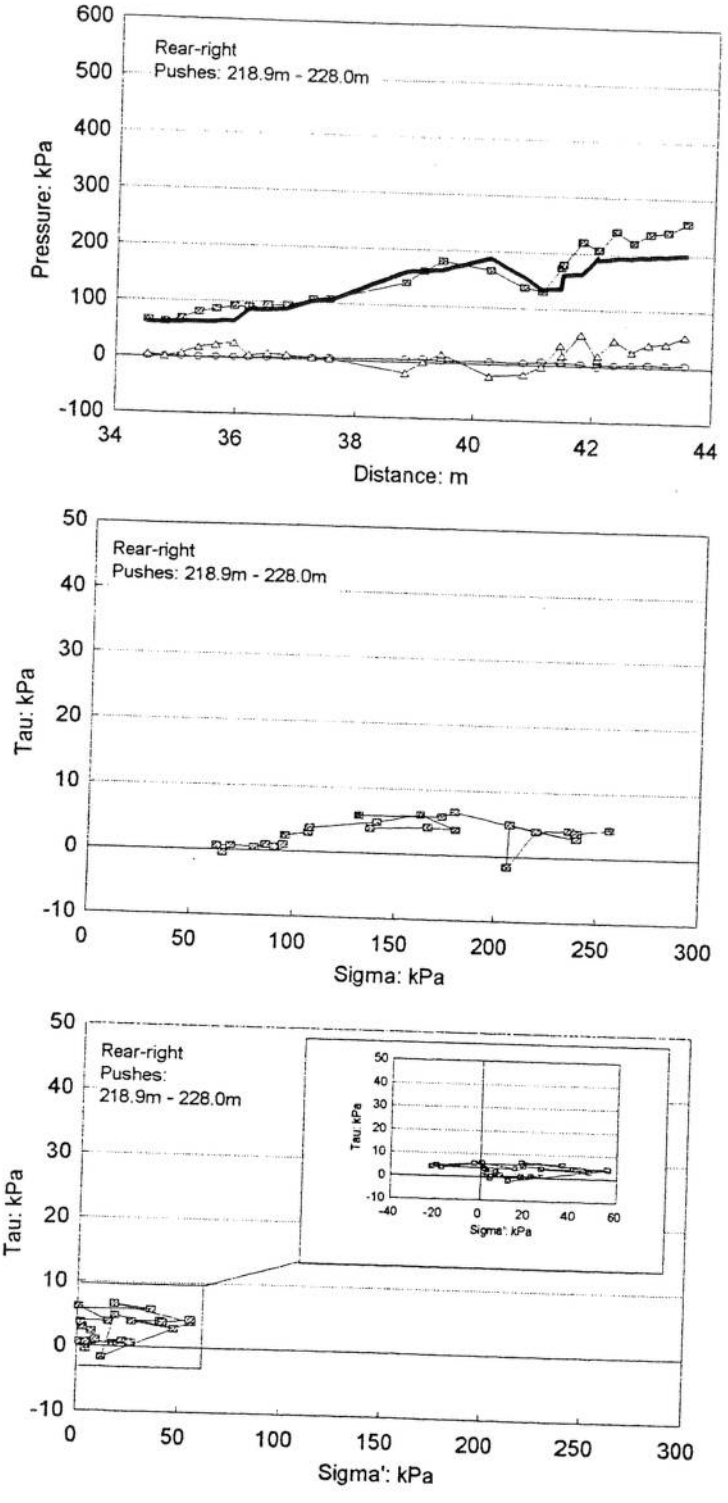

Figure S4.8 Site 3 - radial stress/shear stress relationship

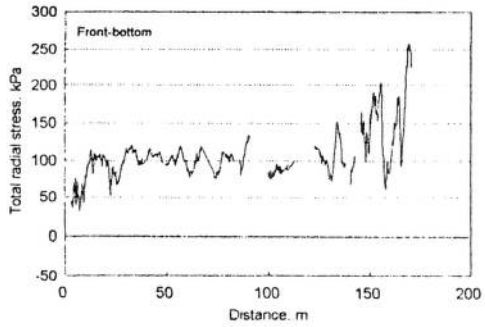
Front-bottom
Total radial stress: kPa
Distance: m

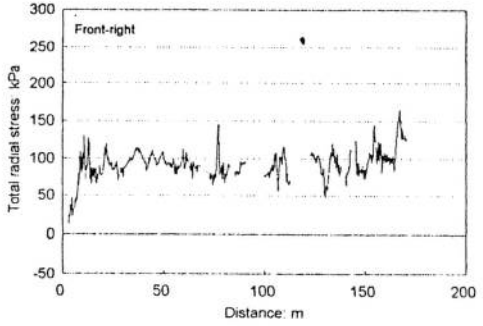
Front-right
Total radial stress: kPa
Distance: m

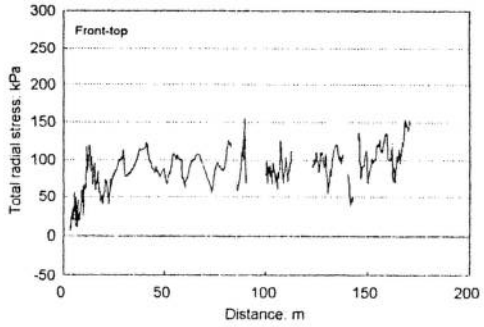
Front-top
Total radial stress: kPa
Distance: m

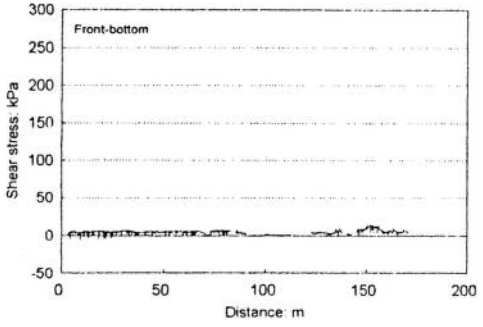
Front-bottom
Shear stress: kPa
Distance: m

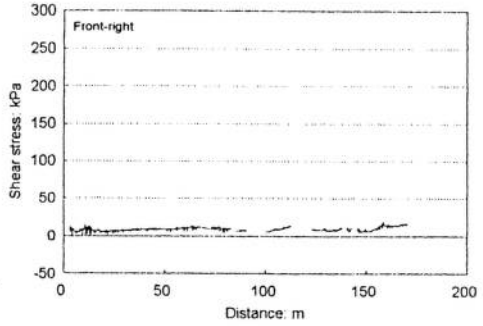
Front-right
Shear stress: kPa
Distance: m

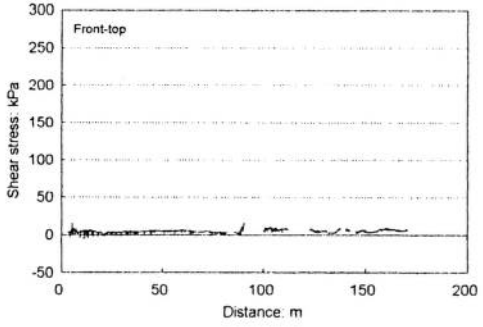
Front-top
Shear stress: kPa
Distance: m

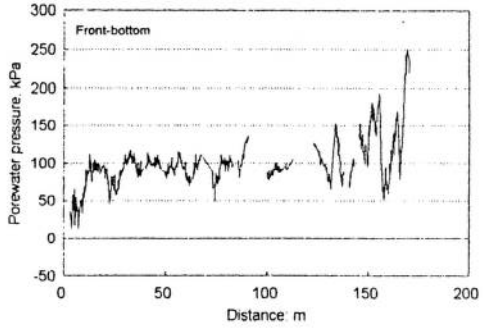
Front-bottom
Porewater pressure: kPa
Distance: m

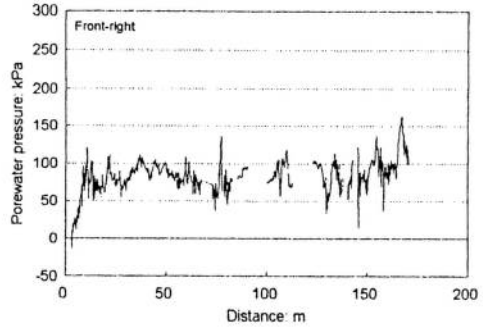
Front-right
Porewater pressure: kPa
Distance: m

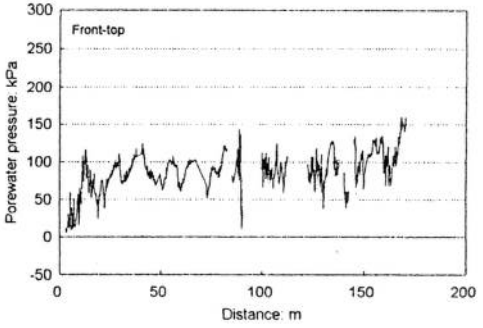
Front-top
Porewater pressure: kPa
Distance: m

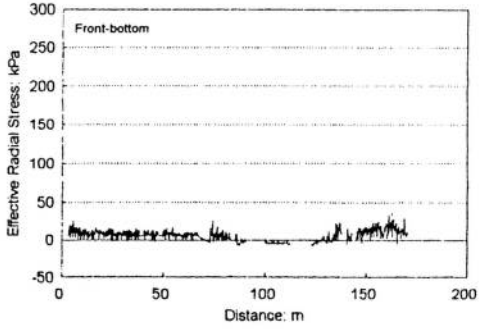
Front-bottom
Effective Radial Stress: kPa
Distance: m

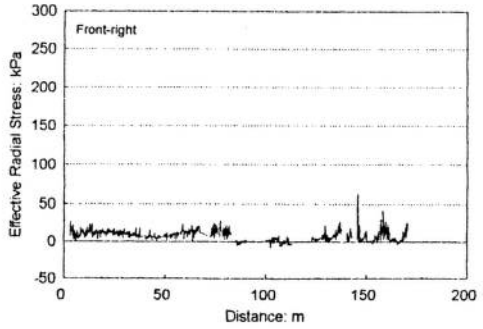
Front-right
Effective Radial Stress: kPa
Distance: m

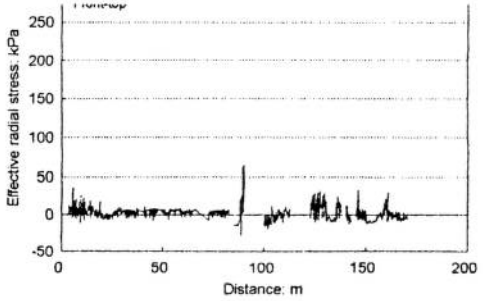
Effective radial stress: kPa
Distance: m

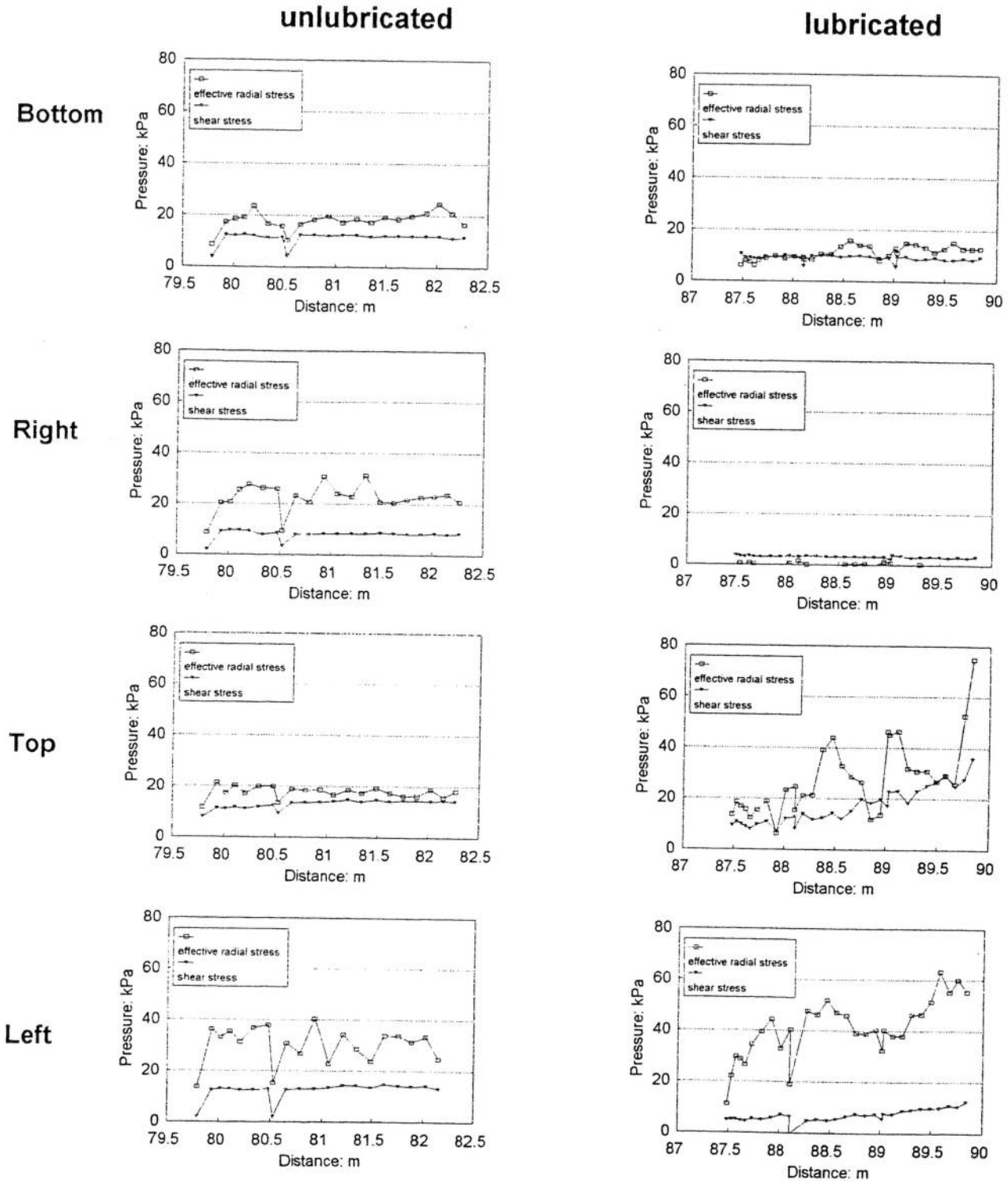

Figure S4.10 Site 4 - contact stresses before and after commencing lubrication

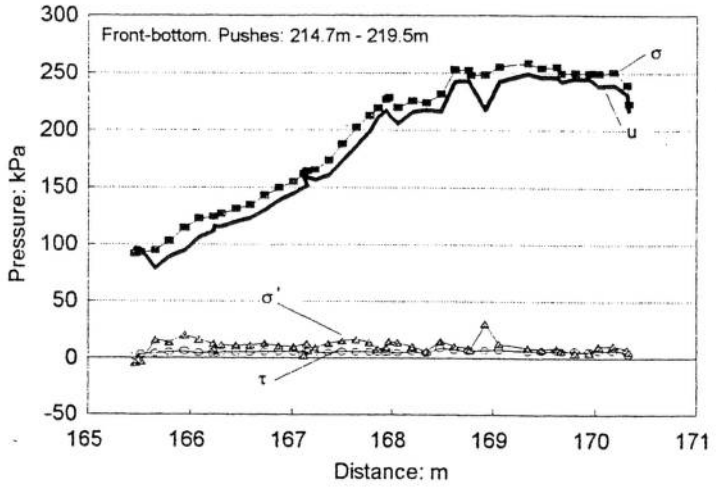

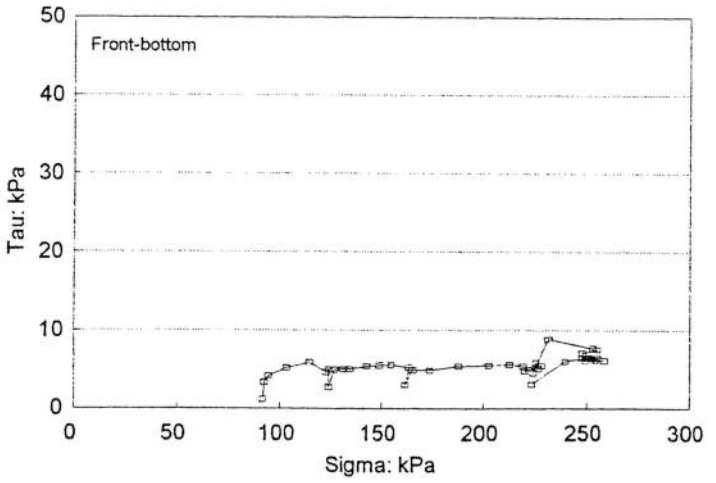

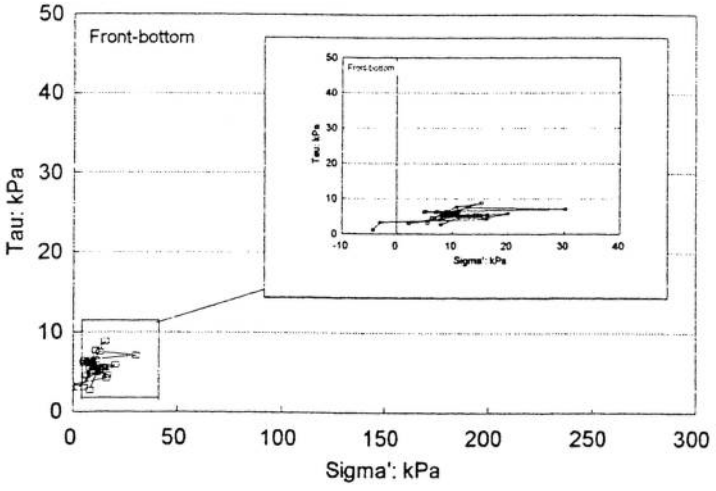

Figure S4.11 Site 4 - radial stress/shear stress relationship

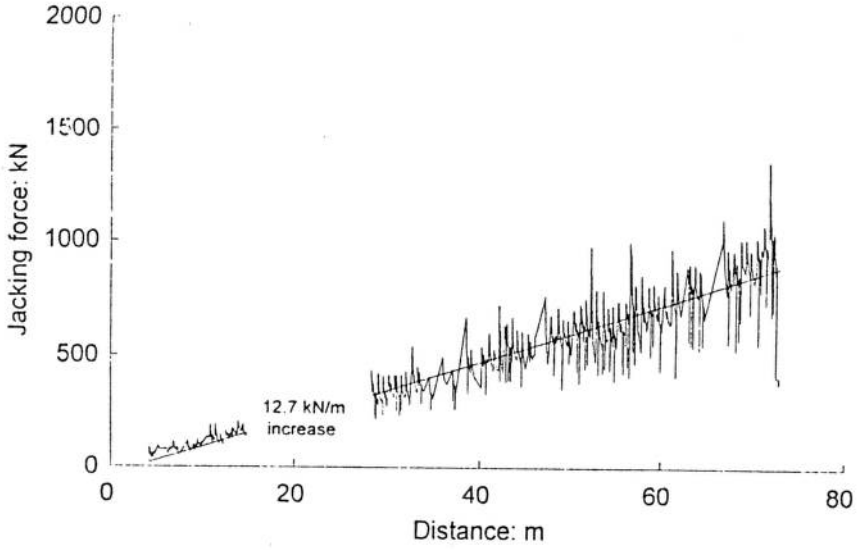

Figure S5.1 Jacking force record, site 1, Leyton

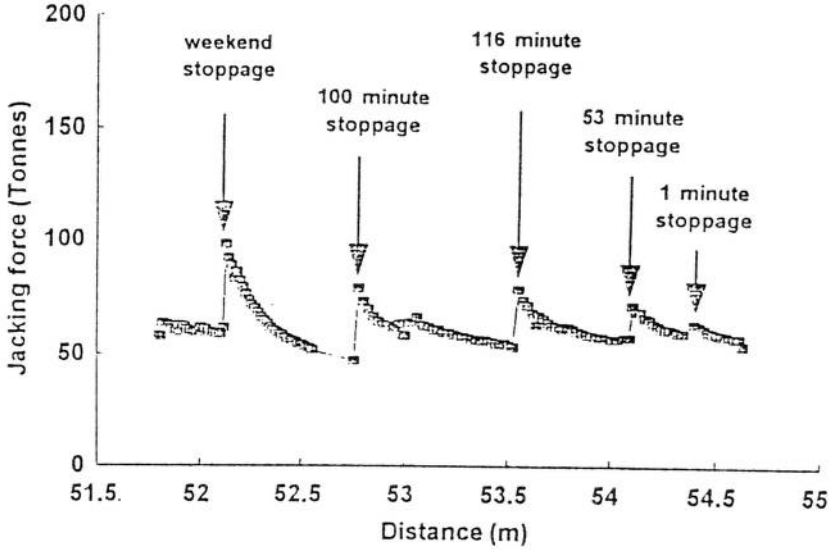

Figure S5.2 Effects of stoppages on jacking forces, site 1

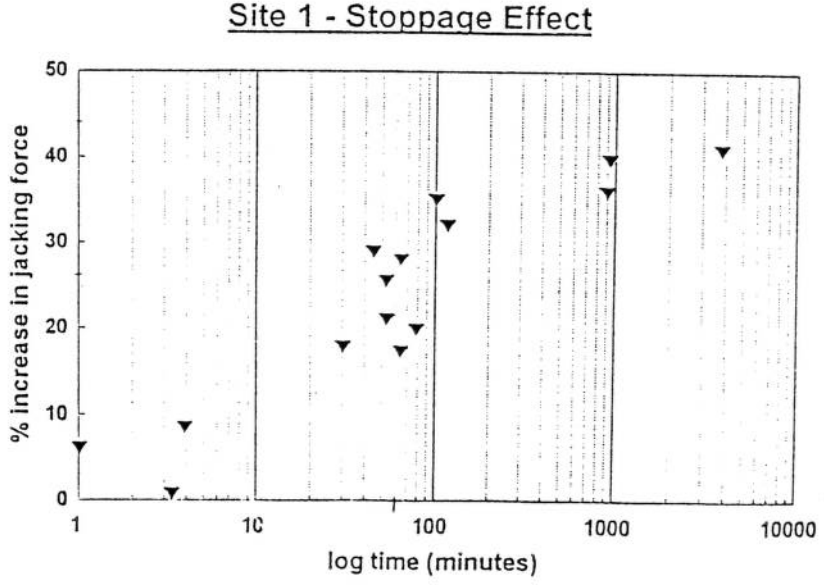

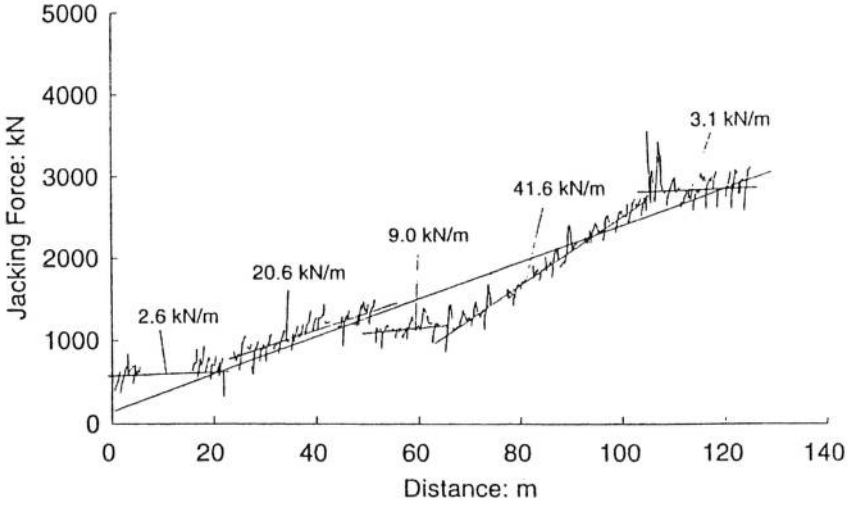

Figure S5.3 Jacking force record, site 2, Southport

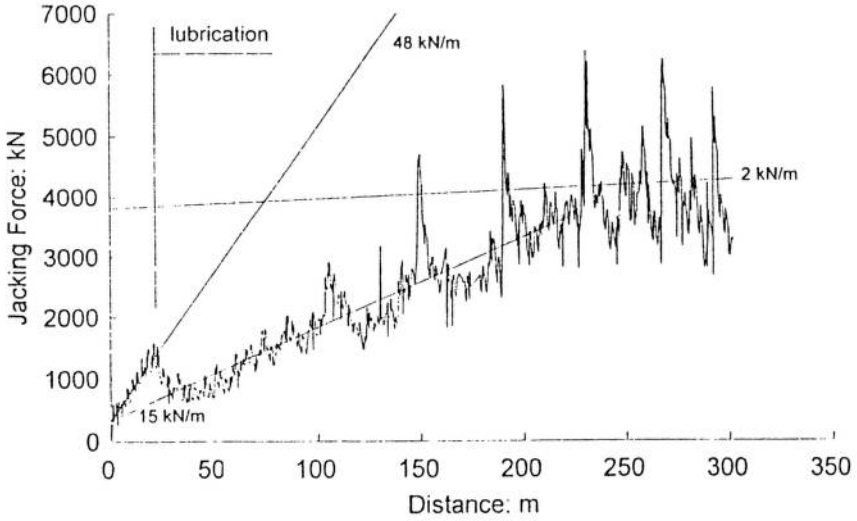

Figure S5.4 Jacking force record, site 3, Seaham

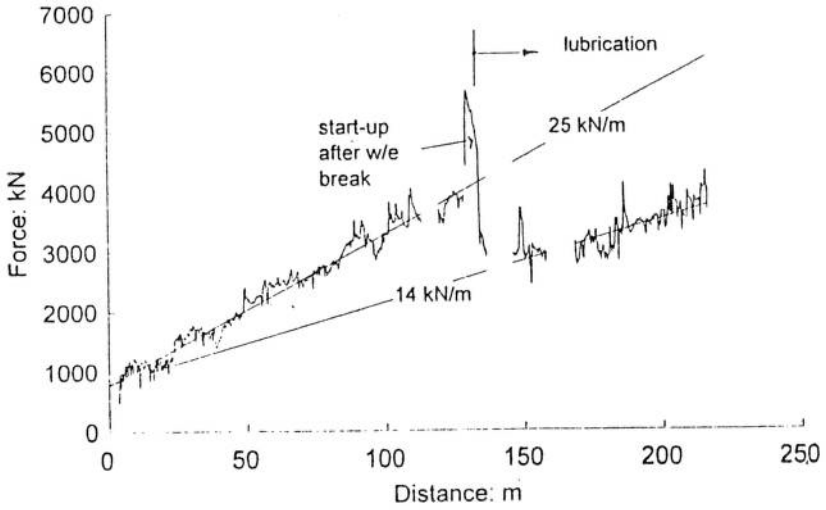

Figure S5.5 Jacking force record, site 4, Thurrock

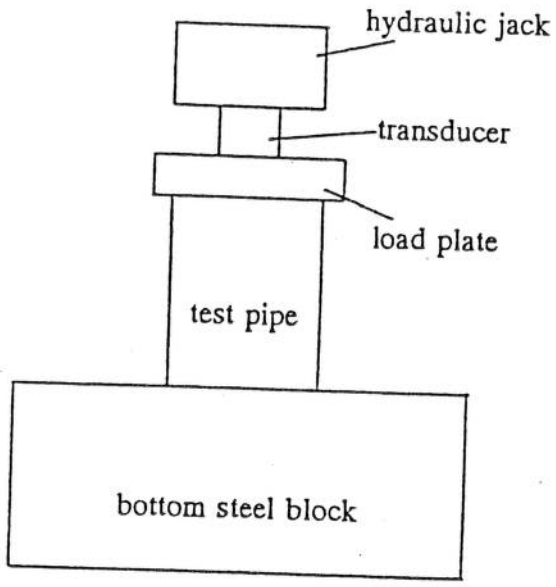

Test arrangement (schematic)

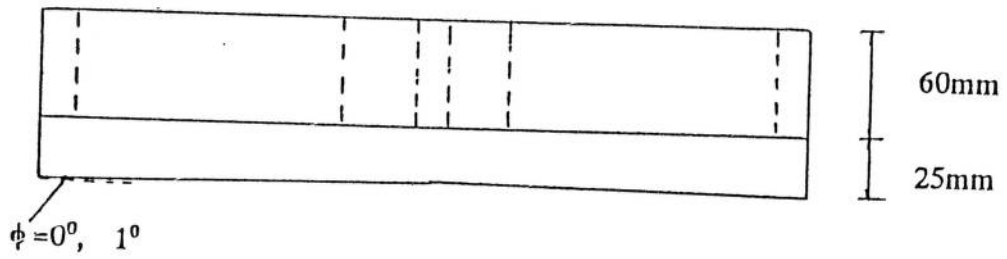

Details of loading plates

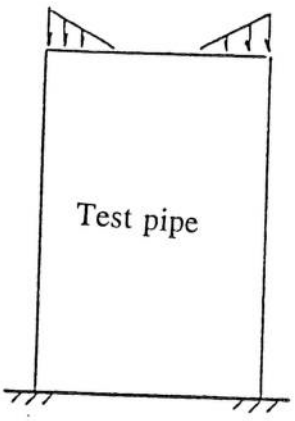

Load distribution with bevelled loading plate B

Figure S7.1 Load tests on model pipes

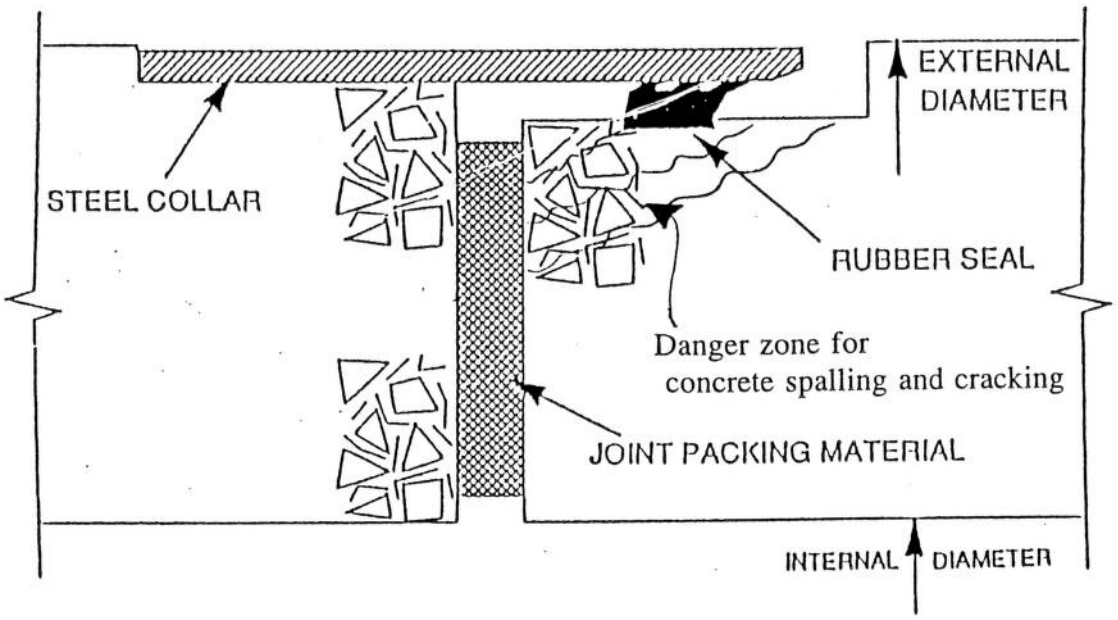

Pipe joint with steel collar

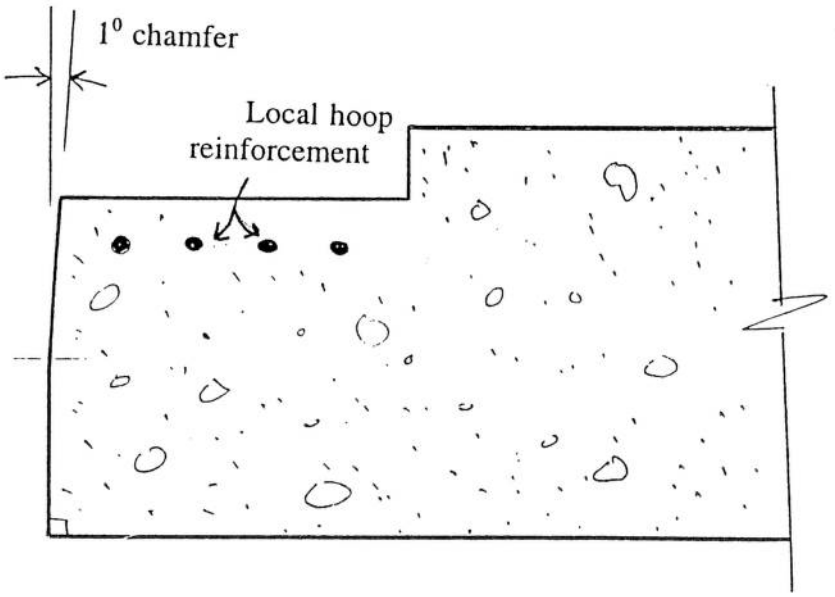

Modified pipe joint end detail

Figure S7.2 Standard pipe joint and modified joint detail

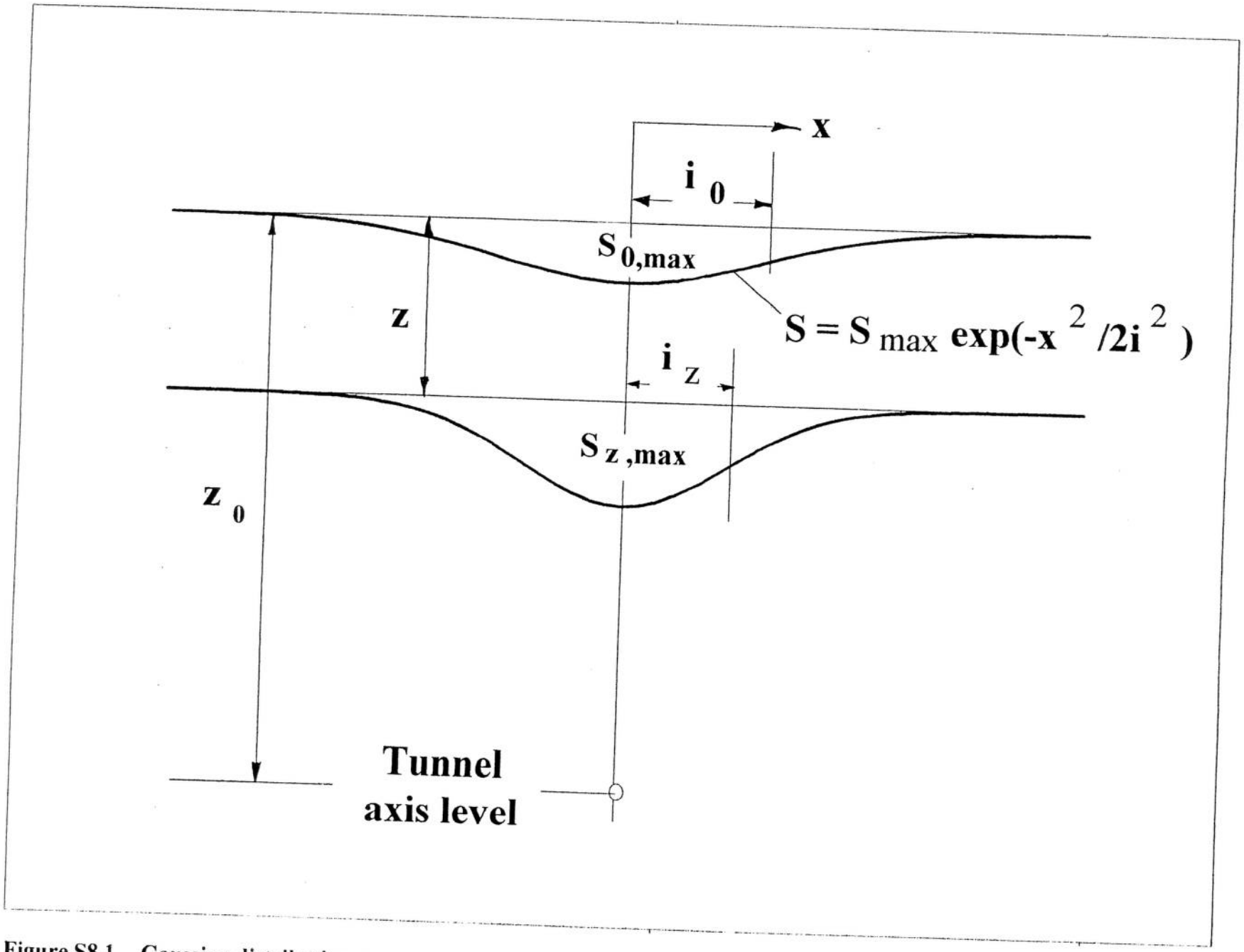

Figure S8.1 Gaussian distribution curve

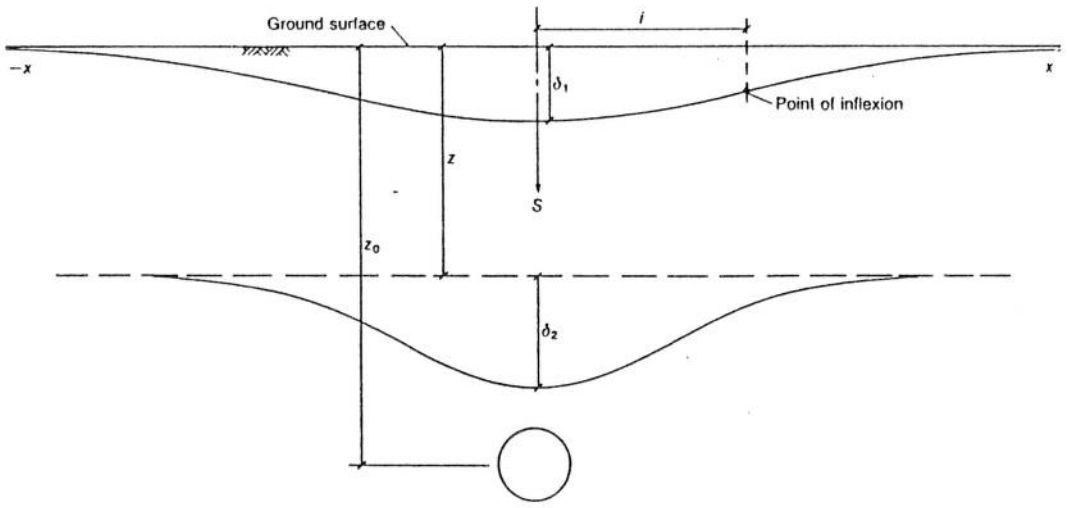

Form of surface and subsurface settlement profiles

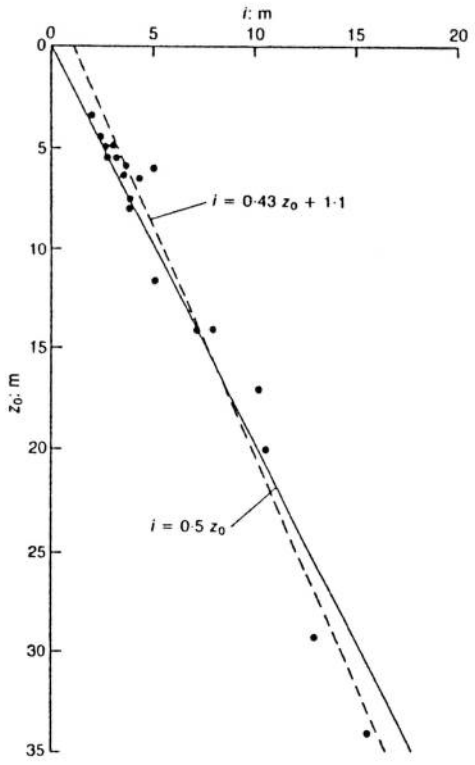

Variation of surface settlement trough width parameter with tunnel depth for tunnels in clays (after O'Reilly & New, 1982)

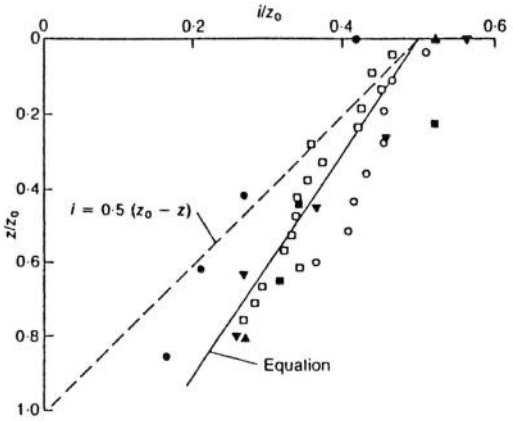

	Location	Soil type	D: m	z_0: m	Reference
•	Green Park	London Clay	4·1	29	Attewell & Farmer (1974)
▲	Regent's Park (northbound)	London Clay	4·1	20	Barratt & Tyler (1976)
▼	Regent's Park (southbound)	London Clay	4·1	34	Barratt & Tyler (1976)
■	Willington Quay	Soft clay	4·3	13.5	Glossop (1978)
○	Centrifuge* model 2DP	Soft clay	0·06	0·13	Mair (1979)
□	Centrifuge* model 2DV	Soft clay	0·06	0·22	Mair (1979)

*Models tested at 75g: equivalent full-scale D = 4·5 m, z_0 = 9·8 m (2DP), 16·5 m (2DV)

Variation of subsurface settlement trough width parameter with depth for tunnels in clays

For subsurface settlements in cohesive soil

$$\frac{i}{z_0} = 0.175 + 0.325\left(1 - \frac{z}{z_0}\right)$$

Figure S8.2 Subsurface settlements in cohesive soils (From Mair et al. 1993)

For conditions of uniform initial stress σ_0 at the tunnel boundary,

$$\frac{\delta}{a} = \frac{s_u}{2G}\left(\frac{a}{r}\right)\exp\left(N^*-1\right)$$

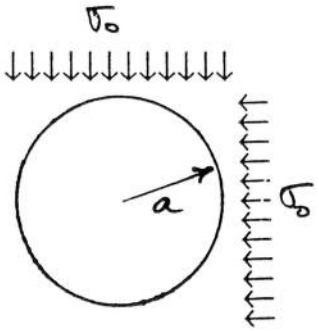

where δ = radial inward movement at radius r
a = radius of tunnel bore
N^* = stability ratio = σ_0/s_u
s_u = undrained shear strength
G = elastic shear modulus

Typically in stiff clay e.g. London Clay, G/s_u = 80 - 100

then for example, if a = 900 mm
G/s_u = 80
N^* = 1.6 ,
corresponding to a 1.8 m O.D. tunnel at about 8 m depth in clay of 100kPa shear strength

δ = 10.25 mm

at the tunnel surface where $r = a$

Results of field measurements near tunnels in London Clay:-

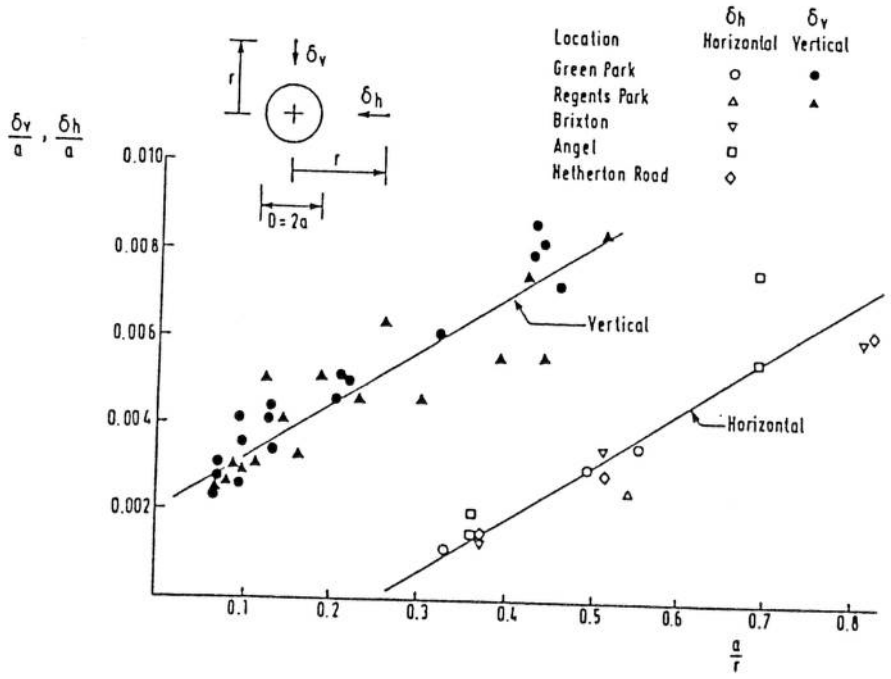

Figure S8.3 Subsurface movements near tunnels in London Clay (From Mair and Taylor 1993)

Site 1 - Surface Settlement

Raod nails in stiff pavement

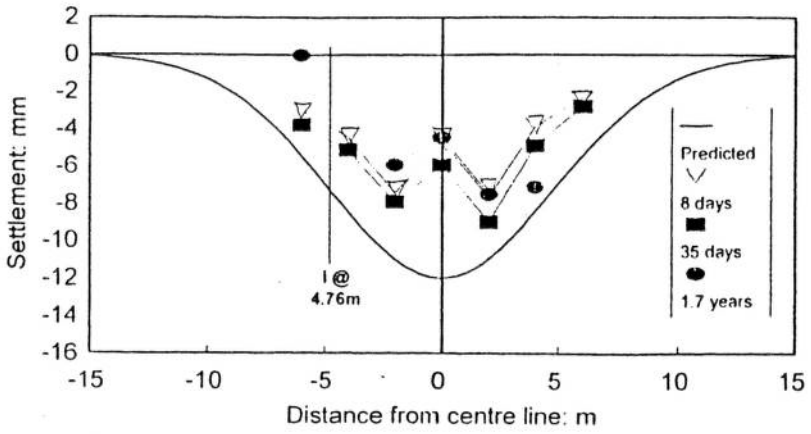

Figure S8.4

Site 1 - Tube B

Transverse movement into tunnel

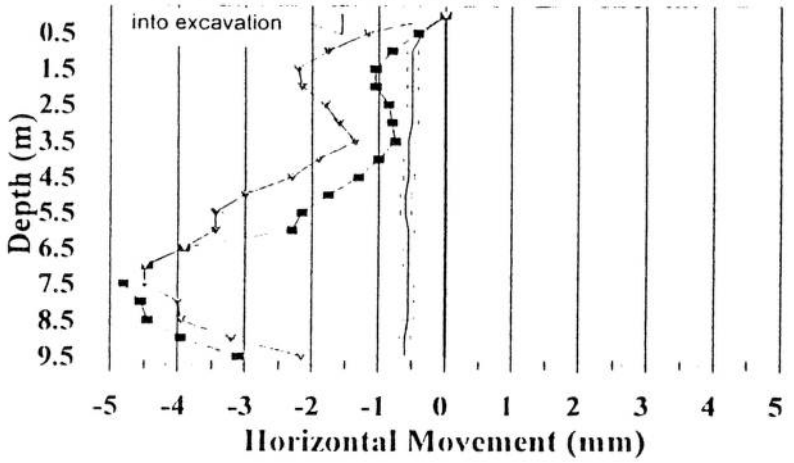

Site 1 - Tube C

Transverse movement into tunnel

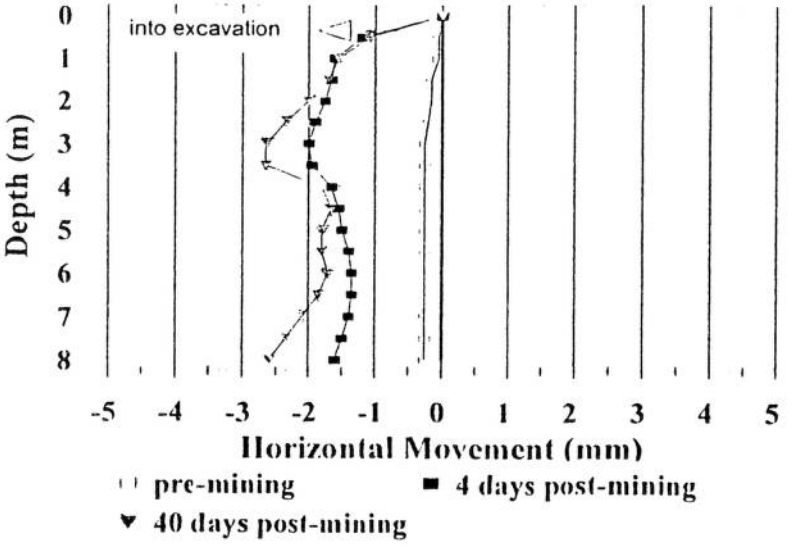

Figure S8.5

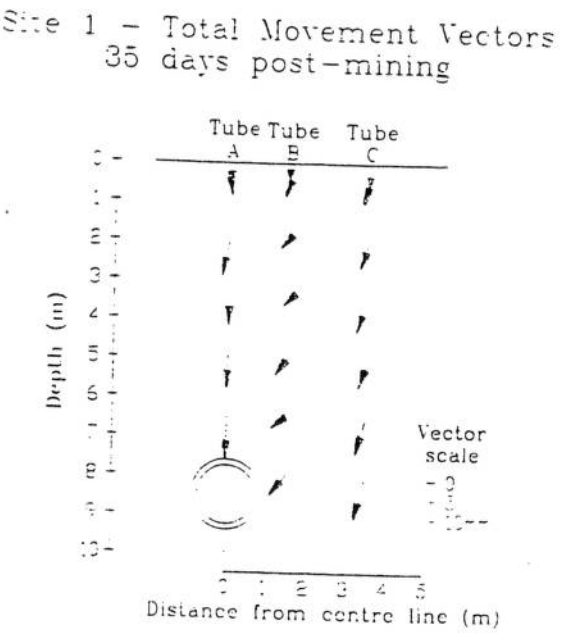

Figure S8.6

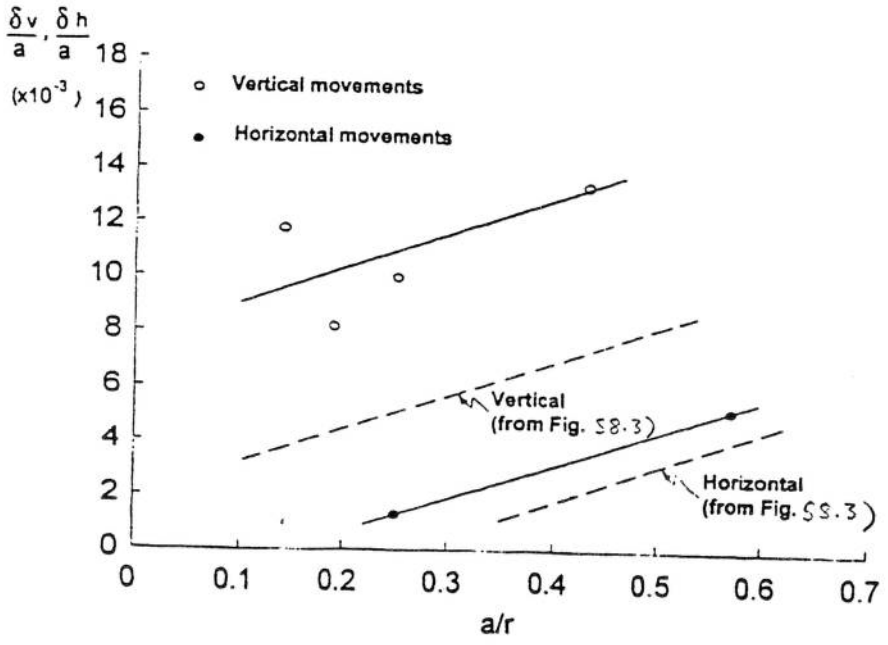

Figure S8.7 Comparison of subsurface movements with deeper 4m diameter tunnels

Site 2 - Surface Settlement

Observed levels - 4 days post-mining

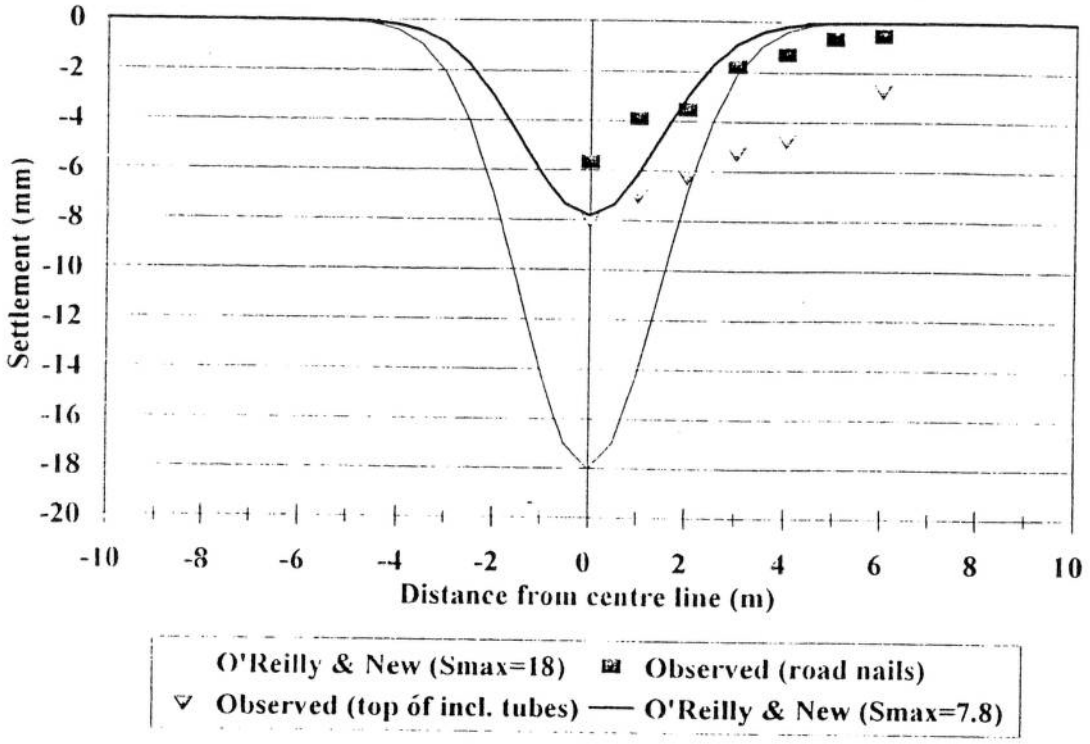

Figure S8.8

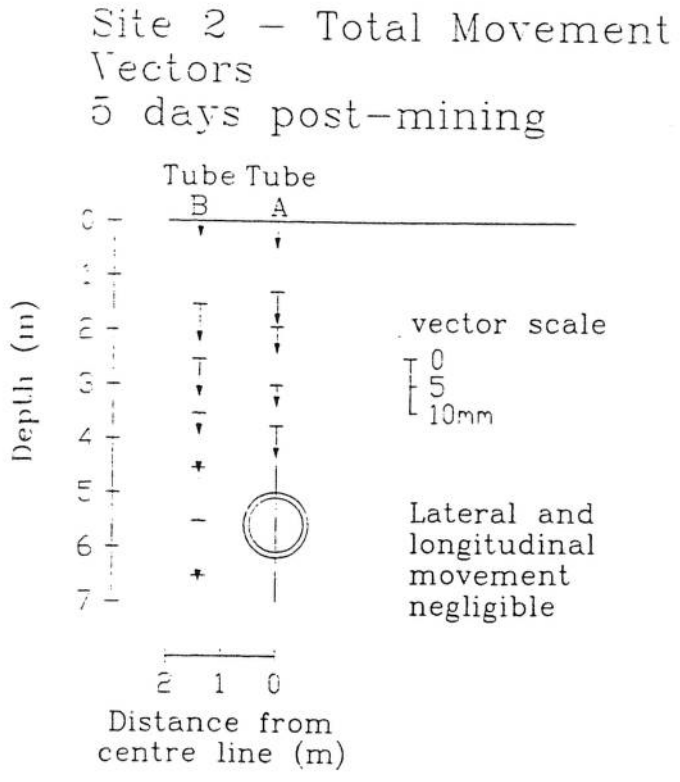

Figure S8.9

Site 3 - Surface Settlement

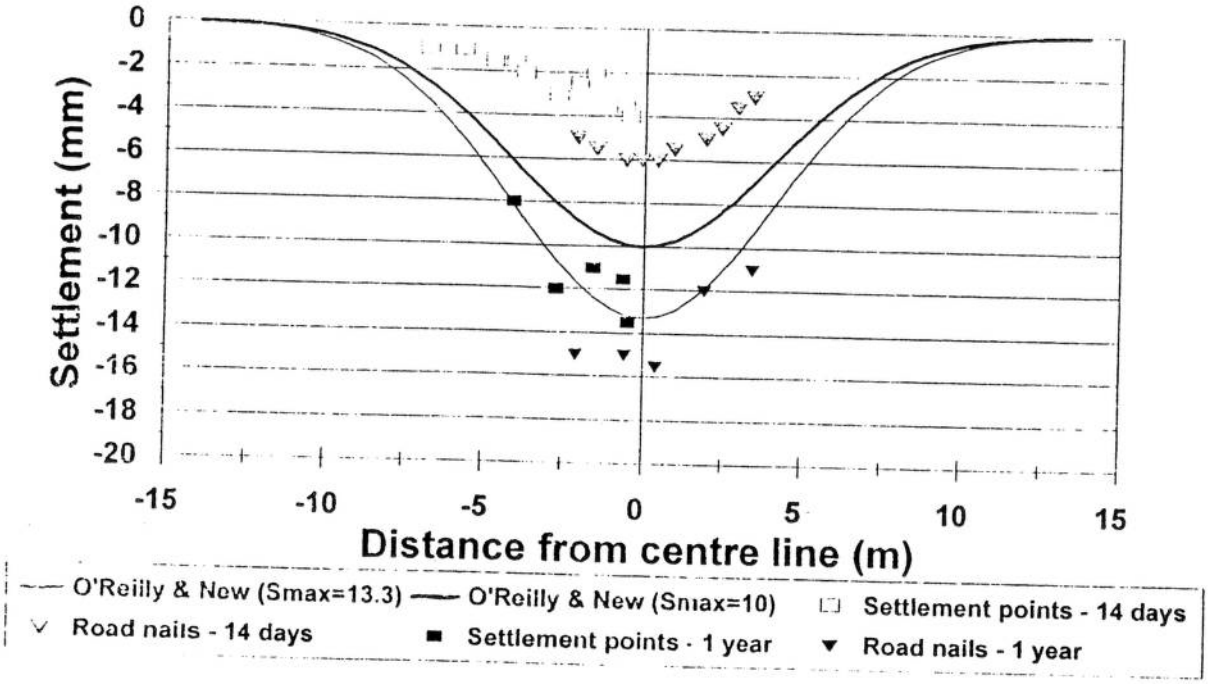

Figure S8.10

Site 3 - Tube B

Transverse movement into tunnel

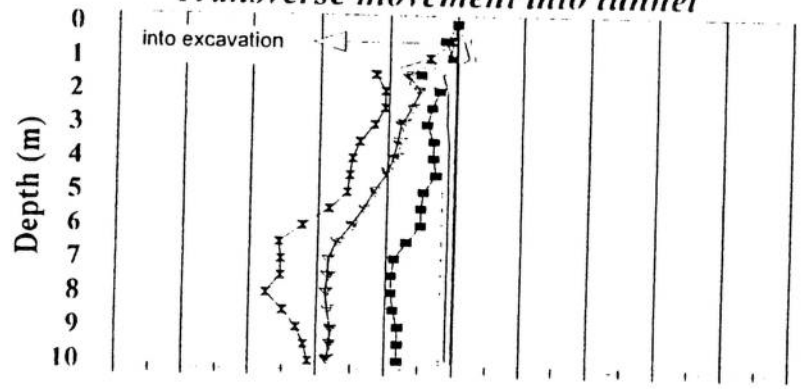

Site 3 - Tube C

Transverse movement into tunnel

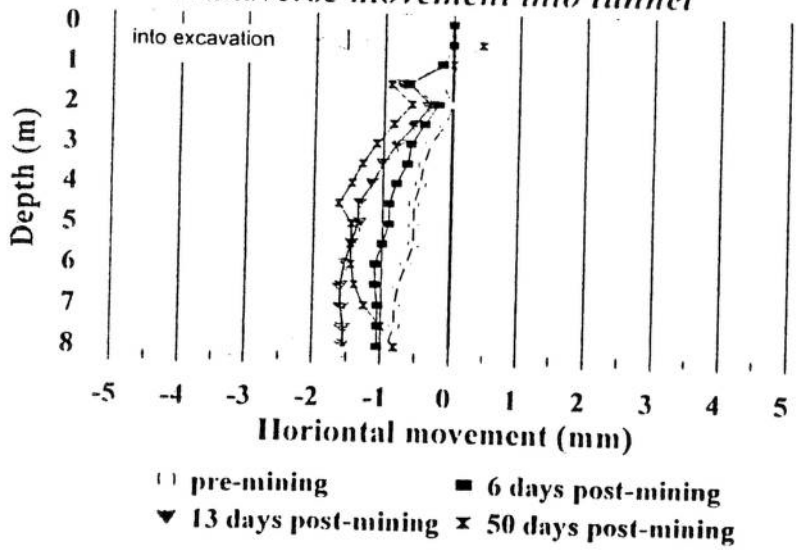

Figure S8.11

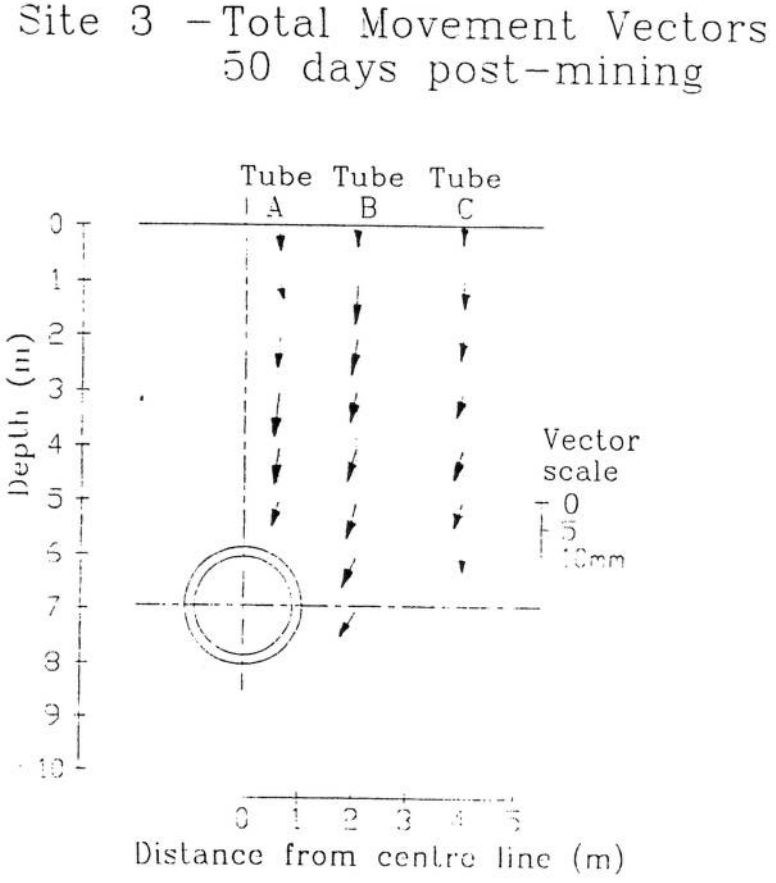

Figure S8.12

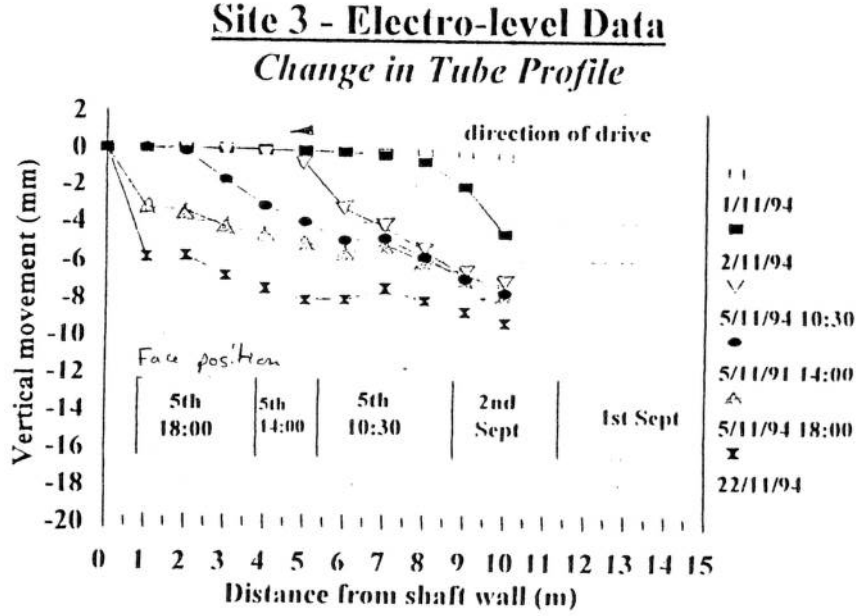

Figure S8.13

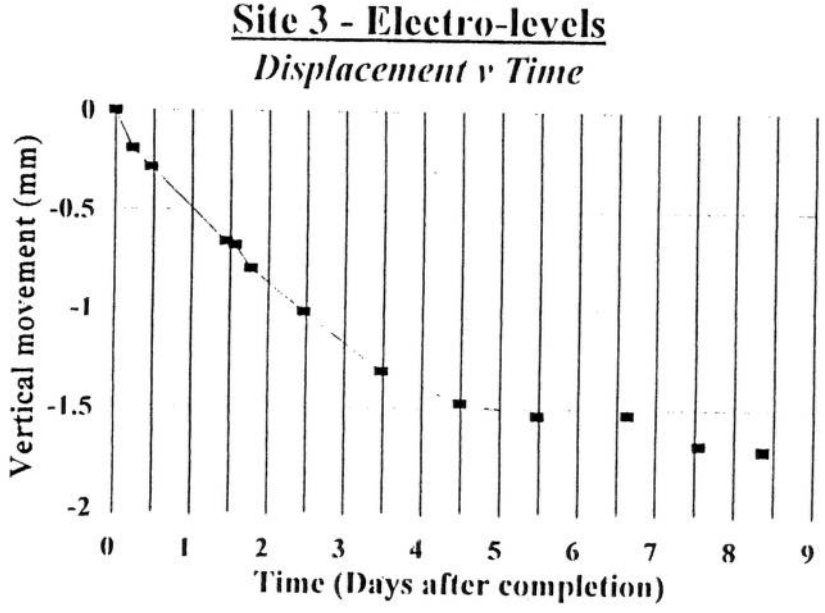

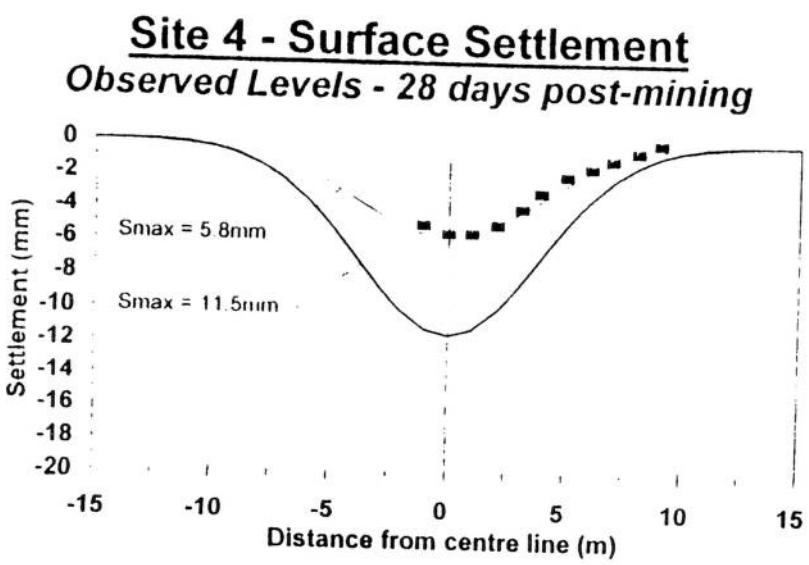

Figure S8.15

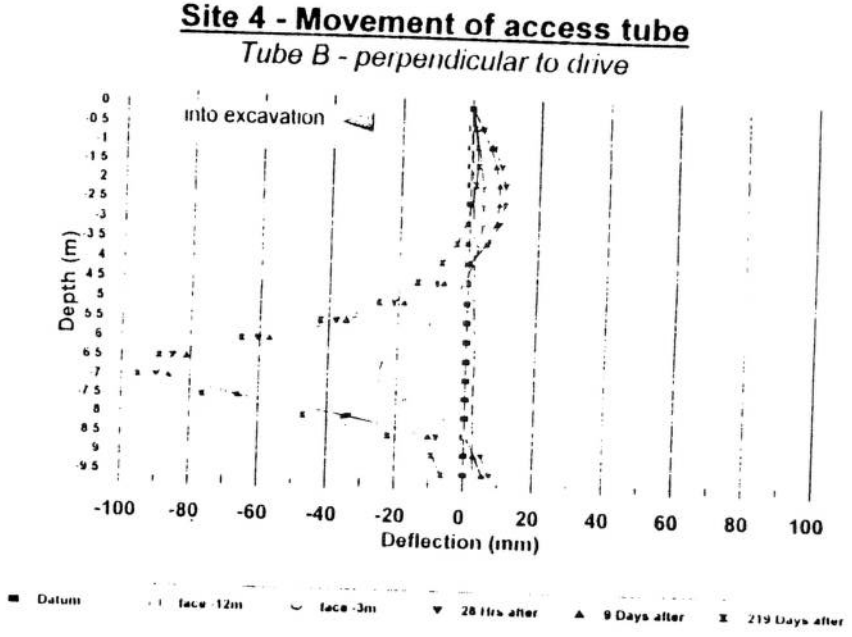

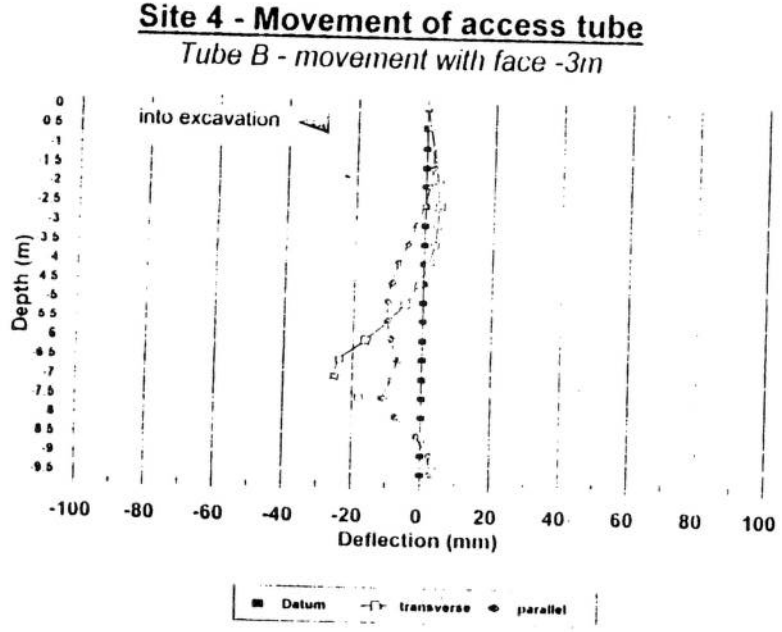

Figure S8.17

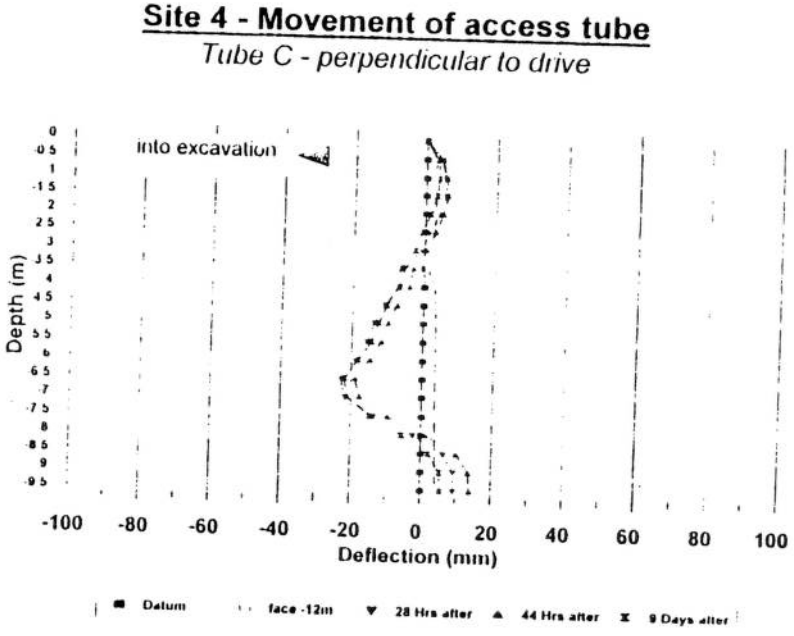

Figure S8.16